RESEARCH REPORT

ANNUAL SUMMARY REPORT

(June 11, 1971--June 10, 1972)

on

THE EFFECT OF ALLOY COMPOSITION ON THE MECHANISM OF STRESS-CORROSION CRACKING OF TITANIUM ALLOYS IN AQUEOUS ENVIRONMENTS

to

NATIONAL AERONAUTICS AND SPACE ADMINISTRATION

June, 1972

by

R. A. Wood, J. D. Boyd, D. N. Williams and R. I. Jaffee

BATTELLE
Columbus Laboratories
505 King Avenue
Columbus, Ohio 43201

TABLE OF CONTENTS

THE EFFECT OF ALLOY COMPOSITION ON THE MECHANISM OF STRESS-CORROSION CRACKING OF TITANIUM ALLOYS IN AQUEOUS ENVIRONMENTS

by

R. A. Wood, J. D. Boyd, D. N. Williams, and
R. I. Jaffee

PROGRAM SYNOPSIS

This program, which was initiated in early 1967, was aimed at determining the effect of alloying elements on the stress-corrosion cracking of titanium alloys in N_2O_4, hot salt, and salt water. The experimental work was designed to afford an understanding of the mechanisms of stress corrosion operative in titanium alloys of several types but chiefly related to compositions of commercial significance.

Numerous compositions were investigated with a major emphasis given to alloys made with combinations of aluminum and the beta stabilizers molybdenum and vanadium. The effect of combinations of aluminum and oxygen were also studied as were other combinations of alloying elements which included tin, zirconium, gallium, indium, manganese, palladium, columbium, and tantalum. Each of the alloys were processed, insofar as practical, to afford minimum differences in microstructure and strength levels. However, selected compositions were evaluated after alternate processing conditions to determine combined effects of composition and variable metallurgical condition.

The principal test condition was a stabilized annealed condition wherein continuous equiaxed alpha was the dominant metallographic feature with beta phase at grain boundaries and triple points (in compositions alloyed with the beta stabilizing elements). Submicroscopic features such as the Ti_3Al phase were present in some compositions; the influence of the phase for its effects on the stress-corrosion susceptibility of selected alloys was evaluated.

The experimental alloys of this program were found to be susceptible to stress-corrosion cracking in oxygenated (red) N_2O_4 at ambient temperatures. However, alloy composition was found to markedly influence the corrosion resistance and the stress-corrosion fracture mode. Corrosion resistance was decreased with

increasing additions of molybdenum, vanadium, and oxygen (Ti-5 to 7 Al, weight percent). The binary alloys, Ti-(6-7) Al-0.1 O, have good corrosion resistance as does the Ti-7Al-2Mn alloy which also was the most resistant alloy to stress-corrosion cracking in the N_2O_4 environment. Some information was obtained which suggested that chemical activity in the alpha-beta alloys may arise through dissolution of the beta phase in N_2O_4. The localized breakdown of the oxide film, and its inability to repair itself, is probably the most important factor in considering mechanisms for stress-corrosion cracking in N_2O_4.

The experiments in hot-salt environment 590K(600 F), were conducted chiefly to characterize selected materials under a broader range of hostile conditions. The tests revealed that there were major differences in cracking susceptibility due to composition. Exposures were adjusted so that each composition deformed plastically to within a specified strain range in a specified time (0.2 to 1.0 percent in ~96 hours). Under these conditions, the lower strength Ti-4Al base alloys (with and without Mo and/or V additions) were considerably less susceptible to hot-salt stress-corrosion cracking than the higher strength Ti-8Al-base materials. A marked improvement in the resistance to hot-salt stress-corrosion was observed for both Ti-4Al- and Ti-8Al-base alloys put into an acicularized microstructural condition by means of either beta fabrication or beta heat treatment.

The major emphasis of this program was directed toward the study of composition effects on salt-water stress-corrosion susceptibility and mechanisms. The aluminum content studied, 4 to 8 weight percent, proved to encompass the apparent critical aluminum content for susceptibility, ~6 weight percent, although several additional factors were observed to markedly affect the criticality of this composition. For example, an increased oxygen content can render an otherwise immue Ti-6Al-base composition susceptible. Further, the immunity or susceptibility of a Ti-4 to 8 Al-base alloy can be markedly affected by processing and/or heat treatment to (a) increase the strength level to increase susceptibility, (b) change the microstructure to decrease susceptibility (e.g., by acicularizing the structure) or to increase susceptibility (e.g., by precipitation of a large volume fraction of Ti_3Al phase).

The effect of the various beta-stabilizer contents (1 to 4 weight percent) on the susceptibility of Ti-4 to 8 Al-base alloys is not pronounced except as a given addition to a given base affects strength, and serves to control the aluminum content of the continuous alpha phase in a mixed two-phase structure. Additions of beta stabilizers to binary Ti-Al increase the yield strength at all aluminum levels, but the resistance to salt-water stress-corrosion cracking is principally determined by the aluminum content. Beta stabilizers serve to modify the aluminum concentration of the alpha phase through their effect upon the volume fraction of the beta phase. Thus, in addition to the strengthening effect of the beta stabilizers, they may also promote increasing amounts of Ti_3Al in the alpha phase leading to an increased stress-corrosion susceptibility of an otherwise marginal aluminum content alloy. Processing and heat treatment to promote various microstructures and strength levels are also factors in developing immunity or susceptibility.

The criticality of aluminum content toward susceptibility appears related to the presence of Ti_3Al and to the quantity and particle size thereof. A reasonably good correlation was found between salt-water stress-corrosion susceptibility and the presence of Ti_3Al in Ti-4 to 8 Al-1.5 Mo-0.5 V alloys as alpha-beta annealed and stabilized at 920 K (1200 F). Thermal exposures promoting Ti_3Al formation (in accordance with the alpha/alpha-Ti_3Al phase boundary in the Ti-Al system) result in alloy susceptibility without significantly altering the yield strength of compositions. The specific effect of the Ti_3Al particles was suggested to be the promotion of a nonhomogeneous planar slip character and an enhanced chemical potential of the slip bands. The experimental work has shown that the Ti_3Al particles are sheared by glide dislocations. This fragmentation of the Ti_3Al particles in the slip bands leads to a higher chemical potential of this material than for the adjacent matrix, thus favoring a sustained anodic reaction at this specimen surface site. Further, it was found that the glide dislocations in the alpha phase act as heterogeneous nucleation sites for the precipitation of hydrides and that hydrogen diffusion is sufficiently rapid so that significant hydride growth can occur during deformation at ordinary strain rates. In a Ti-8Al-1Mo-1 V alloy charged with 200-400 ppm hydrogen, hydrides were found on the $(\bar{1}100)$ slip planes in specimens deformed at room temperature.

Research initiated recently was directed at modifying the composition of the Ti-Al-alpha-base with the hope of maintaining the strength of the alpha while interrupting the formation of the Ti_3Al phase. Substitutions of gallium, indium, tin, zirconium, columbium, and tantalum were made for some of the aluminum in a Ti-7Al-base composition stabilized with 1.5 Mo and 0.5 V additions. While this investigation was terminated prior to completion, very attractive improvements in the strength/stress-corrosion susceptibility ($YS/K_{I_{scc}}$) combinations were found for the alloys with indium or columbium substitutions for some of the aluminum. Work was not progressed to the point where reasons for the improvement were shown. However, the merits of composition modification in promoting resistance to salt-water stress-corrosion cracking were indicated.

Experiments were conducted to examine the slow crack growth of Ti-4Al-base alloys which are generally considered immune to the salt-water stress-corrosion reaction. Crack growth can occur in such moderate-strength, high-toughness alloys at quite low stress intensity values but characteristically is soon arrested possibly due to relaxation of the triaxial stress pattern. Further, slow crack growth can occur in an air environment developing fracture surface characteristics (cleavage regions) identical to those considered typical of stress-corrosion cracking. This work was also terminated prior to the development of full interpretations but suggested that while titanium-subcritical-aluminum-content alloys are immune to salt-water stress-corrosion degradation in the usual tests, it is not possible to estimate the true stress-corrosion susceptibility of notch ductile materials in samples of practical thickness and that immunity per se does not in fact exist.

The studies on the effects of composition on various aspects of microstructure, susceptibility, and on the morphology of stress-corrosion cracks and crack-tip regions, together with the results obtained by other workers have been used to formulate a phenomenological model for aqueous (neutral solutions) stress-corrosion cracking of the titanium alloys included in this investigation. Pertinent observations are:

(1) There is a threshold stress intensity, $K_{I_{scc}}$, below which sub-critical crack growth does not take place. $K_{I_{scc}}$ is sensitive to the chemistry of the environment, but it is principally independent

of the temperature of the environment (over the limited range of temperatures which can be investigated). $K_{I_{scc}}$ is also dependent on alloy composition, heat treatment, and applied electrode potential. A finite plane-strain region at the crack front is required for subcritical cracking to proceed; hence, in thin sections, $K_{I_{scc}}$ increases rapidly with decreasing specimen thickness.

(2) The subcritical crack velocities are usually very high (10^{-3}-10^{-2} in./sec).

(3) The subcritical crack velocity is initially dependent on the applied stress intensity, but at higher stress intensities the crack velocity approaches a constant value which is independent of stress intensity.

(4) During subcritical cracking the cracks follow a predominantly transgranular path. At high stress intensities the main crack front is branched, and consists of numerous long (~0.030 inch), narrow (~0.002 inch), exceedingly straight transgranular cracks.

(5) The fracture surfaces resulting from subcritical crack growth contain a high density of cleavage facets. By contrast, areas of rapid fracture have the "dimpled" appearance characteristic of ductile rupture.

Embrittlement is most probably related to a hydrogen generating reaction at the slip bands at the specimen-electrolyte interface and its transport path to the crack tip may be through the electrolyte, along the crack surface, or through the bulk of the metal. Once there, hydrides form and these nucleate cleavage cracks in the plane-strain region ahead of the crack tip where the tensile stress is highest. The hydrides raise the stress required to create and move dislocations in the plane-strain plastic zone, and hence raise the maximum tensile stress above the intrinsic cleavage strength of the material.

INTRODUCTION TO THE CURRENT WORK

The objectives of this program were to further the understanding of the effects of composition on the mechanism of stress corrosion cracking in titanium alloys. Work summarized in this report was conducted during the period from June 11, 1971, through June 10, 1972. The studies described are, in several cases, continuations of work started in earlier portions of this program which was initiated in February, 1967. Our earlier studies are described in a series of three summary reports issued during the course of the investigation.[1,2,3]

For maximum clarity of presentation, the several separate investigations conducted during the past year are described independently. The interrelationships of these separate investigations, their contribution to the overall program objectives, and the conclusions resulting from the investigations are presented in each section.

Although all measurements in this report are given in U. S. and S. I. units, customary U. S. units were used in making the various measurements. Conversion factors are listed in the Appendix.

EFFECTS OF ALLOY COMPOSITION ON SALTWATER STRESS CORROSION

In previous studies, we have examined the effects of aluminum content, oxygen content, and the composition and amount of beta phase on the saltwater stress corrosion susceptibility of aluminum-strengthened alpha-beta titanium alloys.[1-3] These earlier studies showed susceptibility to saltwater stress corrosion to increase markedly when aluminum content exceeded about 6 weight percent. This behavior has been attributed to the presence of Ti_3Al precipitates by other investigators.[4] The present investigation was designed to determine the effects of replacing portions of the aluminum in alloys of this type with alternate alpha strengtheners. Alpha strengtheners examined included tin, gallium, indium, zirconium, columbium, and tantalum. The first four additions are conventional alpha strengtheners, although less effective than aluminum on a weight percent basis. Equivalent strengthening ability in weight percent was considered to be approximately as follows: 1 Al = 3 Sn = 3 Ga = 3 In = 5 Zr.[5,6] Columbium and tantalum, although actually beta stabilizers, show appreciable alpha solubility in binary titanium alloys (5 weight percent columbium and 15 weight percent tantalum, respectively).[7,8] Alpha soluble additions of beta stabilizer elements have been shown to strengthen titanium by approximately 70 to 140 MN/m^2 (10 to 20 ksi).[9]

Six compositions were selected for study, all of which may be considered modifications of the Ti-7Al-1.5Mo-0.5V alpha-beta alloy examined extensively in prior work. These six compositions were:

Ti-5Al-6Sn-1.5Mo-0.5V
Ti-5Al-6Ga-1.5Mo-0.5V
Ti-5Al-6In-1.5Mo-0.5V
Ti-5Al-10Zr-1.5Mo-0.5V
Ti-6Al-5Ta-1.5Mo-0.5V
Ti-6Al-3Cb-1.5Mo-0.5V

These alloys were evaluated to determine tensile properties and saltwater stress corrosion behavior after selected heat treatments. The results of these evaluations were then compared with the results of earlier investigations of the

Ti-7Al-1.5Mo-0.5V alloy, and of other alloys of similar composition, to determine whether partial replacement of aluminum in alpha-beta alloys of this type was advantageous for improving resistance to stress corrosion.

Materials Preparation

Six 5.4 kilogram (12 pound) ingots were purchased from TMCA for this investigation. The composition of these ingots is given in Table 1. The six ingots were press forged from 10.4 cm (4.1 inch) diameter to 5.6 to 6.1 cm (2.2 to 2.4 inch) thick plate at 1420 K (2100 F). The plate surfaces were ground to remove approximately 2.5 mm (0.1 inch) to eliminate surface contamination and forging defects. The plates were then reduced by hot rolling to provide material at both 0.64 cm (0.25 inch) and 0.32 cm (0.125 inch) thickness. Hot rolling schedules for the six alloys are summarized in Table 2.

Samples cut from the hot rolled sheet were annealed at selected temperatures, quenched, and examined metallographically to determine the beta transus temperature. A standard microstructural condition was then developed in these alloys by alpha-beta annealing at approximately 28 K (50 F) below the beta transus (in argon), furnace cooling to 920 K (1200 F) and stabilizing the structure by annealing for 3 hours at this temperature. Alpha-beta annealing temperatures were as follows:

Ti-5Al-6Sn-1.5Mo-0.5V	1225 K (1730 F)
Ti-5Al-6Ga-1.5Mo-0.5V	1225 K (1730 F)
Ti-5Al-6In-1.5Mo-0.5V	1205 K (1710 F)
Ti-5Al-10Zr-1.5Mo-0.5V	1180 K (1660 F)
Ti-6Al-5Ta-1.5Mo-0.5V	1225 K (1730 F)
Ti-6Al-3Cb-1.5Mo-0.5V	1225 K (1730 F)

Stabilization annealing was conducted in two stages. First stage: 1 hour in argon after alpha-beta annealing, followed by furnace cooling to 920 K (1200 F) at 38 K (100 F)/hour, holding 1 hour at 920 K (1200 F) followed by air cooling and surface conditioning. Second stage: 2 hours at 920 K (1200 F) in vacuum followed by furnace cooling to control hydrogen content. Cooling rate following vacuum annealing was fairly low.

TABLE 1. COMPOSITION OF EXPERIMENTAL TITANIUM ALLOYS

Alloy No.	Nominal Composition	Ingot Analysis Reported by TMCA, weight percent						Interstitial Analysis at Battelle, ppm(b)		
		Al	Mo	V	O	N	Other(a)			
V-4621	Ti-5Al-6Sn-1.5Mo-0.5V	4.92	1.59	0.57	0.122	0.004	5.59 Sn	1300	63	43
V-4622	Ti-5Al-6Ga-1.5Mo-0.5V	4.92	1.50	0.60	0.131	0.007	6.10 Ga	1310	26	39
V-4623	Ti-5Al-6In-1.5Mo-0.5V	4.85	1.52	0.56	0.096	0.005	5.40 In	--	--	--
V-4624	Ti-5Al-10Zr-1.5Mo-0.5V	4.78	1.62	0.58	0.130	0.007	9.88 Zr	1360	78	33
V-4625	Ti-6Al-5Ta-1.5Mo-0.5V	6.22	1.73	0.57	0.100	0.003	4.92 Ta	--	--	--
V-4626	Ti-6Al-3Cb-1.5Mo-0.5V	6.18	1.74	0.53	0.112	0.003	3.00 Cb	--	--	--

(a) In addition, the average iron content was 0.086 percent (range 0.078 to 0.102 percent).

(b) As determined following fabrication and heat treatment (alpha-beta anneal plus stabilization).

TABLE 2. FABRICATION SCHEDULE FOR TITANIUM ALLOYS

Composition[a] weight percent	1420 K (2100 F) Press Forging[b] Thickness, cm(in.)	Rating	Cross Rolling to 18-cm(~7.1 in.)Width Temp,K(F)	Thickness, cm(in.)	Direct Rolling Temp, K(F) To 1.3 cm (~0.5 In.)[c] Thick	To 0.64 cm (~0.25 In.)[d] Thick	To 0.32 cm (~0.125 In.) Thick	Fabrication Rating
Ti-5Al-6Sn-1.5Mo-0.5V	5.9 (2.32)	Good	1230(1750)	3.8(~1.5)	1180-1200(1660-1700)	1180(1660)	1165(1640)	Good
Ti-5Al-6Ga-1.5Mo-0.5V	6.1 (2.40)	Good	1230(1750)	4.2(1.65)	1180-1230(1660-1750)	1180(1660)	1165(1640)	Good to Fair[e]
Ti-5Al-6In-1.5Mo-0.5V	5.9 (2.32)	Good	1230(1750)	3.8(~1.5)	1180-1200(1660-1700)	1180(1660)	1165(1640)	Good
Ti-5Al-10Zr-1.5Mo-0.5V	5.6 (2.20)	Good	1200-1230 (1700-1750)	3.2(1.26)	1180-1200(1660-1700)	1180(1660)	1165(1640)	Good
Ti-6Al-5Ta-1.5Mo-0.5V	5.9 (2.32)	Good	1200-1230 (1700-1750)	3.2(1.26)	1180-1200(1660-1700)	1180(1660)	1165(1640)	Good
Ti-6Al-3Cb-1.5Mo-0.5V	5.6 (2.20)	Good	1200-1230 (1700-1750)	3.2(1.26)	1180-1200(1660-1700)	1180(1660)	1165(1640)	Good

(a) 0.10 percent nominal oxygen

(b) Draw-down-type forging (not upset).

(c) All material subsequently rolled to 1.3-cm (~0.5 in.) thickness with appropriate intermediate conditioning.

(d) One-third length of 0.64-cm (~0.25 in.) thick plates subsequently rolled to 0.32-cm (~0.125 in.) sheet.

(e) Many edge cracks. Balance was good material.

The alpha-beta anneal plus stabilization heat treatment was similar to that used in prior work and developed a fine equiaxed alpha grain structure with beta distributed in a discontinuous fashion at grain boundaries and triple points. Representative microstructures are shown in Figure 1.

Material Evaluation

The measurement of tensile properties and saltwater stress corrosion susceptibility was conducted using procedures followed in prior work. Tensile samples were cut from the 0.32 mm (0.125 inch) rolled sheet with the stress axis parallel to the transverse direction. Sheet-type samples were prepared having a 0.76 cm (0.3 inch) wide by 3.81 cm (1.5 inch) long reduced section and tested at a strain rate of 0.051 cm/minute (0.02 inch/minute). Stress-corrosion measurements were made using fatigue precracked cantilever bend samples cut from 0.64 cm (0.25 inch) plate with the crack propagating along the rolling direction (WR). Specimens were precracked by fatiguing in air for 20,000 to 50,000 cycles at stress levels sufficient to produce a 0.38 cm (0.15-inch) crack with a minimum of plastic deformation. Both step-loaded and static-loaded tests were run. Step-loaded tests were performed in air as well as in 3-1/2 percent NaCl solution. The air tests consisted of step loading at 2 to 5 minute intervals until failure occurred. The same procedure was also used to determine an initial K_{scc} value (salt-water environment). Constant load tests were subsequently performed in salt water at lower loads for a maximum exposure time of 6 hours.

Results

The tensile properties of the six alpha modified alloys are given in Table 3 along with data for the Ti-7Al-1.5Mo-0.5V alloy. All six alpha modified alloys were significantly stronger than Ti-7Al-1.5Mo-0.5V. It appears that equivalent strength conditions could have been obtained with lesser amounts of auxiliary alpha strengtheners. Two of the alloys, Ti-5Al-6Sn-1.5Mo-0.5V and Ti-5Al-6Ga-1.5Mo-0.5V, showed considerably higher strength and were also noticeably less ductile. The remaining four alloys, although up to 70 MN/m^2 (10 ksi) stronger, had approximately equivalent ductilities.

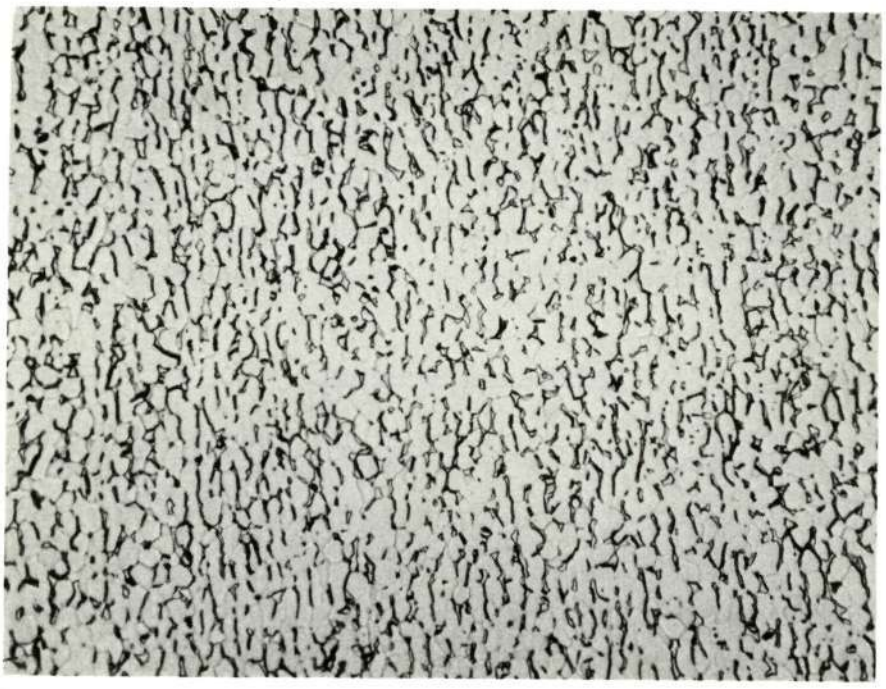

500X 1G808

a. Ti-5Al-6In-1.5Mo-0.5V

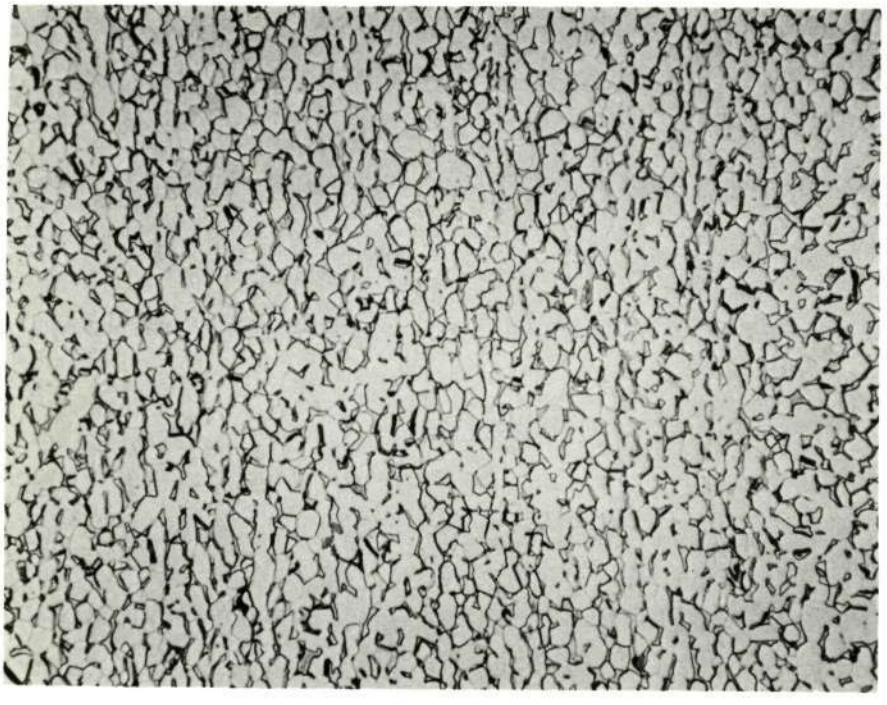

500X 1G809

b. Ti-6Al-3Cb-1.5Mo-0.5V

FIGURE 1. MICROSTRUCTURE DEVELOPED IN EXPERIMENT
BY ALPHA-BETA ANNEALING AND STABI

TABLE 3. TENSILE PROPERTIES OF TITANIUM ALLOYS AS ALPHA-BETA ANNEALED AND STABILIZED

Alloy Composition	Ultimate Tensile Strength, MN/m^2 (Ksi)	Yield Tensile Strength, MN/m^2 (Ksi)	Elongation, percent	Reduction in Area, percent
Ti-5Al-6Sn-1.5Mo-0.5V	1127 (163.6)	1053 (152.9)	9[a]	12
	1085 (157.5)	1030 (149.5)	8[a]	11
Ti-5Al-6Ga-1.5Mo-0.5V	1175 (170.7)	1141 (165.6)	6	7
	1162 (168.7	1130 (164.1	6[a]	7
Ti-5Al-6In-1.5Mo-0.5V	1017 (147.6)	932 (135.3)	18	36
	1018 (147.7)	935 (135.8)	18	34
Ti-5Al-10Zr-1.5Mo-0.5V	1019 (147.8)	1007 (146.2)	18	28
	1002 (145.6)	998 (144.9)	17	28
Ti-6Al-5Ta-1.5Mo-0.5V	998 (143.5)	922 (134.1)	12[a]	21
	976 (141.6)	907 (131.7)	17	31
Ti-6Al-3Cb-1.5Mo-0.5V	960 (139.3)	905 (131.4)	8[a]	23
	979 (142.2)	920 (133.6)	15	27
Ti-7Al-1.5Mo-0.5V[b]	938 (136.1)	852 (123.6)	15	29
	927 (134.5)	838 (121.7)	15	31

(a) Sample broke on gage mark.

(b) From Reference (2), Alloy No. 977, page 6.

The results of saltwater stress corrosion exposure of this series of alloys is shown in Table 4. It is seen that both indium and tantalum substitutions for aluminum produced moderate improvements in stress corrosion resistance while columbium nearly doubled the value of $K_{I_{scc}}$. These trends are especially interesting in view of the improvements in yield strength resulting from alpha-modification. Zirconium modification did not improve stress corrosion resistance in an absolute manner, but it should be noted that the zirconium containing alloy although of equal stress corrosion resistance was stronger than Ti-7Al-1.5Mo-0.5V. Zirconium modification might appear more attractive at an equivalent strength level. Neither tin nor gallium modification appeared attractive from a stress-corrosion standpoint, even when noting the large strength improvement resulting from their use.

The data for Ti-7Al-1.5Mo-0.5V alloy included in Table 4 were obtained using 0.32 cm (0.125 inch) instead of 0.64 cm (0.25-inch) samples. Although the size factor should not affect the measured value of $K_{I_{scc}}$, it probably accounts for the high fracture stress intensity in air observed relative to the other alloys in this table since sample thickness has an effect on air toughness measurements. (See Reference 3, pp 9-11)

It was considered possible that the high strength and low stress corrosion resistance of tin and gallium containing alloys might be related to increased Ti_3Al or omega reaction caused by an alloying effect on reaction kinetics. If so, more rapid cooling following stabilization at 920 K (1200 F) or rapid cooling from a higher stabilization temperature would be expected to reduce strength and improve stress corrosion properties. Hardness measurements (Rockwell C scale) were made on samples from all six alloys after heat treatments involving reannealing for 2 hours at either 920 K or 1055 K (1200 F or 1400 F) followed by water quenching. The effects of these treatments on hardness are shown in Table 5. These data indicate that heat treatment does not have a strong effect on hardness. Since ultimate strength and hardness are closely related, the heat treatments of the type examined would not be expected to affect strength. However, heat treatment might affect stress-corrosion resistance or tensile ductility without affecting strength. To examine this possibility, three alloys were evaluated after reannealing for 2 hours at 1055 K (1400 F) and water quenching. Tensile properties are shown in Table 6. A comparison with

TABLE 4. SALTWATER STRESS CORROSION SUSCEPTIBILITY OF TITANIUM ALLOYS AS ALPHA BETA ANNEALED AND STABILIZED

Composition	Environment	Loading Method	Stress Intensity,[a] $MN/m^{3/2}$ (Ksi $\sqrt{in}$)	Time to Failure, minutes
Ti-5Al-6Sn-1.5Mo-0.5V	Air	Step	32.2 (29.3)	
	Salt water	"	20.7 (18.8)	-
	"	Constant	16.5 (15)	2
	"	"	11.0 (10)	> 360[b]
Ti-5Al-6Ga-1.5Mo-0.5V	Air	Step	22.6 (20.5)	-
	Salt water	"	12.8 (11.6)	-
	"	Constant	7.7 (7)	> 360[b]
Ti-5Al-6In-1.5Mo-0.5V	Air	Step	61.4 (55.8)	-
	Salt water	"	33.9 (30.8)	-
	"	Constant	31.9 (29)	30
	"	"	28.6 (26)	> 360[b]
Ti-5Al-10Zr-1.5Mo-0.5V	Air	Step	77.1 (70.1)	-
	Salt water	"	25.1 (22.8)	-
	"	Constant	24.2 (22)	4
	"	"	22.0 (20)	> 360[b]
Ti-6Al-5Ta-1.5Mo-0.5V	Air	Step	69.5 (63.2)	-
	Salt water	"	39.9 (36.3)	-
	"	Constant	35.2 (32)	3
	"	"	30.8 (28)	> 360[b]
Ti-6Al-3Cb-1.5Mo-0.5V	Air	Step	77.3 (70.3)	-
	Salt water	"	52.7 (47.9)	-
	"	Constant	49.5 (45)	2
	"	"	44.0 (40)	> 360[b]
Ti-7Al-1.5Mo-0.5V[c]	Air	Step	92.4 (84.0)	-
	Salt water	"	26.6 (24.2)	-
	"	Constant	23.8 (21.6)	5
	"	"	20.8 (18.9)	> 360[b]

(a) Plane strain loading can be obtained in 0.64 cm (0.25 inch) thick samples with yield strengths of 930 MN/m^2 (135 Ksi) at stress intensities up to about 47 $MN/m^{3/2}$ (43 Ksi $\sqrt{in}$)[10].

(b) Test stopped before failure.

(c) This alloy tested using 0.32 cm (0.125 inch) thick samples. Data from Reference 2, Alloy No. 977, page 9.

TABLE 5. ROCKWELL C HARDNESS OF HEAT TREATED TITANIUM ALLOYS

Alloy Composition	Original Treatment (Alpha-Beta Anneal Plus Stabilized at 920 K (1200 F)	2 Hours at 920 K (1200 F), Water Quench	2 Hours at 1055 K (1400 F) Water Quench
Ti-5Al-6Sn-1.5Mo-0.5V	33	33	33
Ti-5Al-6Ga-1.5Mo-0.5V	37	35	36
Ti-5Al-6In-1.5Mo-0.5V	30	28	30
Ti-5Al-10Zr-1.5Mo-0.5V	32	31	32
Ti-6Al-5Ta-1.5Mo-0.5V	30	29	30
Ti-6Al-3Cb-1.5Mo-0.5V	29	29	29

TABLE 6. TENSILE PROPERTIES OF THREE ALLOYS AS QUENCHED FROM 1055 K (1400 F)

Alloy Composition	Ultimate Tensile Strength, MN/m^2(Ksi)	Yield Tensile Strength, MN/m^2(Ksi)	Elongation percent	Reduction in Area, percent
Ti-5Al-6Sn-1.5Mo-0.5V	1092 (158.6)	1006 (146.1)	16	24
Ti-5Al-6Ga-1.5Mo-0.5V	1182 (171.7)	1080 (156.8)	13(a)	16
Ti-5Al-6In-1.5Mo-0.5V	989 (143.6)	904 (131.3)	16	27

(a) Broke on gage mark.

the data given in Table 3 shows, as expected, that this heat treatment had little effect on ultimate strength. However, yield strength was reduced somewhat in all three alloys, most significantly in the gallium containing alloy. Moreover, the ductility of both the tin and gallium containing alloys appeared to be improved.

Stress corrosion resistance of the tin and gallium containing alloys was improved only a small amount by the 1055 K (1400 F) heat treatment as shown in Table 7. The indium-containing alloy showed a major improvement in stress corrosion resistance, the value of $K_{I_{scc}}$ increasing from about 31 $MN/m^{3/2}$ (28 ksi $\sqrt{in.}$) as stabilized at 920K (1200 F) to above 50 $MN/m^{3/2}$ (45 ksi $\sqrt{in.}$) as quenched from 1055K (1400 F). These results show the marked sensitivity of these alloys to microstructural factors. Quite possibly, suitable heat treatments would also improve the stress corrosion resistance of Ti-7Al-1.5Mo-0.5V.

Discussion

The critical stress intensity for crack propagation in salt water ($K_{I_{scc}}$) is plotted versus yield strength for alpha-modified alloys in Figure 2. Also included are data for unmodified Ti-(6.5 to 8Al)-(0.5 to 0.2) O_2-1.5Mo-0.5V alloys from earlier work to provide a basis for comparison. It is seen that there is a trend for $K_{I_{scc}}$ to decrease as yield strength increases. In general, the modified alloys appeared to show yield strength -$K_{I_{scc}}$ relationships similar to the behavior of unmodified Ti-Al-Mo-V alloys, although on the high side of the scatter band. Two of the alloys appeared to be significantly improved, however, Ti-6Al-3Cb-1.5Mo-0.5V as alpha-beta annealed and stabilized at 920K (1200 F) and Ti-5Al-6In-1.5Mo-0.5V as reannealed at 1055K (1400 F) and quenched.

As mentioned previously, the superior stress corrosion resistance of the indium-containing alloy seems most likely related to a change in microstructural configuration resulting from heat treatment at 1055K (1400 F). All three alloys reannealed and quenched from 1055K (1400 F) showed some improvement in yield strength -$K_{I_{scc}}$ characteristics and it seems possible that the Ti-Al-Mo-V alloys would be similarly improved, perhaps to the same extent as the indium alloy. The improvements are possibly due to reduced Ti_3Al formation by quenching from the higher temperature.

TABLE 7. SALTWATER STRESS CORROSION SUSCEPTIBILITY OF THREE ALLOYS AS QUENCHED FROM 1055K (1400 F)

	Environment	Loading Method	$MN/m^{3/2}$ (Ksi $\sqrt{in}$)	Time to Failure, hours
Ti-5Al-6Sn-1.5Mo-0.5V	Air	Step	42.8 (38.9)	-
	Salt water	"	24.5 (22.4	-
	"	Constant	23.1 (21)	6
	"	"	19.8 (18)	> 360(a)
Ti-5Al-6Ga-1.5Mo-0.5V	Air	Step	42.1 (38.3)	-
	Salt water	"	20.2 (18.4)	-
	"	Constant	18.7 (17)	3
	"	"	15.4 (14)	> 360(a)
Ti-5Al-6In-1.5Mo-0.5V	Air	Step	66.2 (60.2)	-
	Salt water	"	58.0 (52.8)	-
	"	Constant	55.0 (50)	2
	"	"	49.5 (45)	> 360(a)

(a) Sample removed from test before failure.

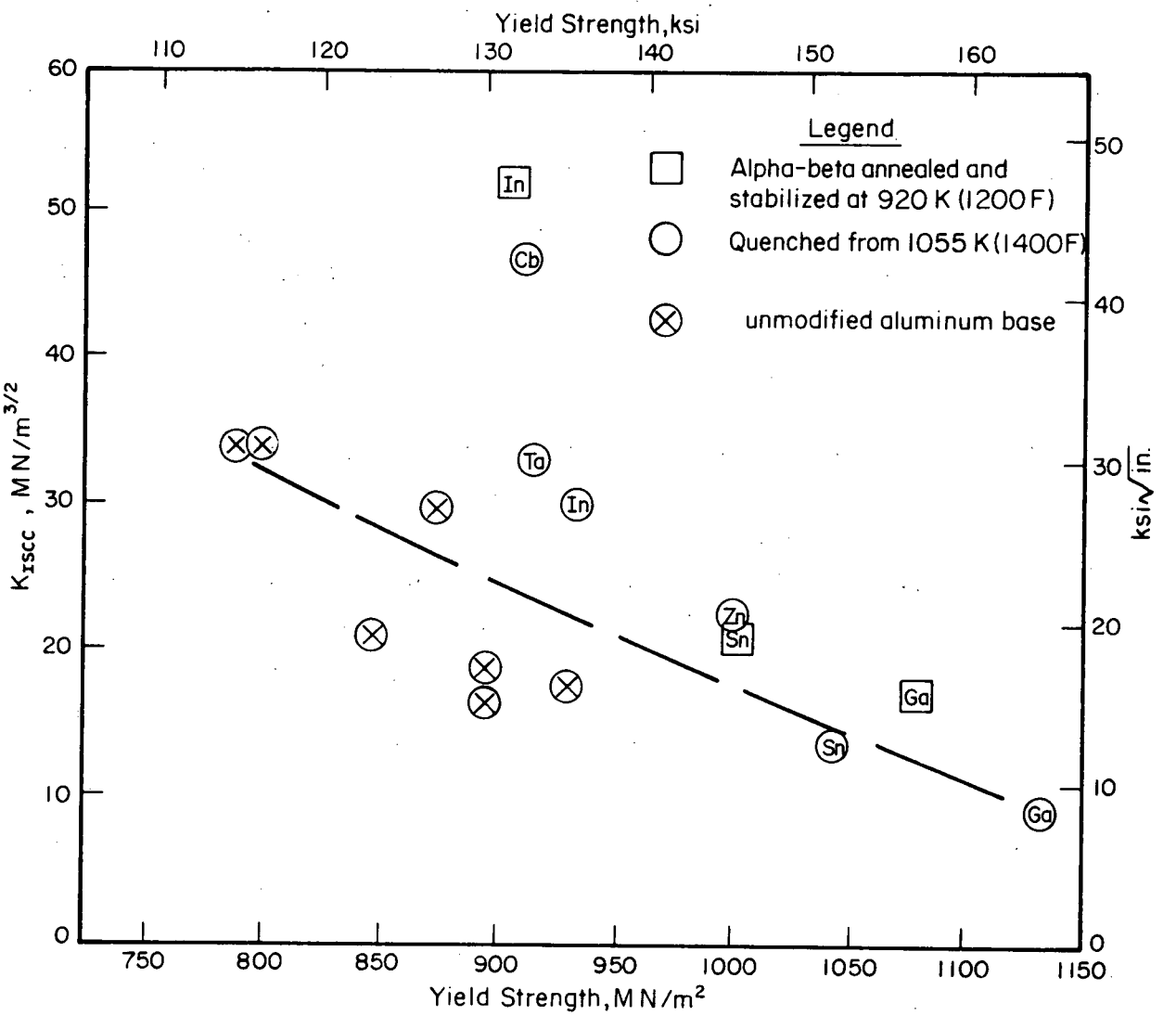

FIGURE 2. STRENGTH-TOUGHNESS CORRELATION FROM SERIES OF Ti-Al-(Sn, Ga, In, Zr, Cb, Ta)-1.5Mo-0.5V ALLOYS

It is possible that the beneficial effects of columbium modification may also represent an effect of columbium on microstructure, perhaps a retardation in Ti_3Al precipitation rates or a reduction in the Ti_3Al solvus temperature. If so, stabilization at a lower temperature or prolonged exposure to moderately high service temperatures may reduce $K_{I_{scc}}$ in the Ti-Al-Cb-Mo-V alloy. The beneficial effects of columbium on the saltwater stress corrosion behavior have been mentioned by previous investigators.[4,11] In these investigations, also, alloying effects were evaluated after similar heat treatments.

The ability of certain alloying additions (eg. indium or columbium) to introduce improved resistance to stress corrosion in aluminum-containing alpha-beta alloys might be attributed to at least two causes other than an intrinsic improvement in stress corrosion resistance. First, alloying may retard Ti_3Al precipitation such that a modified alloy appears superior after a selected heat treatment. If this is the origin of the improved stress corrosion behavior, changes in the heat treatment or fabrication procedures could be made which would alter the effectiveness of the alloy modification if an intrinsic improvement was not real. Second, alloying may reduce the room temperature creep resistance of the alloy, although having no effect on yield strength, leading to crack blunting or general yielding behavior at lower stress intensities, thus making it difficult to conduct a valid measurement of $K_{I_{scc}}$. In this case, modified test procedures may show the alloying benefits to be less attractive than shown by the currently available data. Regardless of the origin of the effect, alloy modification with columbium or indium can be considered beneficial to stress corrosion resistance based on the results of this study.

Conclusions

This investigation of the effects of replacing a portion of the aluminum content in the alpha-beta alloy Ti-7Al-1.5Mo-0.5V with alternate alpha strengtheners has shown the following:

(1) The four alpha stabilizing additions, tin, gallium, indium, and zirconium, which are capable of producing an equivalent strength level in replacing aluminum in

ternary alpha titanium alloys in the ratio (weight percent) of 1Al = 3Sn = 3Ga = 3In = 5Zr are more effective than that in an alpha-beta alloy of the type examined. Replacing 2 percent aluminum with 6 percent tin and gallium resulted in an appreciably greater strength increase than anticipated, while similar replacement with 6 percent indium or 10 percent zirconium resulted in a modest strength increase.

(2) The yield strength -$K_{I_{scc}}$ properties of the modified alloys occupy a position on the high side of the normal scatter band expected for yield strength -$K_{I_{scc}}$ measurement.

(3) Heat treatment of the gallium and tin containing alloys for 2 hours at 1055 K (1400 F) and water quenching, resulted in increased $K_{I_{scc}}$ with a slight reduction in yield strength. The indium-containing alloy, on the other hand, showed a dramatic improvement in $K_{I_{scc}}$ as a result of that treatment. $K_{I_{scc}}$ was doubled with only slight reduction in yield strength.

(4) Replacement of 1 percent aluminum by alpha soluble amounts of beta stabilizers, 5 percent tantalum or 3 percent columbium, resulted in an increased yield strength which is probably related to the alpha soluble portion of the addition since the amount of beta phase was not altered greatly by alloying. The critical stress intensity for saltwater stress corrosion of the columbium-modified alloy was nearly double that of the Ti-7Al-1.5Mo-0.5V alloy while the tantalum modified alloy was only slightly superior to the unmodified alloy.

SUBCRITICAL CRACK GROWTH IN TWO TITANIUM ALLOYS

During the past several years, a number of investigations of the stress corrosion behavior of titanium alloys in salt water have been conducted using fatigue precracked samples following the method originally outlined by Brown.[12] Several of these studies have indicated that susceptibility to stress corrosion is quite sensitive to aluminum content, and that alloys with less than about 5 percent aluminum are relatively immune to saltwater stress corrosion.[4,11,13,14] One of the criticisms common to all of these studies is that there has generally been a failure to maintain plane strain loading at the crack front during determination of the critical stress intensity for crack propagation in salt water (K_{Iscc}). Crack growth in a corrosive environment might occur only under plane strain loading as pointed out by Brown.[15] The basis for such an observation can be rationalized by assuming that stress corrosion requires the development of a critical normal stress in the crack vicinity which exceeds the uniaxial yield strength of the alloy such that crack growth will only be observed under conditions of triaxial loading where elastic stresses appreciably higher than the yield strength can be imposed.

The development of plane strain conditions at the crack front is a function of applied stress, yield strength of the alloy, and sample configuration. Assuming proper sample design, plane strain conditions are usually assumed to predominate when applied stress intensity (K_i), yield strength (Y), and sample thickness (B) meet the following criterion:[10]

$$B \geq 2.5\left(\frac{K_i}{Y}\right)^2 \text{, that is, } \frac{1}{B}\left(\frac{K_i}{Y}\right)^2 \leq 0.4.$$

This relationship shows that plane strain conditions at the crack front are favored by increased sample thickness, increased yield strength, or decreased applied stress intensity.

Effects of sample thickness on measurements of stress corrosion susceptibility have been reported.[16,17] An alloy which is susceptible to saltwater stress corrosion when examined using a thick sample may appear relatively immune when the sample thickness is sufficiently reduced. Less

consideration has been given to the fact that the above relationship indicates that decreased yield strength or increased critical stress intensity for crack propagation could result in a similar transition behavior when evaluating a series of alloys of varying properties using a sample of constant thickness. Yield strength (Y) and $K_{I_{scc}}$ (K_i) changes can alter the stress mode as effectively as sample thickness (B) to result in apparent changes in susceptibility behavior of alloys.

Stress corrosion susceptibility behavior from relatively immune to susceptible behavior was shown to be related to aluminum content in the alpha-beta alloys examined in prior work as shown in Figure 3.[3,14] These data were obtained with a series of Ti-Al-base alloys using 0.32-cm-(0.125-inch) thick samples. Also shown in Figure 3 is the maximum value of stress intensity which it is possible to apply to these samples while maintaining predominantly plane strain loading according to the validity criterion. Apparently stress corrosion susceptibility transition effects are highly dependent on aluminum content as well as on plane strain loading. However, the reported effect of aluminum content on stress corrosion susceptibility could be related to a change in the stress mode brought about by a reduction in yield strength and increase in $K_{I_{scc}}$ accompanying a decrease in aluminum content. A gradual change in properties accompanying the change in aluminum content could lead to an abrupt change in stress corrosion susceptibility when measuring $K_{I_{scc}}$ with samples of constant thickness.

An experiment was conceived whereby the stress corrosion susceptibility of thin specimens of low aluminum content alloys might be determined. The concept considered that upon initially loading a specimen too thin to meet ordinary validity criterion, a condition approaching plane strain might exist at the mid-section of the crack front. Even though the yielding behavior in such thin specimens is such that plastic flow in the thickness direction leads to relaxation of the initial stress triaxiality at the crack front, it is reasonable to assume that this takes place incrementally from specimen surface to center so that specimen centers are triaxially loaded moreso than specimen surface sections. Thus a stress corrosion crack advance might occur after

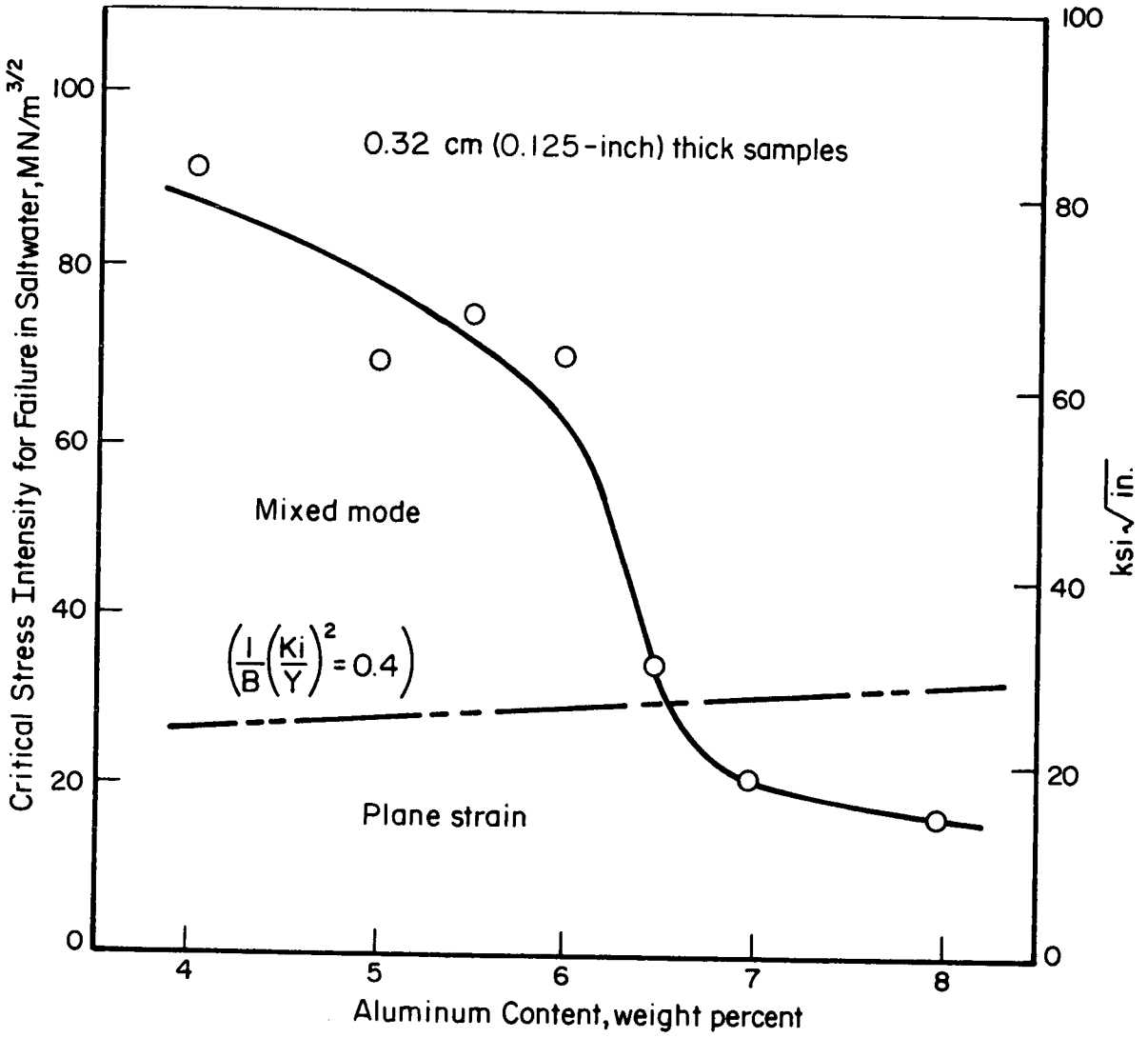

FIGURE 3. EFFECT OF ALUMINUM CONTENT ON THE MEASURED VALUE OF K_{Iscc} IN A SERIES OF Ti-Al-1.5Mo-0.5V ALLOYS(3,14)

loading under conditions approaching plain strain at the mid-section of the specimen. Such preferential crack growth at the mid-section of the specimen effectively thins the specimen. Consequently, none of the specimen would remain under plane strain load after mid-section crack growth and crack arrest might occur before any extension of the crack into the surface sections. Since cracking of this type would be confined to the interior of specimens, it is hereinafter referred to as internal cracking. Examination of statically loaded samples exposed under stress corrosion conditions for evidence of internal crack growth might provide an estimate of K_{Iscc} to be made using samples of inadequate thickness for valid measurement of K_{Iscc} using a failure criterion. The present study was conducted to determine if internal cracking does indeed take place in thin samples, to discover how to accurately measure the extent of internal cracking, and to evaluate the usefulness of this technique for measuring K_{Iscc}.

Experimental Procedure

Two titanium-4 percent aluminum alloys, Ti-4Al-1.5Mo-0.5V and Ti-4Al-3Mo-1V, prepared during earlier studies of compositional effects,[1] were used in the present investigation. The properties of these alloys, which were annealed in the alpha-beta field and then stabilized at 920 K (1200 F) are shown in Table 8. The yield strengths of these alloys were such that valid determinations* of $K_{I_{scc}}$ with samples as thin as 0.6 cm (0.25 inch) might not be expected unless $K_{I_{scc}}$ was as low as the calculated $K_{I_{scc}}$ values shown below:

	Yield Strength	Maximum Measurable $K_{I_{scc}}$**	
	MN/m^2 (Ksi)	$MN/m^{3/2}$	(Ksi $\sqrt{in.}$)
Ti-4Al-1.5Mo-0.5V	703 (102)	35	(32)
Ti-4Al-3Mo-1V	785 (114)	40	(36)

* That is, for predominantly plane strain loading.

** From the relationship $B \geq 2.5 \left(\frac{K_i}{Y}\right)^2$.

TABLE 8. PROPERTIES OF TWO TITANIUM-BASE ALLOYS

	Ti-4Al-1.5Mo-0.5V		Ti-4Al-3Mo-1V	
Tensile Properties				
Ultimate Strength, MN/m^2 (Ksi)	744	(108)	820	(119)
0.2 Percent Offset Yield Strength, MN/m^2 (Ksi)	702	(102)	785	(114)
Elogation in 2 inches, percent	20		16	
Reduction in Area, percent	36		46	
Fracture Toughness in Air, $MN/m^{3/2}$ (Ksi $\sqrt{in.}$)[a]	101	(92)	104	(95)
Apparent Value of K_{Iscc}, $MN/m^{3/2}$ (Ksi $\sqrt{in}$)[b]	91	(83)	97	(88)

(a) As measured using precracked cantilever samples 0.32 cm (0.125 inch) thick step loaded to failure in air.

(b) Critical stress intensity for failure of precracked cantilever samples 0.32 cm (0.125 inch) thick statically loaded for up to 6 hours in salt water.

Cantilever bend samples (WR orientation) having dimensions of 0.64 cm (0.25 in) by 2.54 cm (1 inch) were machined and fatigue cracked according to procedures described elsewhere.[1,2,3] These samples were statically loaded for periods of time up to 10,000 minutes in either air or 3.5 percent NaCl solution (pH of 6.2 - 6.4).

Three methods were used to examine the alloys for evidence of internal crack growth during static loading. In the first, a dial gage was attached to the lever arm which applied the bending load, and periodic measurements of arm deflection were made. Three distinctive types of arm deflection versus time curves were observed as shown in Figure 4. The first curve (Type 1) was the result of exhaustion creep, with no crack movement. In this case, a linear relationship was obtained when plotting lever arm deflection versus

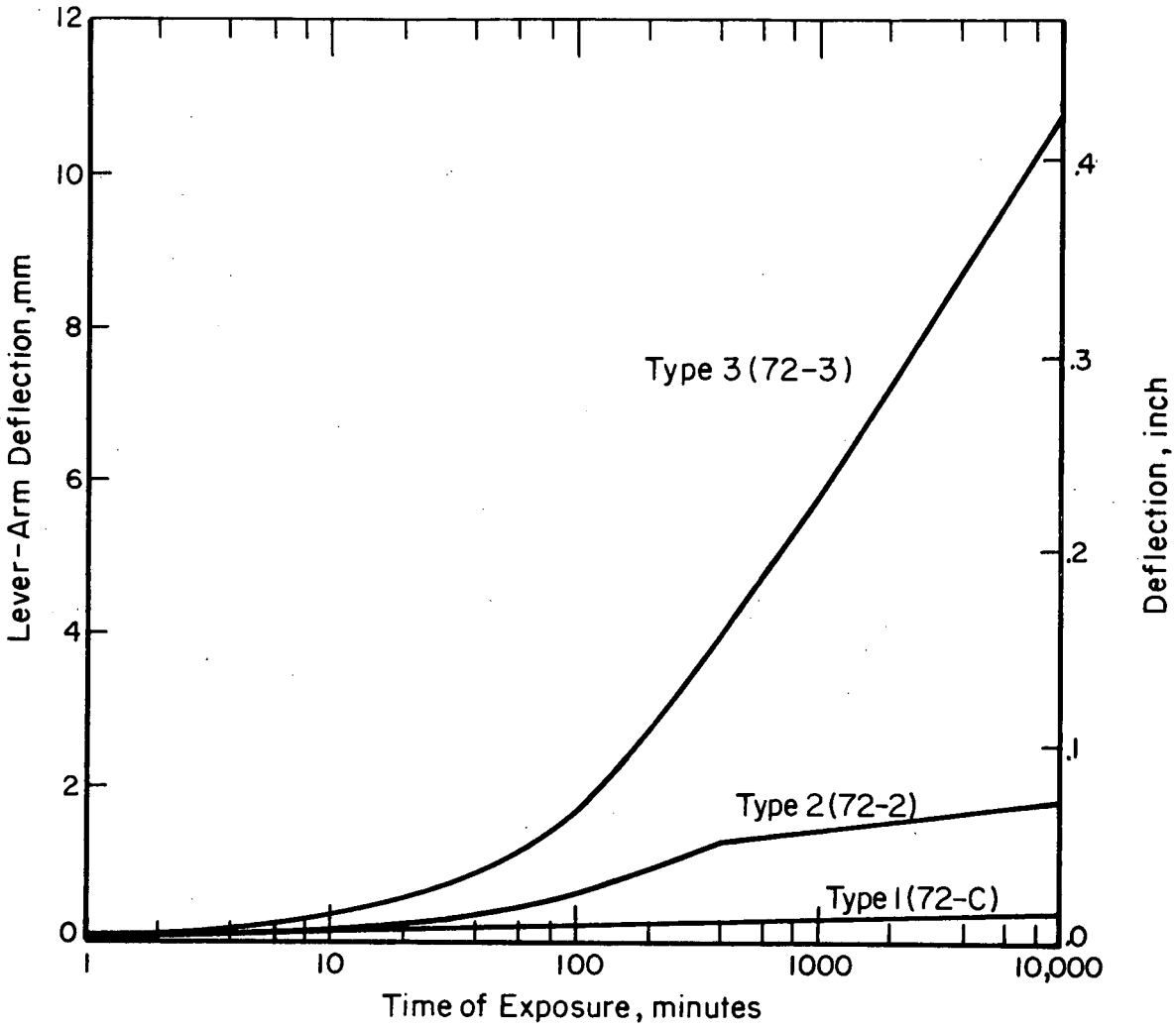

FIGURE 4. LEVER-ARM DEFLECTION AS A FUNCTION OF TIME DURING STATIC LOADING OF THREE TITANIUM ALLOY SAMPLES

Numbers in parentheses identify samples; see Table 9.

log time. The second curve (Type 2) was the result of crack growth followed by crack arrest. After an initial short linear region in which only creep processes were apparently active, the rate of arm deflection began to increase, which was attributed to crack growth. After a variable time period, crack arrest appeared to occur, and a return to linear behavior was observed, suggesting that subsequent arm deflection was occurring only as a result of resumed exhaustion creep. Although the occurrence of crack growth was readily detected, and a qualitative assessment of its extent could be made, efforts to develop a procedure to obtain a quantitative measure of crack growth from lever arm deflection were unsuccessful. The third curve (Type 3) was similar to the second except that crack arrest did not occur. Given adequate time, samples showing Type 3 behavior would presumably fail under static loading.

The second method of detecting crack growth consisted of marking the crack extent at the end of a selected static exposure period with a penetrating dye (Dy-Chek) followed by rapid fracture of the test sample to observe the crack depth. Thorough removal of excess dye (by an air blast) was necessary to avoid continued dye movement during rapid fracture. Typical crack shapes as defined by this method are shown in Figure 5. The third method involved macroscopic examination of the fracture surface after rapid fracture following the static exposure period. As shown in Figure 6, the region of slow crack growth exhibited a distinctive faceted appearance which permitted fairly accurate determination of its extent.

Results and Discussion

The data collected during the experimental period, including the type of deflection-time curve observed, the maximum depth of internal crack growth, and the times during which crack growth occurred, are given in Table 9 for a variety of static loading conditions. Observations resulting from these tests are listed below:

(1) Considerable variation in test results was observed. For example, three samples of Ti-4Al-1.5Mo-0.5V alloy

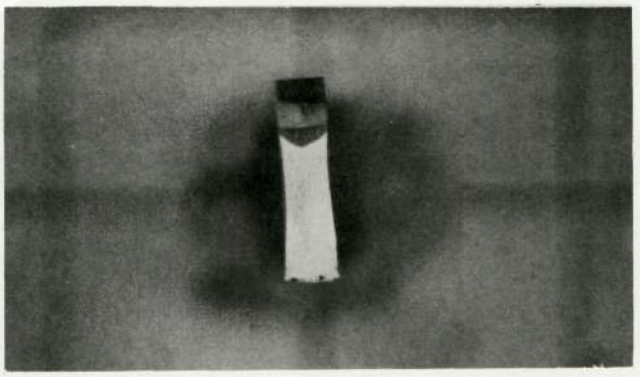

1X

a. Sample 72-2, 60.5 $MN/m^{3/2}$ (55 ksi $\sqrt{in.}$) in Saltwater

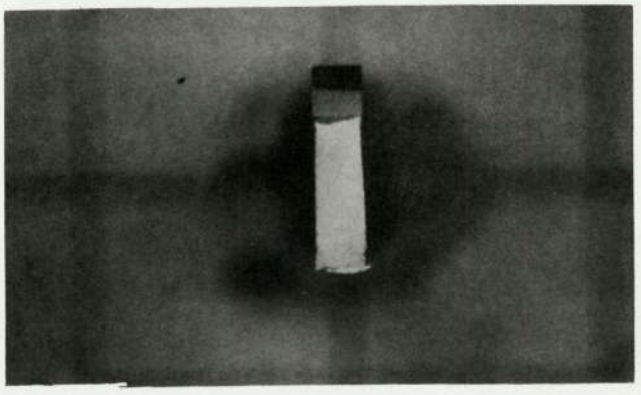

1X

b. Sample 72-1, 49.5 $MN/m^{3/2}$ (45 ksi $\sqrt{in.}$) in Saltwater

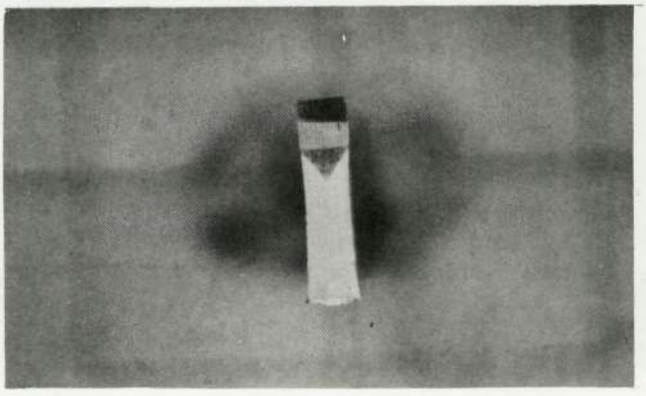

1X

c. Sample 72-3, 71.5 $MN/m^{3/2}$ (65 ksi $\sqrt{in.}$) in Air

FIGURE 5. CRACK GROWTH DURING STATIC LOADING AS SHOWN BY DYE MARKING FOLLOWED BY RAPID FRACTURE

The light area is the fast fracture region and the dark area the slow crack region. The top one-fourth of the sample consists of saw notch and fatigue crack.

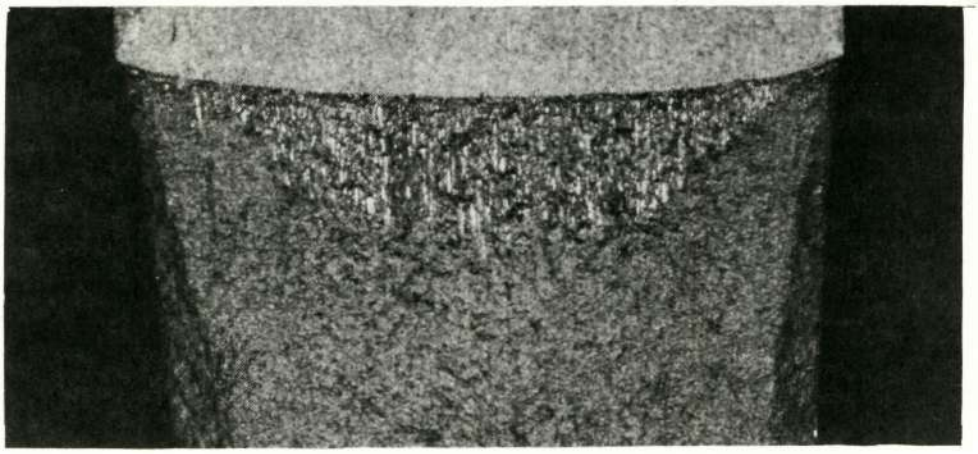

15X 6F948

a. Sample 72-2, 60.5 $MN/m^{-3/2}$ (55 ksi $\sqrt{in.}$) in Saltwater

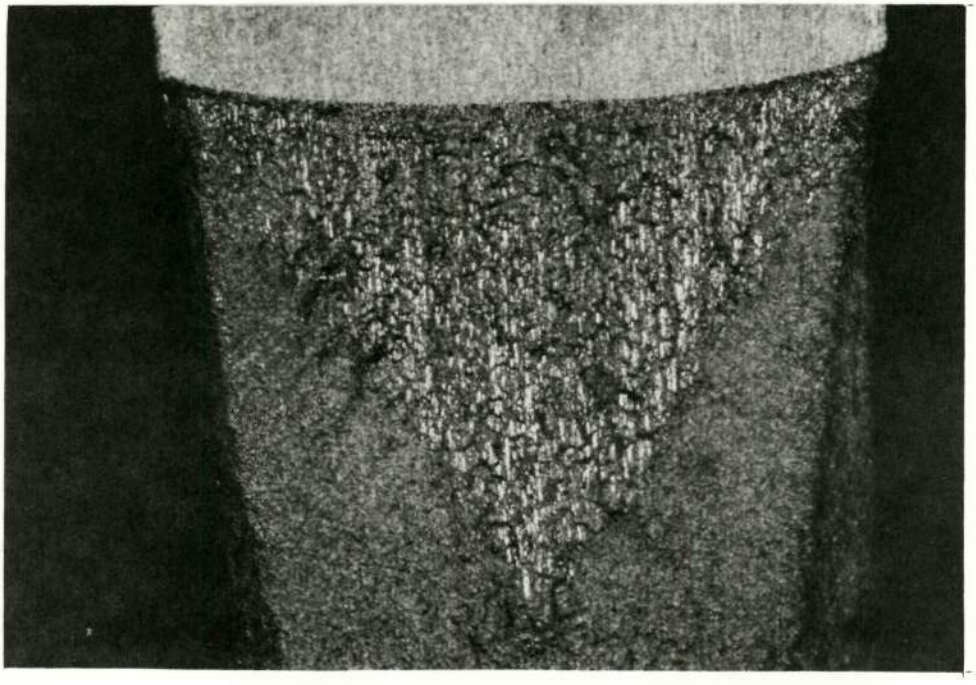

15X 6F949

b. Sample 72-3, 71.5 $MN/m^{3/2}$ (65 ksi $\sqrt{in.}$) in Air

FIGURE 6. MACROPHOTOGRAPHS OF SLOW CRACK REGION

Light area is base of fatigue crack, faceted area is slow crack growth region, gray area is fast fracture region.

TABLE 9. INTERNAL CRACK GROWTH OCCURRING DURING STATIC LOADING IN AIR AND SALT WATER

Sample No.	Environment	Static Loading Conditions: Stress Intensity $MN/m^{3/2}$ (Ksi$\sqrt{in}$)	Static Loading Conditions: Time, minutes	Type of Deflection Curve	Maximum Crack Depth, mm(in x 10^{-3})	Time, minutes, of Crack: Initiation	Time, minutes, of Crack: Arrest
		Ti-4Al-1.5Mo-0.5V Alloy					
72-3	Air	71.5 (65)	11,240	Type 3	4.70 (0.185)	5	--
72-C	Air	49.5 (45)	7,300	Type 1	0 (0)	--	--
72-G	Salt Water	71.5 (65)	7,200	Type 2	0.30 (0.012)	10	1,500
72-2	Salt Water	60.5 (55)	8,640	Type 2	1.47 (0.058)	10	400
72-1	Salt Water	49.5 (45)	8,640	Type 2	0.20 (0.008)	50	3,000
72-B	Salt Water	49.5 (45)	8,480	Type 2	(d)	1,000	1,500
72-H	Salt Water	49.5 (45)	7,300	Type 1	0 (0)	--	--
72-4	Salt Water	38.5 (35)	10,080	Type 2	0.08 (0.003)	30	>10,000
72-D	Salt Water	38.5 (35)	9,980	Type 2	(d)	300	> 9,980
		Ti-4Al-3Mo-1V Alloy					
70-D	Air	71.5 (65)	1,440	Type 3	2.54 (0.100)	4	--
70-1	Air[a]	71.5 (65)	7,220	Type 3	5.28 (0.208)	20	--
70-B	Air	60.5 (55)[b]	1,440	Type 2	0.38 (0.015)	20	200
70-3	Air[a]	49.5 (45)	7,200	Type 2	0.56 (0.022)	75	3,000
70-4	Salt Water	77.0 (70)	<1,440[c]	Type 3	5.28 (0.208)	20	--
70-E	Salt Water	71.5 (65)	1,440	Type 2	0.63 (0.025)	8	40
70-C	Salt Water	60.5 (55)[b]	1,440	Type 2	0.38 (0.015)	100	~1,000
70-2	Salt Water	49.5 (45)	7,200	Type 2	0.38 (0.015)	8	500

(a) A desiccant was included in a closed system to lower moisture content of the air.

(b) Exposed an additional 1440 minutes at 66 $MN/m^{3/2}$ (60 ksi$\sqrt{in.}$) before rapid fracture.

(c) Failed under static load between 480 and 1440 minutes.

(d) Crack depth at end of static loading was not determined.

statically loaded in saltwater to 49.5 $MN/m^{3/2}$ (45Ksi $\sqrt{in.}$) behaved quite differently, one not exhibiting crack growth, the others showing crack growth and arrest over widely different time intervals.

(2) Internal crack growth was observed in both alloys in tests conducted in saltwater. The Ti-4Al-1.5Mo-0.5V alloys showed crack growth followed by arrest at stress intensities between 38.5 and 71.5 $MN/m^{3/2}$ (35 and 65 Ksi $\sqrt{in}$) which were the lowest and highest stress intensities evaluated. The Ti-4Al-3Mo-1V alloy showed crack growth followed by arrest at stress intensities between 49.5 $MN/m^{3/2}$ (45 ksi$\sqrt{in}$, the lowest evaluated) and 71.5 $MN/m^{3/2}$ (65 ksi $\sqrt{in}$). Crack growth to failure occurred in the 4-3-1 alloy loaded to 77 $MN/m^{3/2}$ (70 ksi$\sqrt{in}$, the highest evaluated).

(3) Internal crack growth was observed in both alloys in tests conducted in air. The Ti-4Al-1.5Mo-0.5V alloy showed appreciable crack growth to 71.5 $MN/m^{3/2}$ (65 ksi $\sqrt{in}$, the highest evaluated) but no crack growth at 49.5 $MN/m^{3/2}$ (45 ksi $\sqrt{in}$, the lowest evaluated). The Ti-4Al-3Mo-1V alloy showed appreciable crack growth at 71.5 $MN/m^{3/2}$ (65 ksi $\sqrt{in}$, the highest evaluated) in both laboratory air and desicated air. Crack growth followed by arrest was observed for 4-3-1 loaded in laboratory air at 60.5 $MN/m^{3/2}$ (55 ksi $\sqrt{in}$) and in desicated air at 49.5 $MN/m^{3/2}$ (45 $\sqrt{ksi\ in}$).

(4) Cleavage facets in the slow crack growth portion of the fracture surface were observed to be identical in appearance in the Ti-4Al-1.5Mo-0.5V samples cracked in air and in saltwater, as illustrated in Figure 7.

(5) Internal slow crack growth initiation was apparently always preceeded by creep deformation. No correlation was observed between crack growth initiation time and the applied stress intensity. Crack initiation occurred in 10 minutes or less in 6 out of 15 tests and in 75 minutes or less in 12 of 15 tests. The crack initiation in three other samples occurred in 100, 300, and 1000 minutes, and not at all in two samples exposed for 7300 minutes.

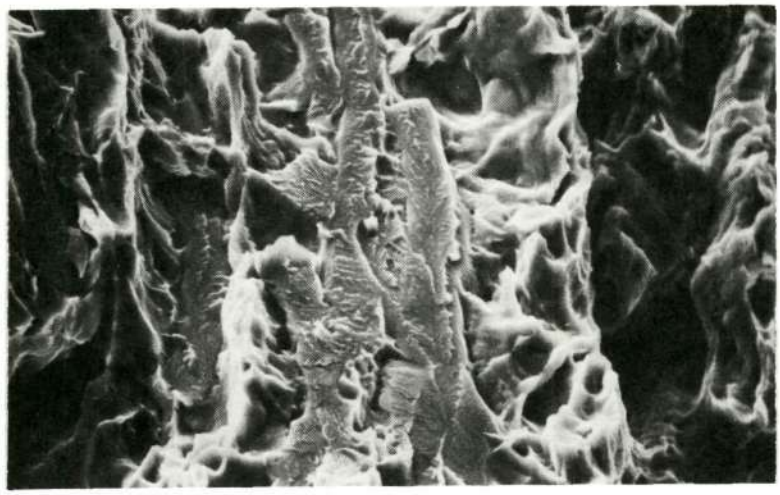

1000X S-5867

a. Sample 72-2, 60.5 $MN/m^{3/2}$ (55 ksi $\sqrt{in.}$) in Saltwater

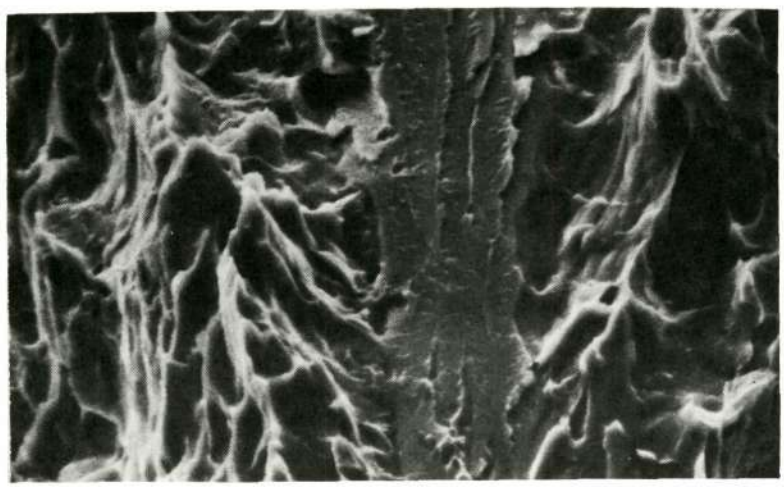

1000X S-5863

b. Sample 72-3, 71.5 $MN/m^{3/2}$ (65 ksi $\sqrt{in.}$) in Air

FIGURE 7. SCANNING ELECTRON MICROGRAPHS OF THE SLOW CRACK GROWTH REGION IN TWO Ti-4Al-1.5Mo-0.5V SAMPLES

Direction of crack growth is vertical.

(6) Internal slow crack growth under constant load was found to occur about as readily in air as in saltwater, and it was apparently more extensive in air than in saltwater at high stress intensity. On the basis of macroscopic measurements of amount of slow crack growth -- which are supported both by lever-arm deflection and dye marking measurements -- the following comparison was made:

Stress Intensity		Maximum Depth of Slow Crack Growth							
		Ti-4Al-1.5Mo-1.5V				Ti-4Al-3Mo-1V			
		Air		Saltwater		Air		Saltwater	
$MN/m^{3/2}$	Ksi $\sqrt{in}$	Mm	(Inch)	Mm	(Inch)	Mm	(Inch)	Mm	(Inch)
71.5	(65)	4.7	(0.185)	0.3	(0.012)	2.5-5.3	(0.1-0.208)	0.6	(0.025)
49.5	(45)	0	(0)	0.2	(0.008)	0.6	(0.022)	0.4	(0.015)
49.5	(45)	-	-	0	(0)	-	-	-	-

Based on the data given in Table 9 and summarized above, it appears possible that the internal slow crack growth observed in salt water statically loaded samples is a stress corrosion reaction which can occur at stress intensities as low as 38.5 $MN/m^{3/2}$ (35 Ksi $\sqrt{in}$) in Ti-4Al-1.5Mo-0.5V alloy or 49.5 $MN/m^{3/2}$ (45 ksi $\sqrt{in}$) in Ti-4Al-3Mo-1V alloy. Assuming $K_{I_{scc}}$ to be as low as these values, a sample thickness of 0.75 (0.29 inch) should be adequate to determine the value of $K_{I_{scc}}$ using the $\frac{1}{B}\left(\frac{K_i}{Y}\right)^2 \leq 0.4$ plane strain criterion for Ti-4Al-1.5Mo-0.5V alloy at yeild strength of 702 MN/m^2 (102 ksi). At the same time, 1 cm (0.39 inch) thick samples should be adequate to test the Ti-4Al-3Mo-1V alloy at yield strength of 785 MN/m^2 (114 ksi). However, stress corrosion susceptibility tests on the 4-3-1 alloy using 1.27-cm (0.5-inch) thick samples did not show a $K_{I_{scc}}$ value as low as 49.5 $MN/m^{3/2}$ (45 ksi$\sqrt{in}$). Similarly, tests run on several alloys similar to Ti-4Al-1.5Mo-0.5V, except with aluminum in the range of 5 to 6 percent, using 0.64-cm (0.25-inch) thick samples, did not show low $K_{I_{scc}}$ values.[3] The apparent $K_{I_{scc}}$ values of these

alloys were lowered by testing with thicker samples as shown by the data of Table 10. However, the $K_{I_{scc}}$ values were not reduced to the level predicted by the present studies.

The $K_{I_{scc}}$ behavior of the thick samples as illustrated by the data of Table 10, compared with the $K_{I_{scc}}$ level predicted by the slow crack growth studies, suggest three possibilities. These are:

(1) The internal slow crack growth measured in the present study is not a representative stress corrosion reaction but relates to a creep phenomenon of largely undefined dimensions.

(2) The $K_{I_{scc}}$ behavior of thick samples may indicate that the validity criterion used to select minimum sample thickness, $\frac{1}{B}\left(\frac{K_i}{Y}\right)^2 \leq 0.4$, is not sufficiently restrictive for moderate strength, high toughness alloys. Fracture toughness studies of similar materials lend some support to this suggestion.[18]

(3) The tests performed on the thick samples described in Table 10, were terminated after 360 minutes, which may be too short, time-wise, to allow crack initiation or if initiated, to allow significant crack growth. As shown by the times for crack initiation and arrest given in Table 9, crack growth rates were fairly low. High aluminum content titanium-base alloys tend to show failure in relatively short times when subjected to stress corrosion exposure in salt water using precracked samples, but this may be a trait specific to them. It has been shown that the rate of stress corrosion cracking of five steel alloys of different compositions, but having essentially the same strength and critical stress intensity for crack propagation in salt water, is highly composition dependent.[19] Times for failure at the critical stress intensity of these five alloys ranged from 100 minutes to 20,000 minutes.

TABLE 10. EFFECT OF SAMPLE THICKNESS ON THE CRITICAL STRESS INTENSITY FOR FAILURE IN SALT WATER USING SELECTED TITANIUM-ALUMINUM BASE ALLOYS(3)

Composition, Weight Percent	Measured $K_{I_{scc}}$, $MN/m^{3/2}$ (Ksi$\sqrt{in}$)					
	0.32 cm (0.125-in) Samples		Thick Samples			
			1.27 cm (0.5 in).		0.64 cm (0.25 in)	
Ti-4Al-3Mo-1V	91-95	(83-86)	78	(71)	--	
Ti-5Al-1.5Mo-0.5V	69	(63)	--		52	(47)
Ti-5.5Al-1.5Mo-0.5V	75	(68)	--		64	(58)
Ti-6Al-1.5Mo-0.5V	70	(64)	--		64	(58)

Slow crack growth was observed in tests on Ti-4Al-1.5Mo-0.5V and Ti-4Al-3Mo-1V alloys conducted in air. At higher stress intensities, Type 3 curves were observed with no evidence of crack arrest. Type 1 and Type 2 curves were obtained at low stress intensities. Although it is unlikely that the plane strain air fracture toughness (K_{Ic}) of either alloy is as low as 49.5 $MN/m^{3/2}$ (45 Ksi $\sqrt{in}$), it has been reported that failure to provide adequate sample thickness in moderate strength, high toughness alloys can result in the measurement of fracture toughness values which deviate toward too low rather than toward too high values as usually expected.(18) Presumably, such behavior is the result of a tensile overload in an essentially notch ductile material.

Subcritical crack growth in air has been reported to occur in certain cases when samples are exposed to plane stress or mixed mode loading.(20,21) Although little study of this phenomenon has apparently been carried out, the mechanism is presumed to be related to creep deformation. It has also been suggested that subcritical crack growth in titanium alloys in air is related to internal hydrogen content.(22) The hydrogen contents of the two alloys examined in this study were relatively low; eg. 26 ppm in

Ti-4Al-3Mo-1V. If crack growth in air is a normal occurrence under mixed mode or plane stress loading, then crack growth in salt water may arise from a similar cause, and measurements of internal crack growth in samples too thin to provide plane strain loading would be of no value in determining K_{Iscc}.

An alternate explanation for the occurrence of crack growth in tests in air is that moisture present in the air is adequate to promote stress corrosion cracking. Such an explanation is favored by the observation of similar appearing regions of cleavage fracture in the slow crack growth regions of samples stressed in either environment, as shown in Figure 7. These regions of cleavage failure are only observed in the portion of the fracture surface formed during slow crack growth. Cleavage regions such as these, occasionally aligned in the direction of crack growth, are commonly observed in high aluminum-titanium-base alloys which have failed in salt water stress corrosion exposure.[1,3,22] Efforts to suppress internal crack growth in air by removing a portion of the moisture from the air were unsuccessful. In these tests, (Samples 70-1 and 70-3) samples were enclosed in a plastic bottle containing a desiccant for several hours prior to loading and were statically loaded in the sealed containers. Cleavage regions have been reported in a Ti-8Al-1Mo-1V alloy showing slow crack growth in air.[22] In this case, cleavage cracking was attributed to the internal hydrogen content of the alloy (48 ppm).

Conclusions

Although further study is required to confirm the results of this investigation, several tentative conclusions can be made as follows:

(1) Crack growth can occur in high-toughness, moderate-strength titanium-base alloys exposed to salt water at stress intensities considerably below the usually accepted critical stress intensity for crack propagation in salt water. Crack arrest can occur after relatively small amounts of crack growth, possibly due to the elimination of the initial triaxial stress pattern caused by crack growth only in the mid-section of samples which effectively thins the samples.

(2) Crack growth at relatively low stress intensities can occur during static loading in a normal air environment. The fracture surface of the slow crack growth region is indistinguishable from that developed during tests in salt water and shows the cleavage regions considered typical of stress corrosion cracking. If slow crack growth is attributed to a stress corrosion reaction, air is as aggressive as saltwater in the case of the two Ti-4Al-base alloys examined.

(3) Crack growth rates are lower in titanium-base alloys containing 4 percent aluminum than observed in alloys containing as much as 8 percent aluminum. Crack initiation time is erratic but can be quite far removed from the time of load application, especially so in low load tests. Therefore, stress corrosion studies of titanium-low and intermediate-aluminum content alloys should be conducted using long time (possibly 24 hour minimum) static loading periods.

(4) Appreciable slow crack growth can occur internally with no visible evidence of crack propagation on the surface. Surface propagation of cracks resulted from ductile failure of the surface region after extensive (non visible) internal slow crack growth. In 0.64 cm (0.25-inch) thick samples of moderate-strength alloys, internal cracking can proceed to a depth of over 0.25 cm (0.1 inch) before any evidence of surface crack extension can be seen.

(5) The usefulness of internal slow crack growth measurement as a method of determining $K_{I_{scc}}$ values in low-strength, high-toughness Ti-Al-base alloys is not clearly established. Procedures for measuring slow crack growth characteristics were developed although results were inconsistent.

(6) The $K_{I_{scc}}$ values indicated by internal slow crack growth measurement were unexpectedly low and may have been the result of some crack growth mechanism other than salt water stress corrosion.

STRESS CORROSION SUSCEPTIBILITY OF Ti-4Al-3Mo-1V THICK PLATE

During an examination of the effects on salt water stress corrosion behavior of increasing sample thickness from 0.32 cm (0.125 inch) to 0.64 cm (0.25 inch), conducted using a series of moderate to high aluminum-content alpha-beta alloys, $K_{I_{scc}}$ was shown to be somewhat sensitive to section size.[3] This phenomenon is well documented in the literature, and it is commonly observed that alloys susceptible to stress corrosion, such as Ti-8Al-1Mo-1V or Ti-6Al-4V, can appear relatively immune if evaluated using samples of inadequate thickness.[16-17] The minimum sample thickness (B) for a reliable test is believed to be related to critical stress intensity for stress corrosion cracking ($K_{I_{scc}}$) and yield strength (Y) of an alloy as follows:[15,23]

$$B \geq 2.5\left(\frac{K_{Iscc}}{Y}\right)^2 .$$

The observation that susceptible alloys may show little evidence of stress corrosion when tested using subsize samples suggests the possibility that alloys presently considered relatively immune to stress corrosion, as, for example, Ti-4Al-3Mo-1V in the annealed condition,[24,25,26] may appear so because of the use of inadequately dimensioned samples. The relative immunity of Ti-4Al-3Mo-1V to salt water stress corrosion being related to testing variables such as sample thickness is further suggested by our observation of arrested crack growth during evaluation of 0.64 cm (0.25 inch) thick samples of this alloy. The objective of this investigation was to examine the effect of sample dimensions on the saltwater stress corrosion behavior of Ti-4Al-3Mo-1V alloy to determine if susceptibility would be increased by conditions favoring plane strain loading, that is, increased sample thickness.

Material

A quantity of 6 cm (2.3 inch) thick rolled plate was supplied by TMCA for use in this investigation. The composition of this plate as

reported by TMCA was as follows: 3.8 aluminum, 3.0 molybdenum, 1.2 vanadium, 0.07 iron, 0.009 nitrogen, and 0.11 oxygen. Interstitial analysis performed at Battelle-Columbus after heat treatment in vacuum showed 1010 ppm oxygen and 4 ppm hydrogen. The plate was sectioned as shown in Figure 8 to provide material at several thicknesses for evaluation. The identification system shown in Figure 8 can be used to locate individual test samples within the plate in subsequent data tabulations.

Sections measuring 0.64 cm (0.25 inch) thick were machined to provide samples for evaluation of tensile properties transverse to the rolling direction. Two samples, one from the surface (B-1) and one from the plate center (B-4) were tested in the as-received condition. Two similarly located samples (A-1 and A-4) were tested after alpha-beta annealing 1 hour at 1170 K (1650 F), furnace cooling to 920 K (1200 F) and holding at this temperature for 1 hour. Samples were heat treated in an argon atmosphere. The properties of the plate as measured in these tests are given in Table 11. A considerable difference in strength between surface and center was observed. Also, an improvement in ductility and a reduction in strength was observed to result from heat treatment.

TABLE 11. TENSILE PROPERTIES OF Ti-4Al-3Mo-1V PLATE

Sample No.	Heat Treatment	Sample Location[a]	Ultimate Tensile Strength, MN/m^2	(Ksi)	0.2% Offset Yield Strength, MN/m^2	(Ksi)	Elongation, percent	Reduction in Area, percent
B-1	As-Received	Surface	861	(125)	772	(112)	10	20
B-4	As-Received	Center	744	(108)	710	(103)	8	18
A-1	Alpha-beta annealed + stabilized	Surface	785	(114)	710	(103)	12	23
A-4	Ditto	Center	751	(109)	661	(96)	11	25

(a) See Figure 8.

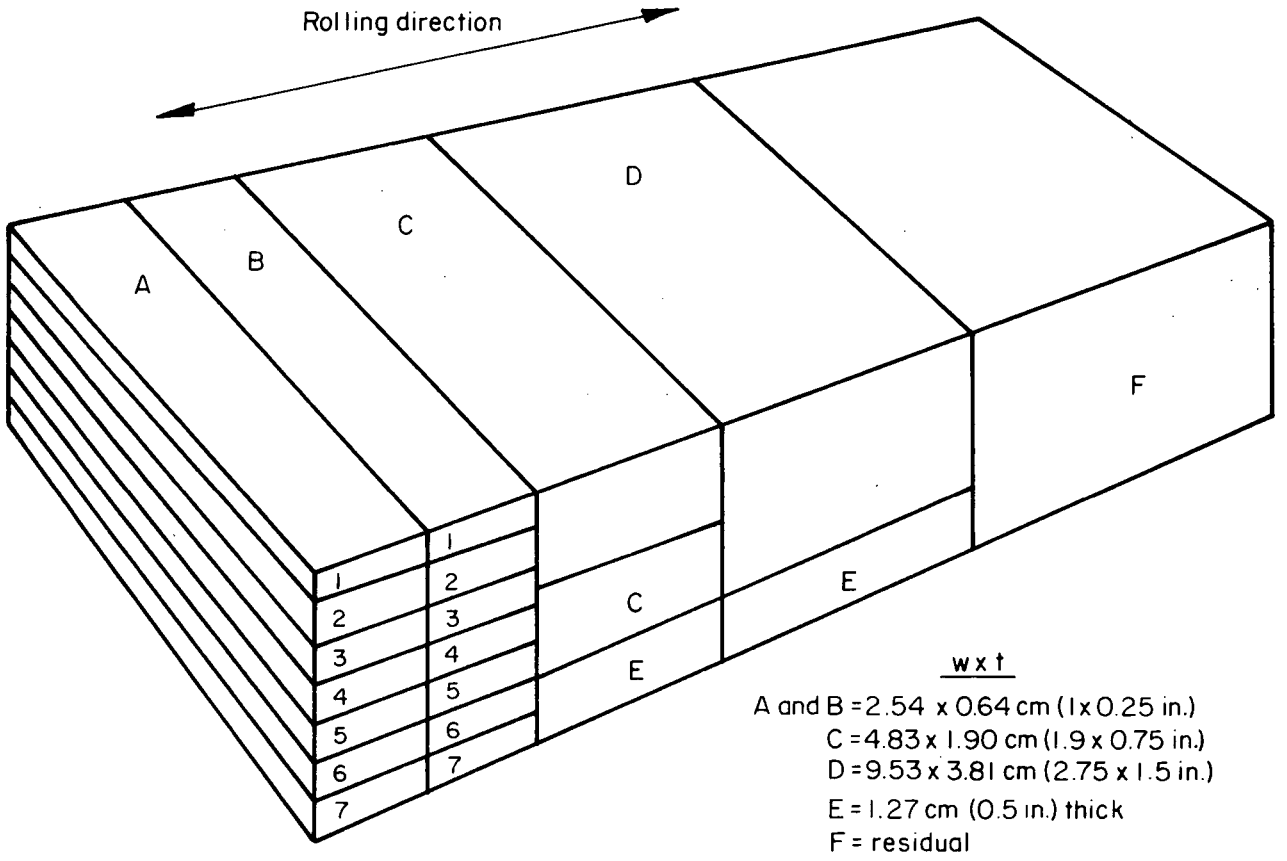

FIGURE 8. SECTIONING PLAN FOR 6-CM (2.36-IN.) THICK Ti-4Al-3Mo-1V PLATE

Metallographic examination showed the as-received plate to have a coarse acicular microstructure. This structure was not altered appreciably by alpha-beta annealing followed by stabilization. All material prepared for evaluation of stress corrosion susceptibility was alpha-beta annealed and stabilized prior to evaluation. Some variation in heat treatment schedule was used in preparing different groups of samples, specifically changes in the length of the stabilization anneal or in the heat treatment atmosphere. These differences are indicated at appropriate points in the discussion of the program.

Experimental Procedures

Based on the validity criterion $B \geq 2.5 \left(\frac{K_{Iscc}}{Y}\right)^2$ and using an average yield strength value of 690 MN/m^2 (100 ksi) (see Table 11), valid plane strain measurements could be performed in samples of varying thicknesses as follows:

Thickness, cm (inch)		Maximum Plane Strain Strain Intensity for Valid Measurements $MN/m^{3/2}$	($Ksi\sqrt{in}$)
0.64	(0.25)	35.2	(32)
1.90	(0.75)	60.5	(55)
3.81	(1.50)	84.7	(77)

Since it was considered unlikely, based on our prior work on 1.27 cm (0.5 inch) thick Ti-4Al-3Mo-1V plate,[3] that K_{Iscc} was above 79 $MN/m^{3/2}$ (72 $ksi\sqrt{in.}$), tests at these three thicknesses appeared adequate to obtain a reliable estimate of K_{Iscc}.

Insufficient material was available for conventional cantilever bend tests at the three thicknesses selected for study. Therefore, it was decided to evaluate the material using the compact tension sample design. The compact tension sample design and methods for determining stress intensity using this sample are described in a recently proposed ASTM Specification.[27]

A drawing showing sample dimensions of the three samples prepared for evaluation is shown in Figure 9. Crack orientation was the same in all cases, the crack plane containing the thickness direction and crack movement occurring along the longitudinal direction. (WR orientation). This orientation is the same as that used in our prior work with cantilever bend samples. Samples were loaded in tension using a suitable yoke and static loading system.

Fatigue cracks were introduced from a few days to a month or more prior to static loading. Fatigue cracking was done using a minimum of 50,000 cycles at stress intensities well below the initial static stress intensity.

A clip-on strain gage unit mounted on the gage support notch shown in Figure 9 was used to monitor crack opening during the course of the loading period. Crack opening displacment at the root of the notch was calculated assuming hinge-type crack opening from a neutral point of the center of the uncracked region:*

$$\text{COD} = \text{gage reading} \times \left(\frac{W - a_o}{2W_1 - W + a_o} \right)$$

with values of W_1, W, and a_o as shown in Figure 9. Crack opening displacement as a function of creep was determined as the difference between crack opening measured 30 seconds after load application and that after the time interval of interest, usually 24 hours (1440 minutes). Salt water was held in a plastic container when this environment was required. Approximately two-thirds of the sample was submerged with the crack plane horizontal. The salt water was added immediately preceeding load application. Upon completion of the loading period unfractured compact tension samples were pulled to failure in tension and the fracture stress intensity was measured. The machine head travel during the test was 0.051 cm (0.02 inch) per minute.

Although the majority of the test samples were run using compact tension samples, a few tests of 0.64 cm (0.25 inch) material were run using the cantilever-bend sample for direct comparison with prior work.

---

* Although a neutral axis located one-third of the ligament distance from crack root is recommended for rising load tests[28], a value of one-half seemed more reasonable under creep conditions.

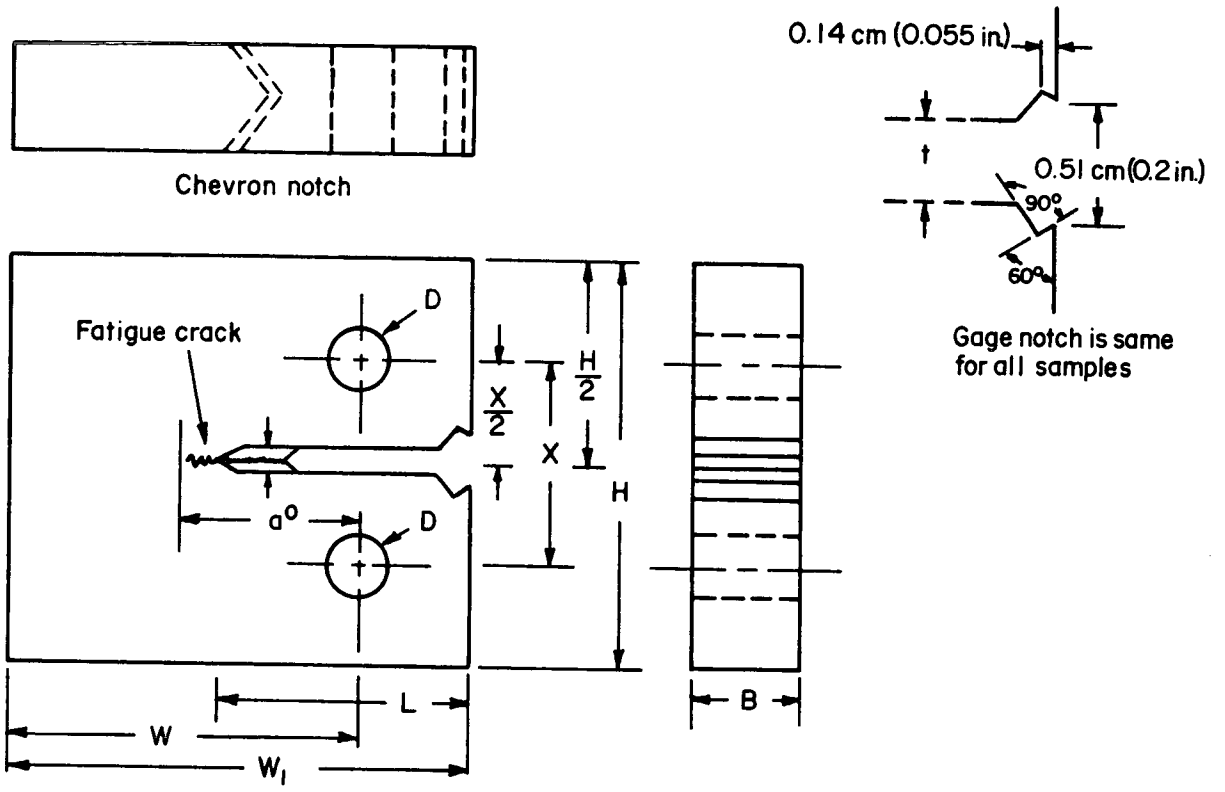

Sample Dimensions

	0.64-cm (0.25-in.) Sample		1.90-cm (0.75-in.) Sample		3.81-cm (1.5-in.) Sample	
	cm	inch	cm	inch	cm	inch
B	0.64	(0.25 ± .01)	1.90	(0.75 ± .01)	3.81	(1.50 ± .01)
W	2.03	(0.800 ± .002)	3.81	(1.500 ± .002)	7.62	(3.000 ± .002)
H	2.44	(9.96 ± .01)	4.57	(1.80 ± .01)	9.14	(3.60 ± .01)
W_1	2.54	(1.000 ± .005)	4.76	(1.875 ± .005)	9.52	(3.750 ± .005)
D	0.51	(0.200 ± .005)	0.95	(0.375 ± .005)	1.90	(0.750 ± .005)
X	1.12	(0.44 ± .01)	2.10	(0.825 ± .01)	4.19	(1.65 ± .01)
L	1.32	(0.52 ± .01)	2.48	(0.975 ± .01)	4.95	(1.95 ± .01)
t	0.13	(0.05 ± .01)	0.24	(0.094 ± .01)	0.48	(0.187 ± .01)
a^o (desired)	1.02	(0.400)	1.90	(0.750)	3.81	(1.500)

FIGURE 9. COMPACT TENSION SAMPLE DIMENSIONS

Results

To provide an initial indication of the stress intensities for failure in air and in salt water, cantilever bend samples were step loaded to failure in air and in salt water using a 3 minute delay period between load increments and approximately 1.1 $MN/m^{3/2}$ (1 ksi$\sqrt{in.}$) stress intensity steps in the vicinity of the failure stress intensity. Failure stress intensities were:

Air (Sample A2): 98.4 $MN/m^{3/2}$ (89.5 Ksi$\sqrt{in}$)

Salt water (Sample A6): 94.4 $MN/m^{3/2}$ (85.8 Ksi$\sqrt{in}$)

Following these tests, a series of sustained load tests were run in both air and salt water using 0.64 cm (0.25 inch) thick samples. The results of these tests are summarized in Table 12.

The samples described in Table 12 were heat treated using three different procedures. Cantilever bend samples A3, A5, and A7 were alpha-beta annealed and stabilized in an argon atmosphere and received only a 1 hour stabilization anneal. The two step-loaded samples described above (A2 and A6) were similarly treated. All samples designated with the letter B were heat treated entirely in vacuum, including the alpha-beta anneal, and received a 3 hour stabilization treatment. Compact tension samples designated with the letter A were alpha-beta annealed and stabilized in argon along with the cantilever bend samples, but were subsequently annealed for an additional 4 hours at 920 K (1200 F) in vacuum. This latter group of samples appeared significantly less creep resistant. In addition, sample location within the plate was a significant variable. Sample location within the original plate can be identified by number with reference to Figure 8 (B7c is a surface sample, etc.). Where comparisons are possible, it appears that surface samples were more resistant to stress corrosion (and more creep resistant) than samples nearer the center of the plate.

Compact tension samples 0.64 cm (0.25 inch) thick appeared capable of sustaining at least 82.5 $MN/m^{3/2}$ (75 ksi$\sqrt{in}$) for 24 hours (1440 minutes) in air even though significant creep was observed at stress intensities as low as

TABLE 12. RESULTS OF SUSTAINED LOAD TESTS ON 0.64 cm (0.25 INCH) THICK Ti-4Al-3Mo-1V ALLOY

Sample No.	Type	Environment	Constant Load Stress Intensity, $MN/m^{3/2}$	(Ksi $\sqrt{in}$)	Time to Failure, minutes[a]	Tensile Fracture Stress Intensity, $MN/m^{3/2}$	(Ksi $\sqrt{in}$)	Creep in 24 hours, COD, μ m	(inch x 10^3)
A7a	CT	Air	88.0	(80)	40	--	--	--	--
A5a	"	"	82.5	(75)	(>1440)	88.0	(80.1)	86	(3.4)
A6b	"	"	73.7	(67)	(>3960)	94.8	(86.2)	25	(1.0)
A6a	"	"	59.4	(54)	(>5700)	97.4	(88.6)	8	(0.3)
A5b	CT	Salt water	88	(80)	<1	--	--	--	--
A3	Bend	"	"	"	23	--	--	--	--
B7a	CT	"	"	"	(>1440)	95.3[b]	(86.7)[b]	51	(2.0)
A5	Bend	"	85.8	(78)	<1	--	--	--	--
B7c	CT	"	"	"	(>10080)	110.6	(100.6)	20	(0.8)
A6a	"	"	"	"	480 to 5760[c]	--	--	43	~(1.7)
A7b	"	"	82.5	(75)	<1	--	--	--	--
A7	Bend	"	81.4	(74)	(>1440)	--	--	--	--
B5c	CT	"	80.3	(73)	550	--	--	--	--
B7b	"	"	"	"	(>5700)	97.0	(88.2)	28	(1.1)
A6b	"	"	77.0	(70)	(>1400)	82.3	(74.8)	96	(3.8)
B3b	"	"	75.9	(69)	1	--	--	--	--
B5b	"	"	72.6	(66)	(>4020)	102.0	(92.8)	8	(0.3)
B3a	"	"	66.0	(60)	(>5520)	81.4	(74.0)	23	(0.9)
B5a	"	"	"	"	(>4620)	94.0	(85.5)	13	(0.5)
B6a	"	"	49.5	(45)	(>7080)	99.2	(90.2)	5	(0.2)

(a) Time in parenthesis indicates sample removed from test before failure.

(b) Step-loaded to failure in salt water.

(c) Failed over a weekend without gage attached.

59.4 $MN/m^{3/2}$ (54 ksi $\sqrt{in.}$). The degree of creep correlated moderately well with applied stress. Tensile loading to failure upon completion of the sustained loading period gave an average stress intensity for failure of 93.5 $MN/m^{3/2}$ (85.0 ksi $\sqrt{in.}$) with a rather broad variation in test results, most probably related to heat treatment and sample location.

Behavior in salt water was considerably less consistent than that in air. Two of three samples tested at 88 $MN/m^{3/2}$ (80 ksi $\sqrt{in.}$) failed rapidly, but one was removed from test after prolonged exposure without failure. Somewhat similar behavior was observed at 85.8 $MN/m^{3/2}$ (78 ksi $\sqrt{in.}$). Additional failures were observed at 82.5 (75), 80.3 (73), and 75.9 $MN/m^{3/2}$ (69 ksi $\sqrt{in.}$). On the other hand, samples were removed from test without failure after exposure for extended times at 81.4 (74), 80.3 (73), and 77.0 $MN/m^{3/2}$ (70 ksi $\sqrt{in.}$). The differences can be correlated with differences in sample location and heat treatment in most cases. Samples loaded to failure in tension in air after variable sustained loading periods in salt water also showed a wide range of failure stress intensities, from 81.4 (74.0 to 110.6 $MN/m^{3/2}$ (100.6 ksi $\sqrt{in.}$), with an average value of 88.0 $MN/m^{3/2}$ (80.0 ksi $\sqrt{in.}$). Again, it seems likely that a major portion of the variation in fracture stress can be attributed to sample location and heat treatment differences. The amount of creep deflection observed during testing was also quite variable although a reasonable correlation with stress intensity was observed. Measurable creep deflection was observed at the lowest stress intensity examined, 49.5 $MN/m^{3/2}$ (45 ksi $\sqrt{in.}$).

None of the samples exposed in salt water showed evidence of slow crack growth or crack arrest in measurements of crack opening displacement as a function of time. Typical examples of gage deflection versus time behavior are shown in Figure 10. The deflection behavior shown is believed related entirely to creep deflection. No evidence of a slow crack growth region could be detected on macroscopic examination, nor did a correlation appear to exist between fracture stress intensity in tensile tests after exposure and either crack opening displacement or the sustained loading conditions.

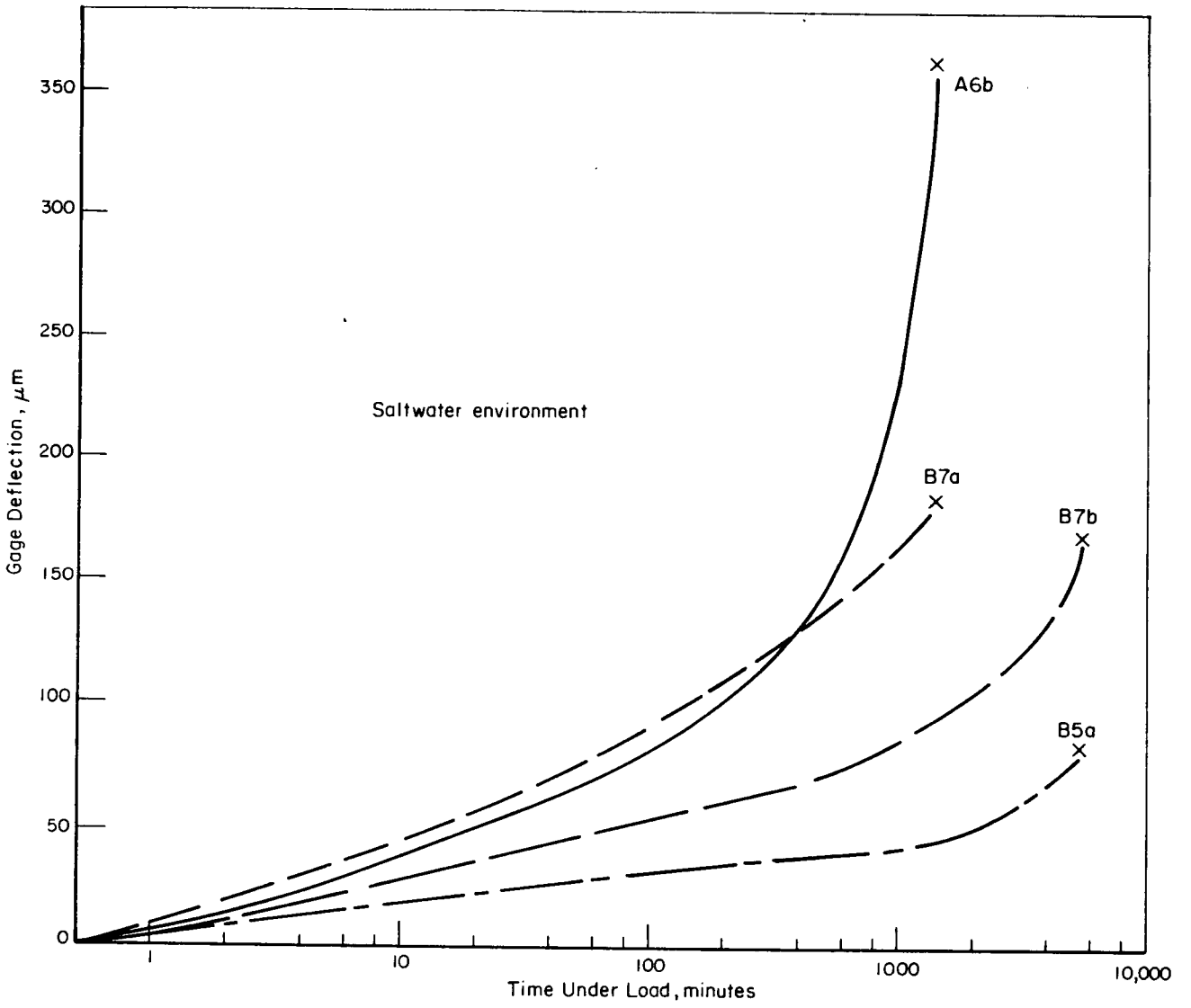

FIGURE 10. CRACK-OPENING MEASUREMENTS ON FOUR 0.25-INCH-THICK CT SAMPLES REMOVED FROM TEST BEFORE FAILURE

Despite our failure to observe any evidence of slow crack growth in this material of the type previously observed in laboratory processed Ti-4Al-3Mo-1V, it was decided to proceed with the evaluation of the 1.90 cm (0.75 in.) thick samples. Six compact tension samples were loaded at varying stress intensities, using a maximum loading time of 1440 minutes, with the results shown in Table 13. All six of these samples were heat treated entirely in vacuum in the same manner, alpha-beta annealed for 1 hour at 1170 K (1650 F), furnace cooled to 920 K (1200 F), and held 3 hours. The crack opening versus time curves were all of Type 3 as shown in Figure 11 and can apparently be related to creep deflection under load. No evidence of crack growth was seen on macroexamination although a difference in the appearance of the fracture surface between tests in air and salt water appeared to exist. Salt water fracture surfaces seemed to show more cleavage of the acicular alpha phase.

The critical stress intensity for failure was somewhat higher in air than in salt water, perhaps as much as 5.5 $MN/m^{3/2}$ (5 ksi $\sqrt{in.}$). Creep was apparent at the lowest stress intensity examined, 82.5 $MN/m^{3/2}$ (75 ksi $\sqrt{in.}$), it appeared to decrease with decreased stress intensity in a regular manner. The increase in crack opening displacement in 24 hours in 1.90 cm (0.75 in.) samples was approximately the same at a given stress intensity as that measured in 0.64 cm (0.25 in.) samples.

An appreciable load would be required to test the 3.8 cm (1.5 in.) 4-3-1 plate material at stress intensities in the range suggested by the results on 1.90 cm (0.75 in.) material. A stress intensity of 88 $MN/m^{3/2}$ (80 ksi $\sqrt{in.}$), for example, would require a load of approximately 11,300 Kg (25,000 lbs). It was therefore decided not to attempt to carry out tests on the 3.8 cm (1.5 in.) material.

A limited study of the Ti-4Al-1.5Mo-0.5V alloy examined previously in the investigation of subcritical crack growth was carried out to determine whether the apparent absence of crack growth in the thick plate Ti-4Al-3Mo-1V might have been related to test method (CT samples instead of cantilever bend samples) rather than to microstructure. Compact tension samples were

TABLE 13. RESULTS OF SUSTAINED LOAD TESTS ON 1.90 cm (0.75 in.) THICK Ti-4Al-3Mo-1V ALLOY

Sample No.	Environment	Constant Load Stress Intensity, $MN/m^{3/2}$	(ksi$\sqrt{in.}$)	Time to Failure, minutes[a]	Tensile Fracture Stress Intensity, $MN/m^{3/2}$	(ksi$\sqrt{in.}$)	Creep in 24 hours, COD, μ m	(inch x 10^{-3})
C5	Air	99.0	(90)	240	--	--	--	--
C4	"	93.5	(85)	(>1440)	110.4	(100.4)	63	(2.5)
C3	Salt water	93.5	(85)	<1 min.		--	--	--
C6	"	91.3	(83)	(>1440)	108.2	(98.4)	63	(2.5)
C2	"	88.0	(80)	(>1440)	116.8	(106.2)	25	(1.0)
C1	"	82.5	(75)	(>1440)	108.0	(98.2)	18	(0.7)

(a) Time in parenthesis indicates sample removed from test before failure.

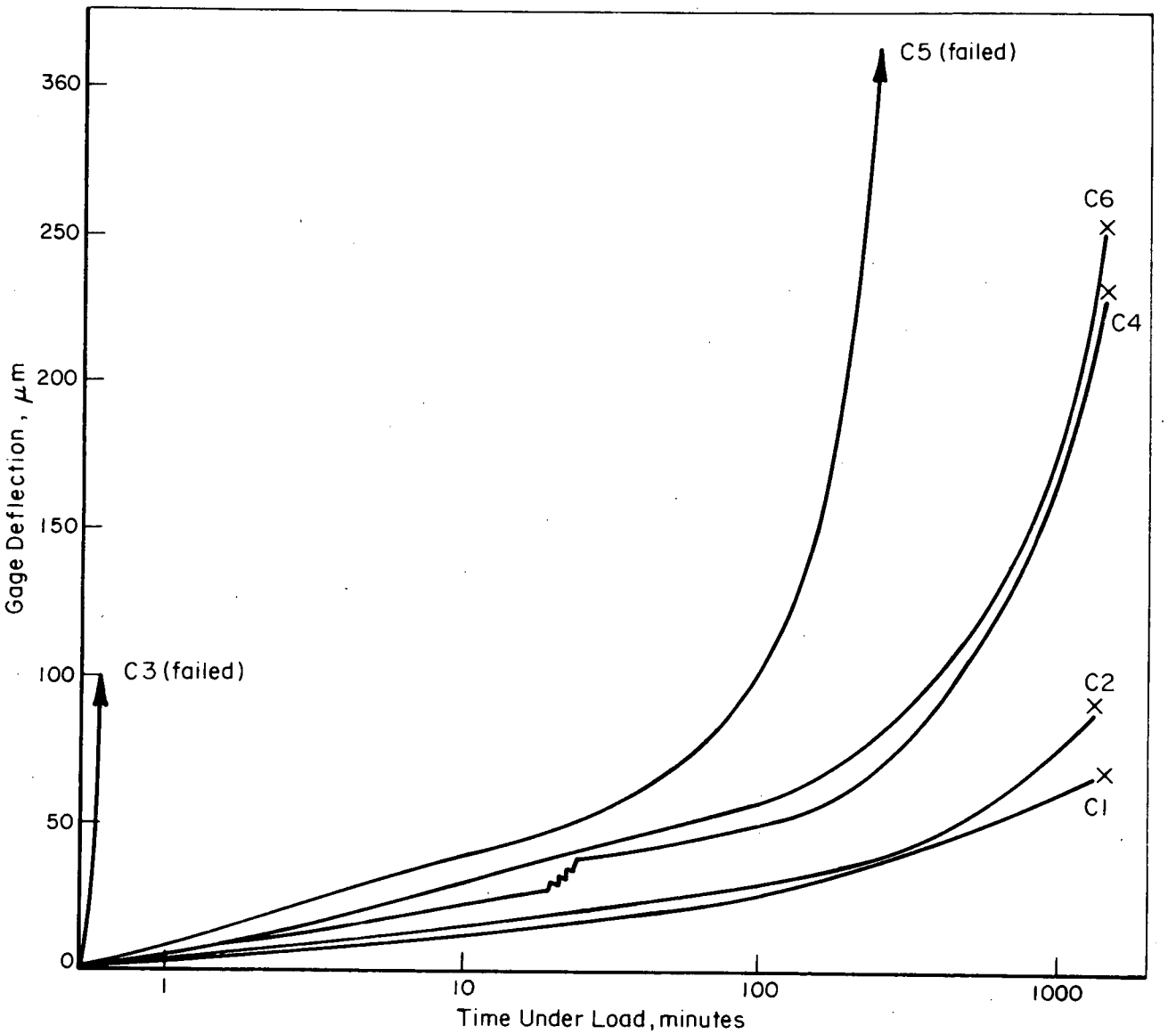

FIGURE 11. CRACK OPENING MEASUREMENTS ON 1.90-CM (0.75-INCH) THICK CT SAMPLES

prepared from remnants of previously tested cantilever bend samples. Results of these tests are summarized in Table 14. The results of these tests paralleled those previously observed with cantilever bend samples (see Table 9, previous section) indicating that the compact tension test provides essentially similar behavior to that observed in cantilever bend tests. However, stress intensity levels did not appear directly comparable. For example, failure occurred in CT samples loaded in air at 60.5 $MN/m^{3/2}$ (55 ksi $\sqrt{in}$) in less then 1 day, but a cantilever bend sample was loaded in air at a stress intensity of 71.5 $MN/m^{3/2}$ (65 ksi $\sqrt{in.}$) for over 7 days without failure. In addition, in compact tension tests in salt water at 60.5 $MN/m^{3/2}$ (55 ksi $\sqrt{in.}$), only 0.38 mm (0.015 in) of slow crack growth was evident whereas 1.47 mm (0.058 in) was seen in the cantilever bend test at the same stress intensity.

Clear evidence of crack growth followed by arrest at 60.5 $MN/m^{3/2}$ (55 ksi$\sqrt{in.}$) in salt water (726 T-5), and of exhaustion creep at 49.5 $MN/m^{3/2}$ (45 ksi $\sqrt{in.}$) in air (71CT-4), was observed from gage defection measurements during constant load testing of compact tension samples as shown in Figure 12. These observations also suggest that the failure to observe slow crack growth in the thick plate 4-3-1 material was not related to the test method.

Although more data are required before reliance can be placed upon this method, tensile tests of samples after constant load exposure may prove useful in detecting internal crack growth. As shown in Table 14 the two samples which showed crack growth (72CT-1 and 72CT-5) had lower fracture stress intensities than the sample which did not show crack growth (72CT-4). Such behavior would be an expected result of internal crack growth since fracture stress intensity determination from failure load is based on external crack dimensions.

Discussion

Samples cut from the Ti-4Al-3Mo-1V thick plate used in this investigation did not show susceptibility to salt water stress corrosion. No

TABLE 14. SUSTAINED LOAD TESTS OF 0.64 cm (0.25 inch) THICK COMPACT TENSION SAMPLES OF Ti-4Al-1.5Mo-0.5V ALLOY

Sample No.	Environment	Constant Load Stress Intensity, $MN/m^{3/2}$	(ksi$\sqrt{in}$)	Time to Failure, minutes(a)	Deflection Curve(b)	Apparent Depth of Slow Crack Growth, mm	(inch x 10^{-3})	Tensile Fracture Stress Intensity, $MN/m^{3/2}$	(ksi$\sqrt{in}$)	Creep in 24 hours, COD, μm	(inch x 10^{-3})
72CT-2	Air	60.5	(55)	480 to 1300	Type 3	3.81	(152)	--	--	--	--
72CT-3	"	60.5	(55)	870	Type 3	4.09	(162)	--	--	--	--
72CT-4	"	49.5	(45)	(>1440)	Type 1	0	(0)	82.9	(75.4)	2	(0.1)
72CT-1	Salt water	60.5	(55)	(>1200)	Type 2	0.38	(15)	75.4	(68.6)	--	--
72CT-5	"	60.5	(55)	(>1440)	Type 2	0.38	(15)	79.0	(71.8)	18	(0.7)

(a) Time in parenthesis indicates sample removed from test before failure.

(b) See Figure 4 for an illustration of curve designations.

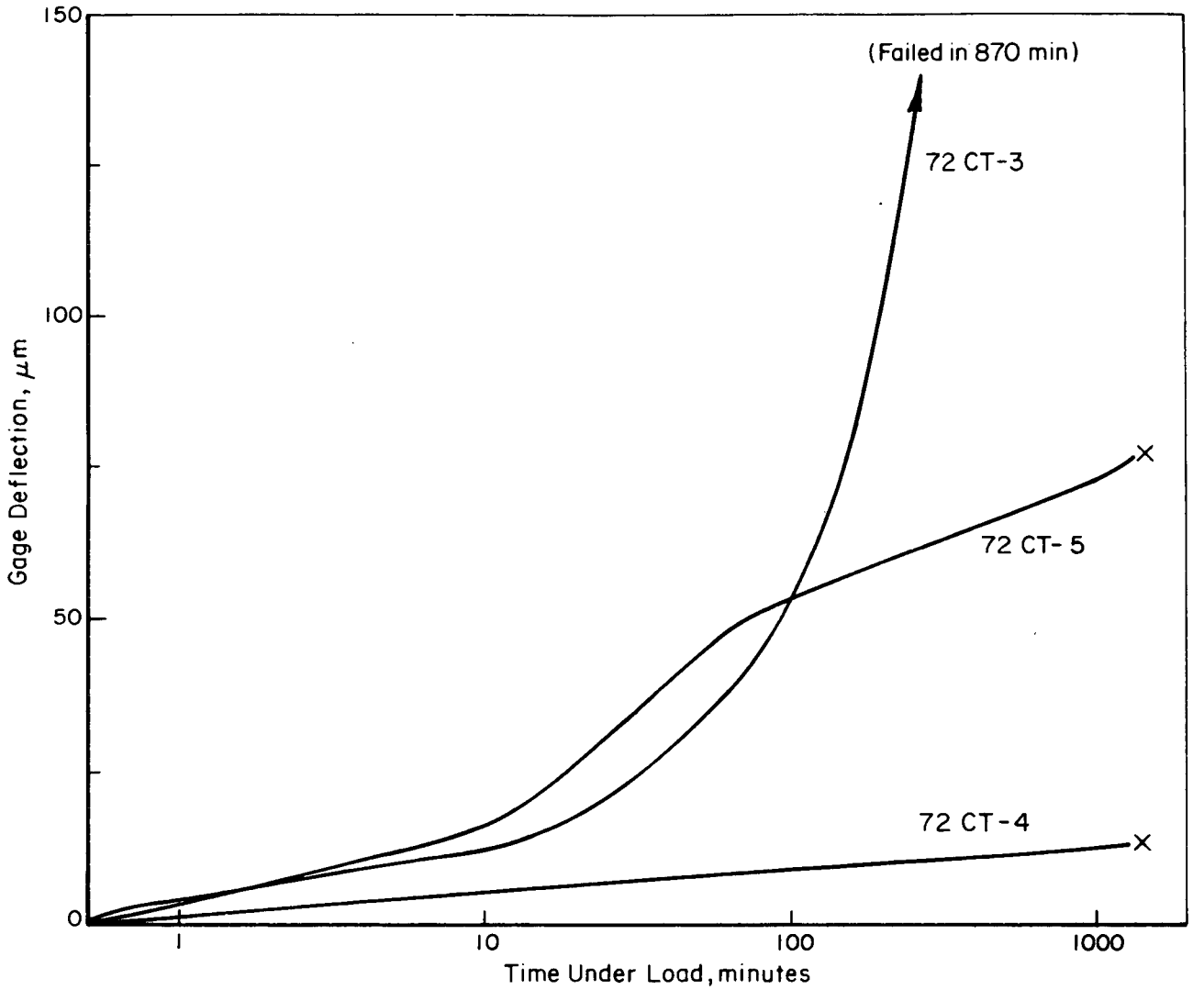

FIGURE 12. CRACK OPENING MEASUREMENTS OF 0.64-CM (0.25-INCH) COMPACT TENSION SAMPLES OF Ti-4Al-1.5Mo-0.5V ALLOY

evidence was obtained to indicate that increased sample thickness (to increase the plane strain character of the loading conditions) increased stress corrosion susceptibility. In fact, an increase in air and salt water stress intensity for failure was observed for samples of increased thickness as shown below (data from Tables 12 and 13).

Thickness	Air	Salt Water
0.64 cm (0.25 inch)	88.0 $MN/m^{3/2}$ (80 Ksi$\sqrt{in}$)	82.5 $MN/m^{3/2}$ (75 Ksi$\sqrt{in}$)
1.90 cm (0.75 inch)	99.0 $MN/m^{3/2}$ (90 Ksi$\sqrt{in}$)	93.5 $MN/m^{3/2}$ (85 Ksi$\sqrt{in}$)

It is believed that the 4-3-1 plate used in this experiment was more resistant to stress corrosion cracking than the 4-3-1 material examined previously. Observations leading to the above explanation of the present results are as follows.

Prior experiments with other heats of 4-3-1 alloy indicated that strength level and microstructural condition are quite important with regard to susceptibility.[2] For example, the prior 4-3-1 material examined was found to be more tough and resistant to salt water cracking in the acicularized microstructural condition (116.5 $MN/m^{3/2}$ (106 Ksi$\sqrt{in}$) in air, and 197.8 $MN/m^{3/2}$ (98 Ksi$\sqrt{in}$) in salt water) than in the equiaxed alpha-beta annealed condition (104.5 $MN/m^{3/2}$ (95 Ksi$\sqrt{in}$) in air, and 96.8 $MN/m^{3/2}$ (88 Ksi$\sqrt{in}$) in salt water). Further, prior material modified by heat treatment to a higher strength level showed reduced air toughness and greater stress corrosion susceptibility. Thus, the present material in its low strength, acicularized microstructural condition behaved predictably based on the previous experience with a similar alloy.

Another set of observations concerns the notch ductility of the 4-3-1 used in the present study. The crack opening versus time curves showed no evidence of either crack movement, or at low stress intensities, of exhaustion creep. Instead, a curve shape suggesting cubic creep behavior was observed. No macroscopic evidence of slow crack growth was seen on the fracture surface. Thus, the data suggest that the 4-3-1 material was very notch

ductile and of quite low strength so that gross yielding, together with crack blunting, occurred at the crack front. It was further observed that increasing the sample thickness from 0.64 to 1.90 cm (0.25 to 0.75 inch) increased rather than decreased the apparent air toughness of the 4-3-1 alloy (for example from 88 to 99 $MN/m^{3/2}$ (80 to 90 $Ksi\sqrt{in}$)). Such behavior has been previously reported as an indication of notch ductility [29].

The present results are of interest in explaining the beneficial effects of an acicular microstructure of a low strength material (and possibly in high strength acicularized materials as well) on both stress corrosion susceptibility and fracture toughness. Possibly, acicularity is effective through its ability to induce crack blunting. This behavior may be analogous to the beneficial effects of a laminated structure.[30] On the basis of this analogy, the effectiveness of microstructural methods for controlling toughness or stress corrosion resistance of alpha-beta alloys should be a function of the void or crack forming propensity of the beta phase, the distribution of the beta phase, and the toughness of the alpha phase. Further work in the area of microstructural control should prove valuable in improving both stress corrosion resistance and fracture toughness.

Conclusions

The Ti-4Al-3Mo-1V alloy in the low strength, annealed condition with acicular microstructure can be considered for practical purposes and at practical thicknesses, immune to the salt water stress corrosion reaction. Failure to observe a reduction in K_{Iscc} with increasing sample thickness is atrributed to the notch ductility of the thick plate material. The notch ductility observed in this material is an intrinsic property of 4-3-1 alloy in the low strength, annealed condition and is enhanced by an acicularized microstructural condition.

RELATIONSHIP BETWEEN STRESS-CORROSION SUSCEPTIBILITY AND THE PRESENCE OF Ti_3Al

Titanium alloys containing variable amounts of aluminum show increased susceptibility to salt water stress corrosion as aluminum content increases. Several investigations have shown an abrupt decrease in the measured value of $K_{I_{scc}}$ as aluminum content exceeds about 6 percent.[4,11,13,14] The increased salt water stress-corrosion susceptibility of high aluminum alloys has been attributed to Ti_3Al precipitation which is known to occur at about this same aluminum level.[31] Ti_3Al precipitation can be embrittling to titanium-aluminum alloys,[32] so a relationship between Ti_3Al precipitation and susceptibility to salt water stress corrosion might be expected.

The objective of the present investigation was to examine a series of titanium alloys containing different aluminum contents for evidence of Ti_3Al precipitation to determine whether salt water stress-corrosion susceptibility could be correlated with the presence of Ti_3Al.

Materials and Procedures

Seven Ti-4 to 8 Al-1.5Mo-0.5V alloys prepared in earlier portions of this program were selected for study.[1,2,3] The properties of these alloys, as determined from 0.32 cm (0.125-inch) thick sheet samples, are summarized in Table 15. The $K_{I_{scc}}$ values for these alloys are plotted versus aluminum content in an earlier section of this report (see Figure 3). All alloys had been stabilized at 920 K (1200 F) following alpha-beta annealing.

Material for examination by transmission electron microscopy was cut from failed 0.32 cm (0.125 inch) thick stress-corrosion samples from a region within 1 cm (0.2 inch) of the fracture, but outside the shear lip area. Samples were cut parallel to the sheet surface about midway between the surface and the center. After thinning, these samples were examined for general microstructural details. Electron diffraction was used to detect the presence of Ti_3Al and when Ti_3Al was found, dark field techniques were applied in an attempt to resolve Ti_3Al particles.

TABLE 15. AVERAGE PROPERTIES OF Ti-(4-8)Al-1.5Mo-0.5V ALLOYS[1,2,3]
(Transverse Tensile Samples, WR Fracture Samples)[a]

Nominal Composition, weight percent[b]	Ultimate Tensile Strength, MN/m^2 (Ksi)	0.2% Offset Yield Strength, MN/m^2 (Ksi)	Elong. % in 1 inch	Red. in Area, %	Stress Intensity in salt water[c] $MN/m^{3/2}$ (Ksi $\sqrt{in.}$)
Ti-4Al-1.5Mo-0.5V	744 (108)	701 (102)	20	36	91 (83)
Ti-5Al-1.5Mo-0.5V	825 (120)	805 (117)	14	28	69 (63)
Ti-5.5Al-1.5Mo-0.5V	833 (121)	791 (115)	16	30	75 (68)
Ti-6Al-1.5Mo-0.5V	881 (128)	840 (122)	14	32	70 (64)
Ti-6.5Al-1.5Mo-0.5V	846 (123)	791 (115)	14	26	34 (31)
Ti-7Al-1.5Mo-0.5V	930 (135)	846 (123)	15	30	22 (20)
Ti-8Al-1.5Mo-0.5V	1005 (146)	895 (130)	18	29	16.5(15)

(a) Alpha-beta annealed at 1185-1245K (1670-1785 F) depending on aluminum content, furnace cooled to 920 K (1200 F), and stabilized approximately 4 hours at 920 K (1200 F).

(b) Nominally 0.1 percent oxygen content.

(c) Maximum constant stress intensity which will not result in sample failure in 6 hour exposures.

Results and Discussion

The alpha grain size of these alloys was relatively small as shown in Figure 13. Since all seven alloys showed essentially the same microstructure, only two are shown. Alpha grain size measurements indicated the grain diameter of the Ti-4Al-1.5Mo-0.5V alloy was approximately 0.0004 cm (0.00016 inch).

Electron diffraction patterns for the seven alloys are shown in Figure 14. No Ti_3Al was detected in alloys containing 4, 5, or 5.5 weight percent aluminum. Alloys containing 6, 6.5, 7 and 8 weight percent aluminum contained Ti_3Al although in amounts too small to detect by means of dark field techniques. Only trace amounts of Ti_3Al were observed in the 6 and 6.5 percent aluminum alloys. The 7 and 8 percent aluminum alloys contained larger amounts of Ti_3Al. The Ti_3Al detected in the 7 and 8 percent aluminum alloy probably precipitated during the stabilization annealing at 920 K (1200 F). (Ti_3Al is reported to form in binary Ti-8Al alloy on annealing below 965 K (1260 F)).[33] The apparently smaller amounts of Ti_3Al present in the intermediate aluminum content alloys most likely precipitated on cooling following the stabilization anneal rather than during annealing. The cooling rate was relatively low, the samples being cooled in a vacuum furnace, thus permitting samples to cool through the Ti_3Al field for some short period of time.

The Ti-4Al-, Ti-5Al-, and Ti-5.5Al-base alloys which do not show Ti_3Al phase by the electron diffraction techniques used in this study were relatively immune to stress corrosion while the Ti-7Al- and Ti-8Al-base alloys which had the strongest Ti_3Al reflections, were very susceptible to stress corrosion. The Ti-6Al- and Ti-6.5Al-base alloys do not fit the susceptibility, Ti_3Al correlation exactly since while similar amounts of Ti_3Al were found in these alloys, widely different stress-corrosion susceptibilities were found. The Ti-6Al-base alloy was relatively immune to stress corrosion. On the other hand, the Ti-6.5Al-base alloy was susceptible to stress corrosion. Therefore, one of the difficulties in observing a complete correlation between stress-corrosion susceptibility and the presence of Ti_3Al appears to be the inability to quantify the small amounts of Ti_3Al detected in the borderline alloys. It is possible that there are progressively increasing amounts of Ti_3Al in the Ti-6Al- and Ti-6.5Al-base alloys even though not revealed by the diffraction technique.

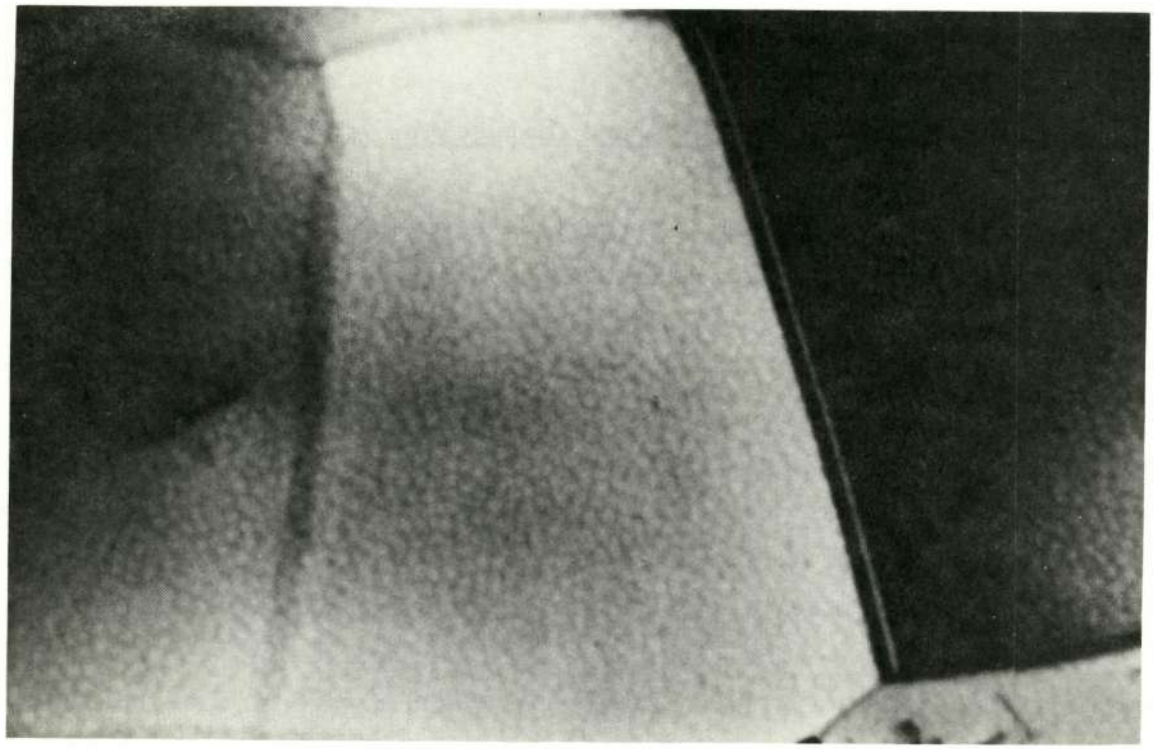

33,000X 15108

a. Ti-4Al-1.5Mo-0.5V

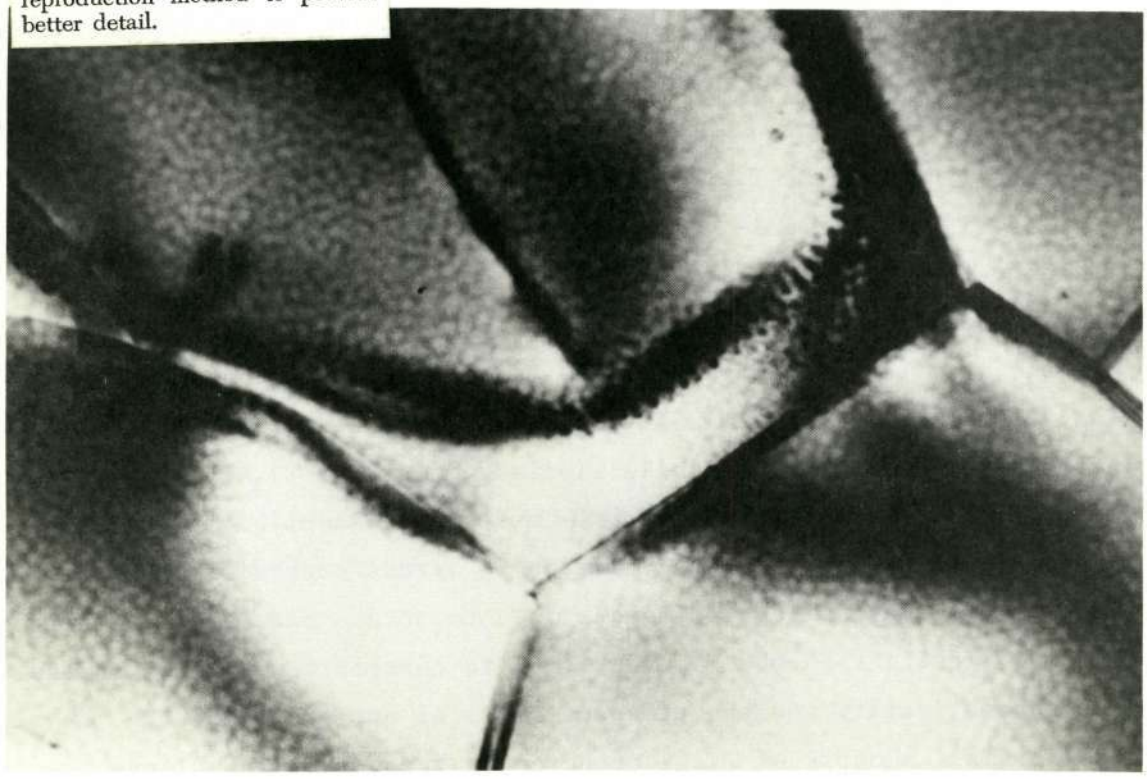

32,000X 15109

b. Ti-8Al-1.5Mo-0.5V

FIGURE 13. TRANSMISSION ELECTRON MICROGRAPHS OF TWO TITANIUM ALLOYS

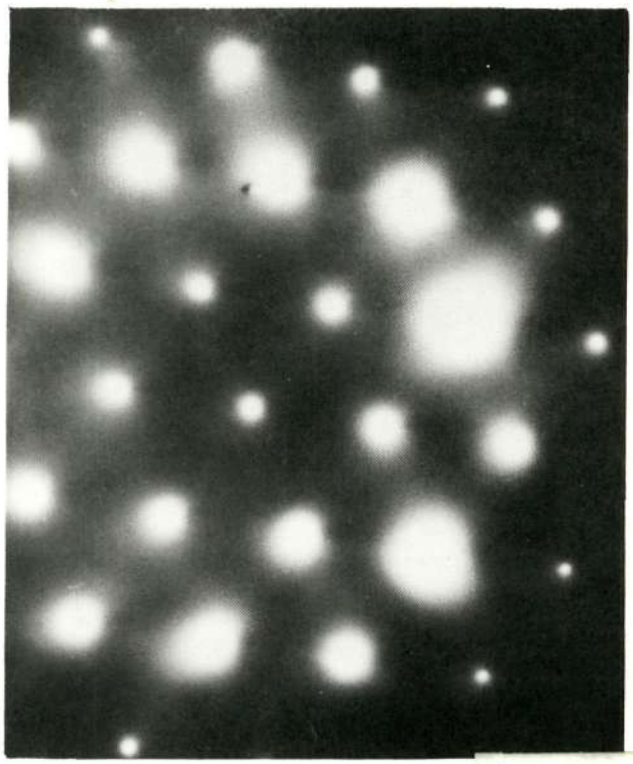

a. Ti-4Al-1.5Mo-0.5V

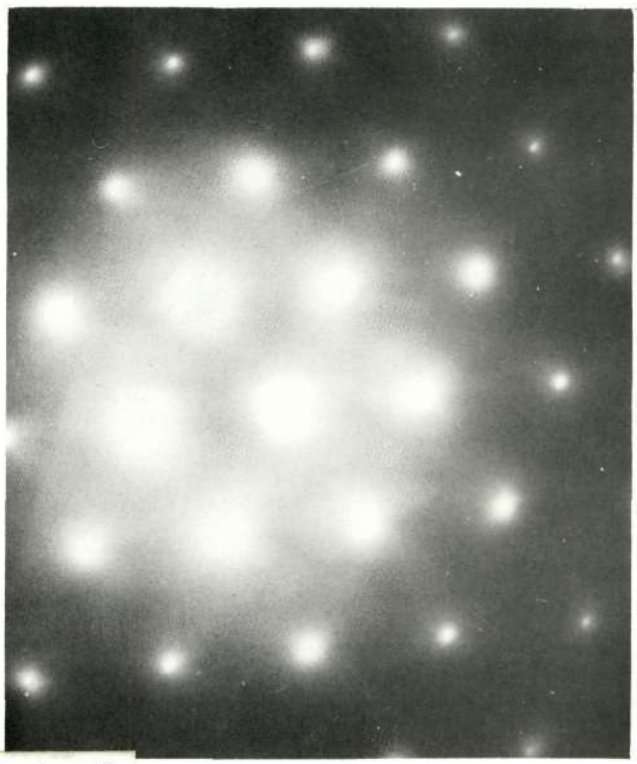

b. Ti-5Al-1.5Mo-0.5V

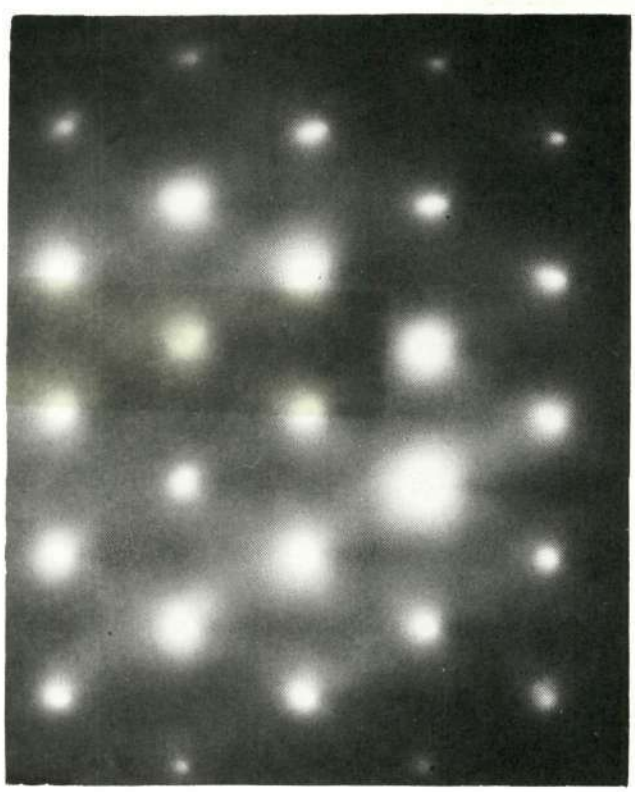

c. Ti-5.5Al-1.5Mo-0.5V

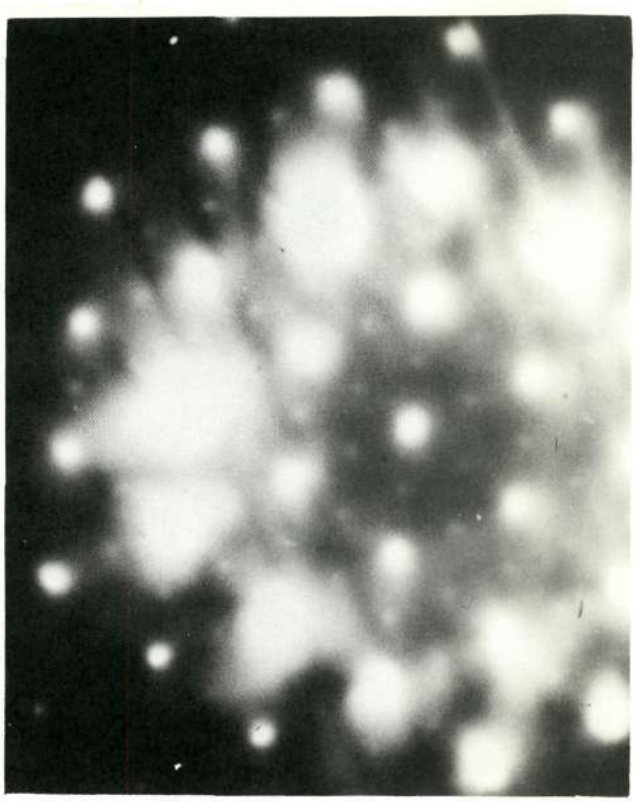

d. Ti-6Al-1.5Mo-0.5V

FIGURE 14. ELECTRON-DIFFRACTION PATTERNS FOR SEVEN TITANIUM-ALUMINUM ALLOYS

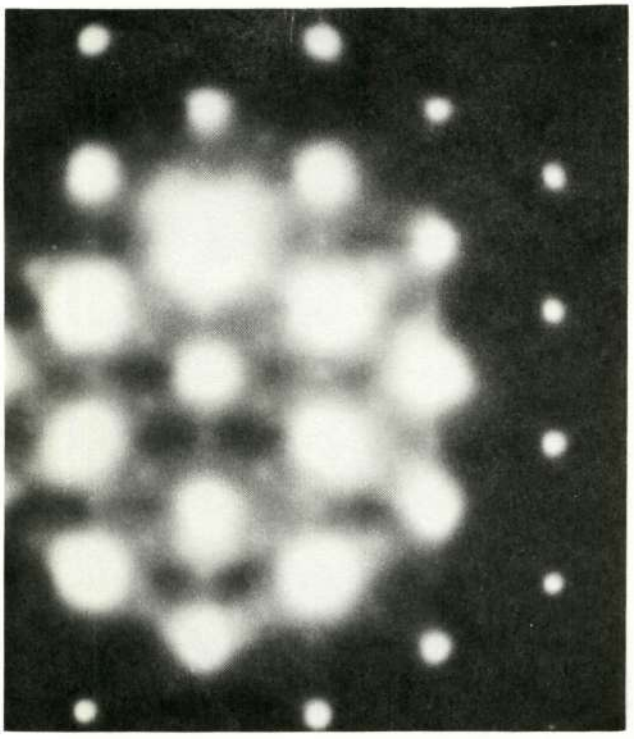

e. Ti-6.5Al-1.5Mo-0.5V

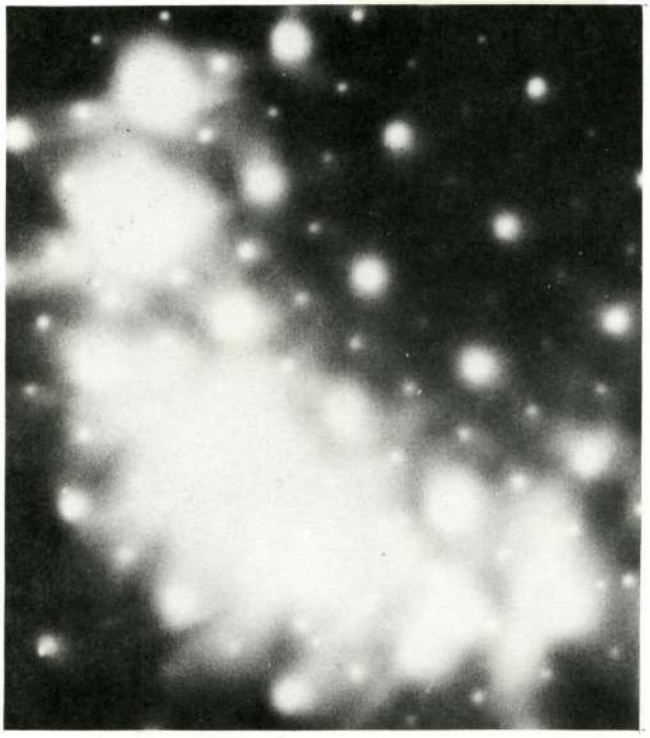

f. Ti-7Al-1.5Mo-0.5V

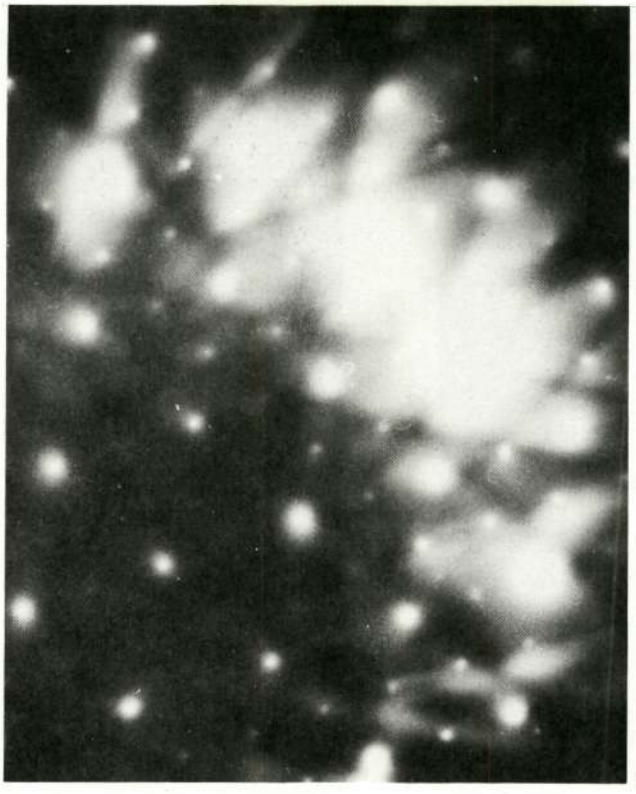

g. Ti-8Al-1.5Mo-0.5V

FIGURE 14. (CONTINUED)

The four alloys containing the Ti_3Al phase, are, on the average, as ductile in the tension test as are the three alloys not showing Ti_3Al (Table 15). Thus, this is additional evidence that the amount of Ti_3Al phase is small and no correlation exists between this small amount of Ti_3Al and tensile ductility. Similarly, no correlation exists between tensile ductility and stress-corrosion susceptibility. No correlation exists between tensile yield strength and stress-corrosion susceptibility either, since among the five intermediate aluminum content alloys there is only a 55 MN/m^2 (8 ksi) yield strength spread and within this spread, one of the highest strength materials is not very susceptible while one of the lowest strength materials is susceptible.

Conclusions

A reasonably good correlation was found between salt water stress-corrosion susceptibility and the presence of Ti_3Al phase in Ti-4 to 8 Al-1.5Mo-0.5V alloys as alpha-beta annealed and subsequently stabilized at 920 K (1200 F). The correlation is weakened somewhat by the behavior of the intermediate aluminum content alloys inasmuch as there were gross differences in stress-corrosion susceptibility among compositions showing no obvious differences in amounts of Ti_3Al present (trace amounts). This resulted from the experimental difficulty in obtaining a quantitative measurement of the amount of Ti_3Al present.

METALLURGICAL MECHANISMS OF STRESS-CORROSION CRACKING

Background

Several independent investigations have shown that the precipitation of long-range-ordered Ti_3Al particles in the alpha phase has a profound effect on the aqueous stress-corrosion behavior of titanium-aluminum-base alloys. This was pointed out first by Lane and Cavallaro[4], and subsequently by others.[14, 26, 31-34] It has been established that alloys containing Ti_3Al exhibit lower values of $K_{I_{scc}}$ and higher rates of subcritical crack growth than disordered alloys having the same aluminum content. However, the specific effect of the Ti_3Al particles on the mechanism of subcritical crack initiation and growth has not been adequately demonstrated. The following factors are thought to be germane to the problem.

(1) The coherent, ordered precipitates promote nonhomogeneous, planar slip. This slip mode generally occurs in alloys hardened by coherent precipitates because the areal fraction of precipitate in a given slip plane decreases with passage of each dislocation. Hence, it requires a lower stress to move dislocations in an active slip plane than to initiate slip in an area where the particles have not been previously sheared. Consequently, the slip bands tend to be narrow and widely spaced, and to have large shear displacements. The ordered nature of the particles causes the dislocations to move as pairs of perfect $\frac{a}{3}[11\bar{2}0]$ dislocations separated by a strip of antiphase boundary, which makes it difficult for obstacles to be bypassed by cross slip. The result is that long coplanar pileups of dislocations form at obstacles, and large shear displacements occur at free surfaces. The former effect produces high normal stresses which could cause cleavage, and the latter exposes large areas of bare metal to the environment which could act as active anodic sites.

(2) The slip bands have a higher chemical potential than the undeformed material. This is a consequence of the increased density of antiphase

boundary in the sheared particles, their decreased size (Gibbs-Thompson Effect), and the tendency toward particle dissolution in the slip bands[34-36]. The enhanced chemical potential of the slip bands caused by the sheared Ti_3Al particles is expected to increase the rate of any electrochemical reaction occurring at surface slip steps.

(3) Ti_3Al particles make an alloy intrinsically more brittle[32,35,37].

Recently it has been demonstrated by Cavallaro and Wilcox[33] that the degree of embrittlement, in air as well as in saltwater, is a function of the aging time at a temperature at which Ti_3Al forms. Their results also indicate that in certain cases toughness in air and in salt water can be recovered by overaging. These observations suggest that the toughness is sensitive to the precise size distribution of the Ti_3Al particles. Work by Lütjering and Weissman[35] suggests an explanation for the relation between the size distribution of Ti_3Al and the fracture toughness in air. Studying a series of alloys containing 14.5 to 18.1 atomic percent aluminum (8.7 to 11.1 weight percent), they showed that the tensile ductility increases when the slip mechanism changes from particle shearing to particle bypass. When the bypass mechanism is operative, the dislocation debris which accumulates in the vicinity of the particles hardens the active slip planes, and results in a more homogeneous slip character. Lütjering and Weissman showed that the particle-bypass mechanism is favored when the Ti_3Al exists as a homogeneous distribution of large (>0.1 μm), widely spaced particles. They obtained such distributions of particles by aging each alloy just below the $\alpha/\alpha+Ti_3Al$) phase boundary. Lütjering and Weissmann did not consider the effects of slip character on stress-corrosion cracking, but it can be argued that when the particle-bypass mechanism is predominant, the detrimental effects of Ti_3Al described above are alleviated. Furthermore, if the enhanced chemical potential of the slip bands is an important factor in the mechanism of stress-corrosion cracking, this effect should be greatest for very small particles (<.005 μm). Hence, the susceptibility to stress-corrosion cracking could be a function of the Ti_3Al size distribution even when the particles are sheared by glide dislocations.

In order to further investigate these postulated effects of Ti_3Al, a detailed study has been made of the relation between the tensile properties in air and in salt water, and the size distribution of Ti_3Al particles in a binary Ti-8Al alloy. Since the different size distributions of Ti_3Al particles were obtained by isothermal aging treatments, it was necessary to first evaluate the coarsening kinetics of the precipitates. The complete results are reported below. Some results have been presented at 2 meetings[34,36], and will be published in the proceedings.

Materials

Titanium-8 weight percent (13.4 atomic percent) aluminum was the single alloy composition investigated throughout this program. Two different lots of material were used during the course of the experiments, and these are identified as "alloy 73" and "alloy 27". The manufacturer's chemical analyses for both alloys are given in Table 16.

TABLE 16. VENDOR ANALYSES OF EXPERIMENTAL ALLOYS

Alloy No.	Elements, Weight percent					
	Al	Fe	C	O	N	H
73	8.03	0.053	0.022	0.096	0.003	0.015
27	8.07	0.074	--	0.108	0.004	--

Experimental Procedures

The as-received ingots were press forged and hot rolled, with intermediate anneals, to approximately 3.175 mm (0.125 in.) thick sheet. Blanks for tensile specimens were then cut from this material, and the blanks were annealed

for 2-4 hr. at 920 K (1200 F) in a dynamic vacuum of 10^{-5} torr. This treatment lowered the hydrogen content of the material to less than 10 ppmw. The specimen blanks were then heat treated and machined into tensile specimens. Several different specimen geometries and preparation procedures were employed, and these are detailed in Table 17.

The general specimen-preparation procedure was as follows: For all heat treatments the specimens were individually encapsulated in quartz tubes which were evacuated to less than 10^{-5} torr, and back-filled with dry argon to 1/3 atmosphere pressure. After solution treating (24 hr. at 1170 K (1650 F)), the specimens were quenched by breaking the tubes in ice water. After the aging heat treatment the specimens were cooled in air to room temperature before the tubes were broken. Since some of the tensile specimens were replicated to study the surface slip lines, special care was taken in the preparation of the tensile specimens to prevent deformation or chemical contamination of their surfaces. After heat treating, at least 0.635 mm (0.025 in.) was carefully removed from each surface of all tensile specimens by surface grinding. Then, they were metallographically polished through 6-micron diamond paste, and, finally, the gauge length of each specimen was electropolished.

All tensile deformation was carried out at room temperature using an Instron Universal Testing Machine at a crosshead speed of 5×10^{-3} min^{-1}. Tests were performed in air and in 3.5 weight percent NaCl (pH - 6.5). The saltwater tests were accomplished by fastening a plastic container around the specimen such that only the gauge section was immersed in the saltwater. All tests were carried out under open-circuit potential conditions.

Specimens representing all the heat treatments and the two testing environments were deformed to fracture to establish the yielding, work-hardening, and fracture characteristics of each. For these tests engineering stress-strain curves were constructed directly from the Instron charts. Some other specimens were deformed incrementally, and their surfaces were replicated after selected increments of strain. In these tests the strain was measured more accurately by gauge marks scribed on the specimen surfaces.

The surface replicas were prepared by the standard 2-stage technique using cellulose triacetate sheet as replicating material. The replicas were shadowed at an angle of 10 degrees with a 50-50 mixture of carbon and platinum, and then backed with carbon. A surface step in the replica will either appear

TABLE 17. DETAILS OF TENSILE SPECIMEN PREPARATION AND HEAT TREATMENT

Alloy	Specimen Dimensions[a] Thickness mm(in)	Gage Length mm(in)	Aging Heat Treatment[b]	Remarks
27	1.905 (.075)	31.75 (1.25)	0,22,100,500 and 1000 hr. 920K (1200F)	3.18 mm (.125-in.) thick blanks heat treated, then 1.9 mm (.075-in.) thick tensile specimens machined and polished
73	1.270 (.050)	25.4 (1.00)	0,22,100 and 500 hr. 770K (930F)	3.18 mm (.125-in.) thick tensile specimens machined, heat treated, then surface ground and polished to 1.27 mm (.050-in.) thick
73	0.635 (.025)	25.4 (1.00)	0 and 100 hr., 770K (930F)	3.18 mm (.125-in.) thick tensile specimens machined, and given ST & WQ. Same specimens surface ground and polished to 0.635 (.025-in.) thick; others surface ground to 1.14 mm (.045-in), aged, then surface ground and polished to 0.635 mm (.025-in.) thick
73	0.254 (.010)	(c)	0 and 100 hr., 770K (930F), 0,22,100,500 and 1000 hr., 920K (1200F), 0 and 500 hr., 970K (1290F)	0.254 mm (.010-in) thick strip tensile specimens (no reduced section) heat treated.

(a) Specimens were 6.35 mm (0.250 inch) wide in the reduced section.

(b) All specimens were solution treated 24 hours at 1170K (1650F) and water quenched prior to aging.

(c) No reduced section.

as a thin black line if facing toward the Pt-C source, or it will cast a long shadow if facing away. Because of the low shadowing angle, the shadow length is several times larger than the height of the step. A third feature which was prevalent in this study was a depression or crack associated with a slip step (referred to in the text as a "trench"). Since the surface relief of the replica is inverted from that of the metal surface, a trench appears as a ridge with a black line on one side and a shadow on the other.

Some 0.254 mm (0.010-in.) thick material of alloy 73 was prepared by cold rolling. Specimens 10.1 cm x 2.2 cm (4 in. x 0.75 in.) were prepared from this material, and vacuum annealed and heat treated as described above. These specimens were used for transmission electron microscopy (t.e.m.) studies of the precipitate microstructures and dislocation substructures representative of the various heat treatments. In the thin strip specimens plastic deformation was often extremely nonhomogeneous (on a macroscopic scale), especially in the aged condition. For these specimens the reported strains are average values measured over a 2.54 cm (1-in.) gauge length.

Specimens were thinned for t.e.m. by chemical polishing in nitric-hydroflouric acid (60% HNO_3-40% HF), to approximately 0.127 mm (0.005-in.) thickness, followed by electropolishing in a 6% perchloric acid-30% butanol-64% methanol solution.[38] Hydrogen contamination during electropolishing was avoided by keeping the electrolyte cooled below 240 K (-22 F).

Results

All of the heat treatments that were investigated are summarized in Table 17. Representative microstructures are shown in Figure 15. Following the solution treatment, 24 hr at 1170 K (1650 F), and water quench, the microstructure consisted of large, equiaxed alpha grains (average grain diameter $\simeq$ 60μm). Transmission electron microscopy (t.e.m.) revealed that the grains were completely recrystallized (Figure 15a), and there was no evidence of superlattice reflections in the electron diffraction patterns (Figure 15b). All of the aged specimens had pronounced DO_{19} superlattice reflections in their electron

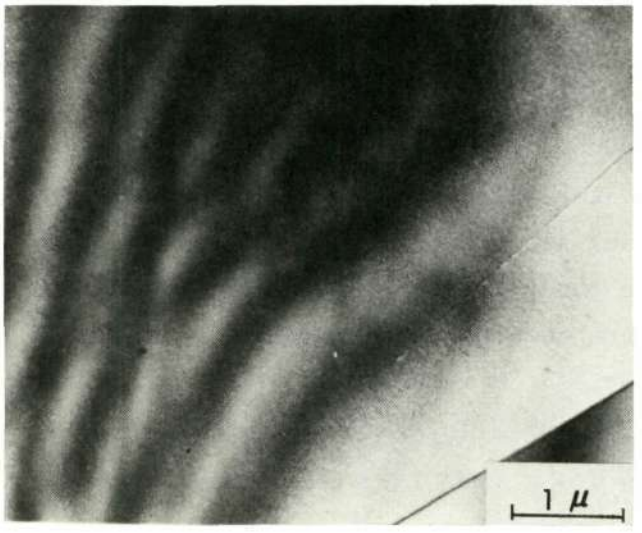

a. 24 hr at 1170 K (1650 F) W.Q., Bright-Field Micrograph

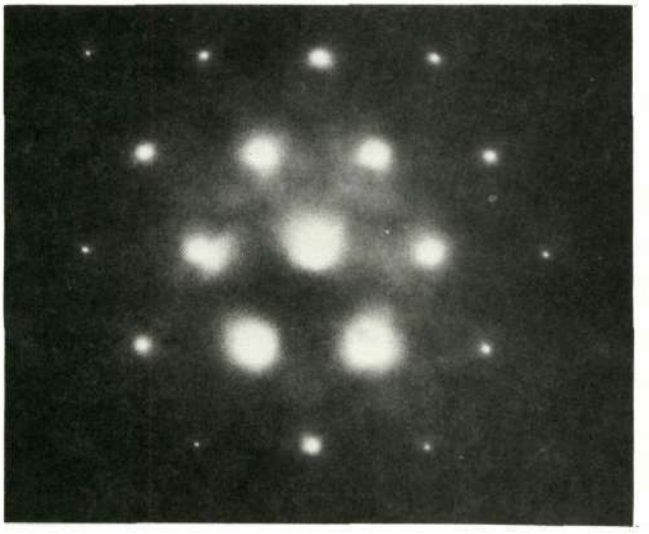

D.P.

b. Same as a, Diffraction Pattern

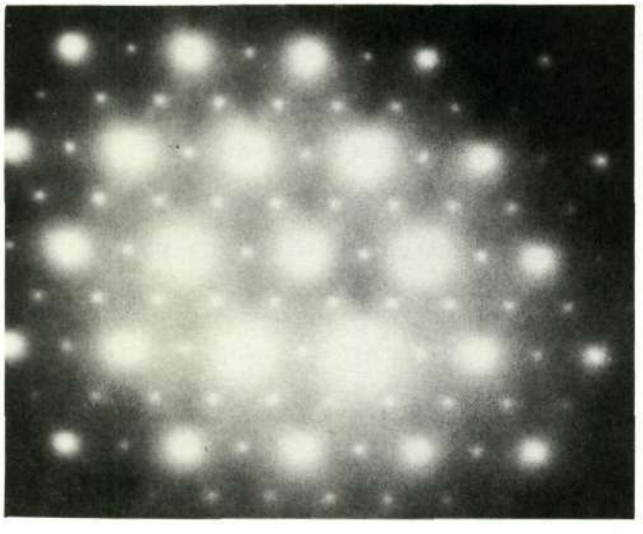

D.P.

c. Aged 100 hr at 770 K (930 F) Diffraction Pattern

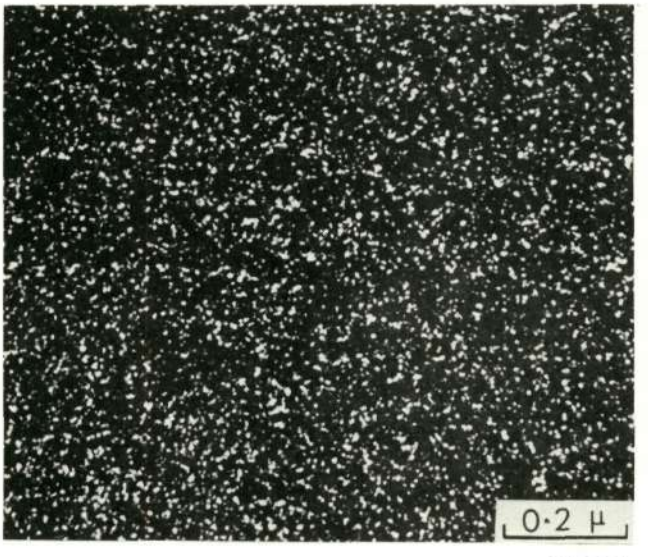

11095

d. Aged 100 hr at 770 K (930 F) Dark-Field Micrograph

FIGURE 15. REPRESENTATIVE MICROSTRUCTURES FOR VARIOUS HEAT TREATMENTS

This page is reproduced at the back of the report by a different reproduction method to provide better detail.

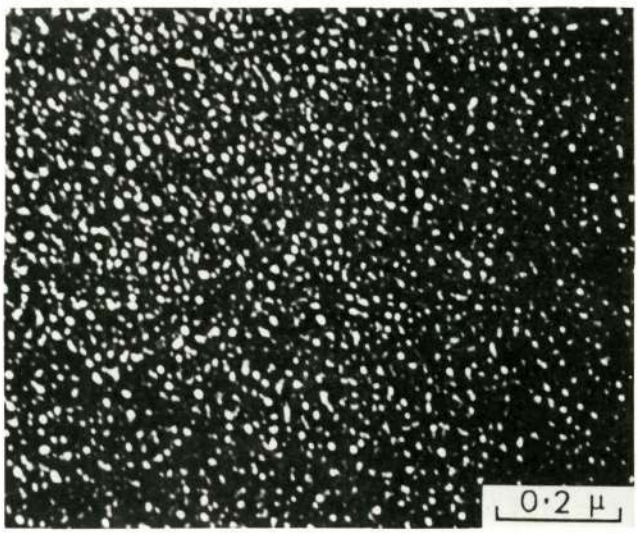

11163

e. Aged 22 hr at 920 K (1200 F)

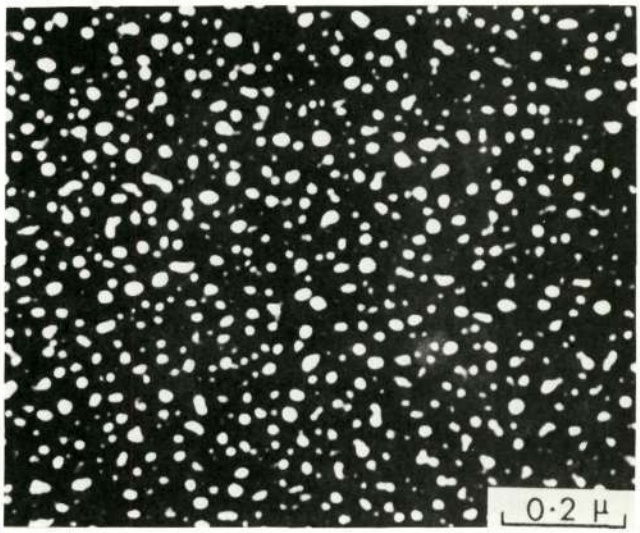

10793

f. Aged 100 hr at 920 K (1200 F)

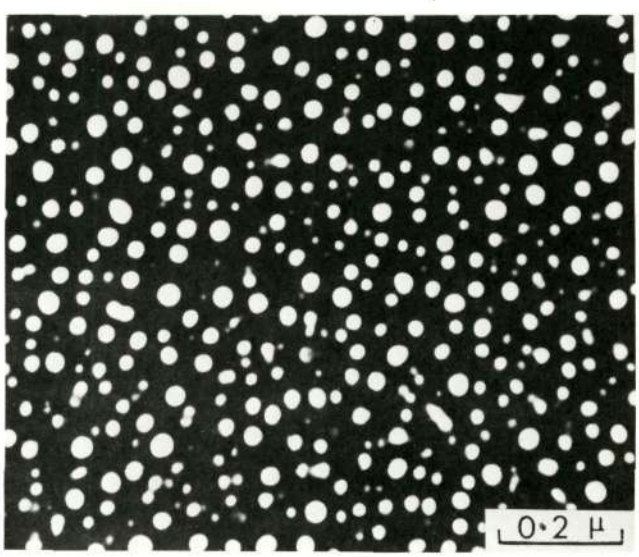

10745

g. Aged 500 hr at 920 K (1200 F)

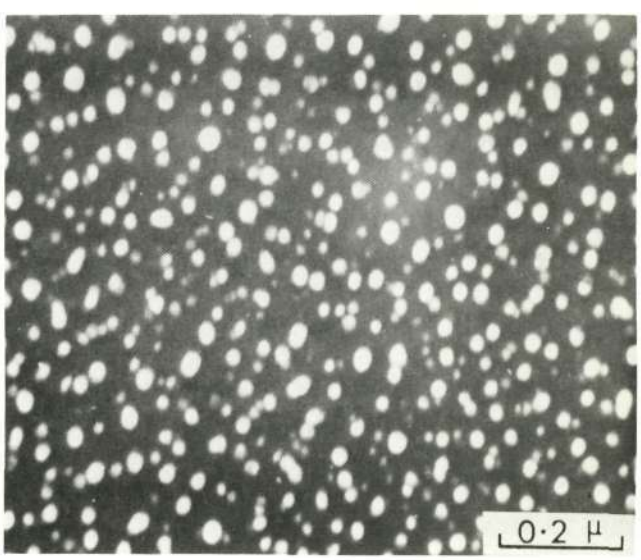

12780

h. Aged 500 hr at 970 K (1290 F)

FIGURE 15. (CONTINUED)

This page is reproduced at the back of the report by a different reproduction method to provide better detail.

diffraction patterns (Figure 15c), indicating the presence of long-range-ordered Ti_3Al. Dark-field micrographs taken using a superlattice reflection (usually $11\bar{2}0_{\alpha_2}$) revealed that the Ti_3Al was in the form of small, discrete particles (Figures 15d-15h). In all of the foil orientations which were examined the Ti_3Al particles were approximately spherical in shape. It has been reported elsewhere that in more concentrated Ti-Al alloys, and with higher aging temperatures than employed here, the Ti_3Al particles are elongated in the $[0001]_\alpha$ direction.[32,35] The particles appeared to be homogeneously nucleated throughout the grains and preferentially nucleated on grain boundaries. There was occasional evidence of preferential nucleation on isolated dislocations. The mean particle diameter varied from 25-30 A for the 100 hr at 770K (932 F) treatment (Figure 15d), to 180 A for the 500 hr at 920K (1200 F) treatment (Figure 15g). Matrix strain-field contrast was observed for the larger particles, but no effort was made to analyze it quantitatively.

The kinetics of coarsening of the Ti_3Al particles were investigated for the specimens aged at 920K (1200 F). Particle-size distributions were obtained for different aging times from t.e.m. prints by means of a Zeiss Particle Analyzer. At least 2000 particles were measured for each size distribution. If the particle-size distribution $n(d) \cdot \Delta d$ is defined as the number of particles per unit volume whose diameter is $d \pm \Delta\, d/2$, then the total number of particles per unit volume, Z, is $\sum_d n(d).\Delta d$. If the particles are truly coarsening by a volume diffusion-controlled process, any arbitrary initial size distribution will evolve to a well-defined steady-state size distribution.[39] Ardell and Nicholson[40] have shown that this requirement of the coarsening theory can be checked conveniently by plotting $9\,\bar{d}\,n(d)/4Z$ against ρ, and comparing it with the theoretical function $\rho^2 h(\rho)$, where $\rho = d/\bar{d}$ and

$$h(\rho) = \left(\frac{3}{3+\rho}\right)^{7/3} \left(\frac{3/2}{3/2-\rho}\right)^{11/3} \exp\left(\frac{-\rho}{3/2-\rho}\right) \; ; \; \rho < 3/2$$

$$h(\rho) = 0 \; ; \qquad \rho \geq 3/2 \qquad (1)$$

The normalized particle-size distributions are plotted this way in Figure 16 (solid lines). In some cases two independent determinations were made. The "steady-state" function $\rho^2 h(\rho)$ is shown by the broken lines.

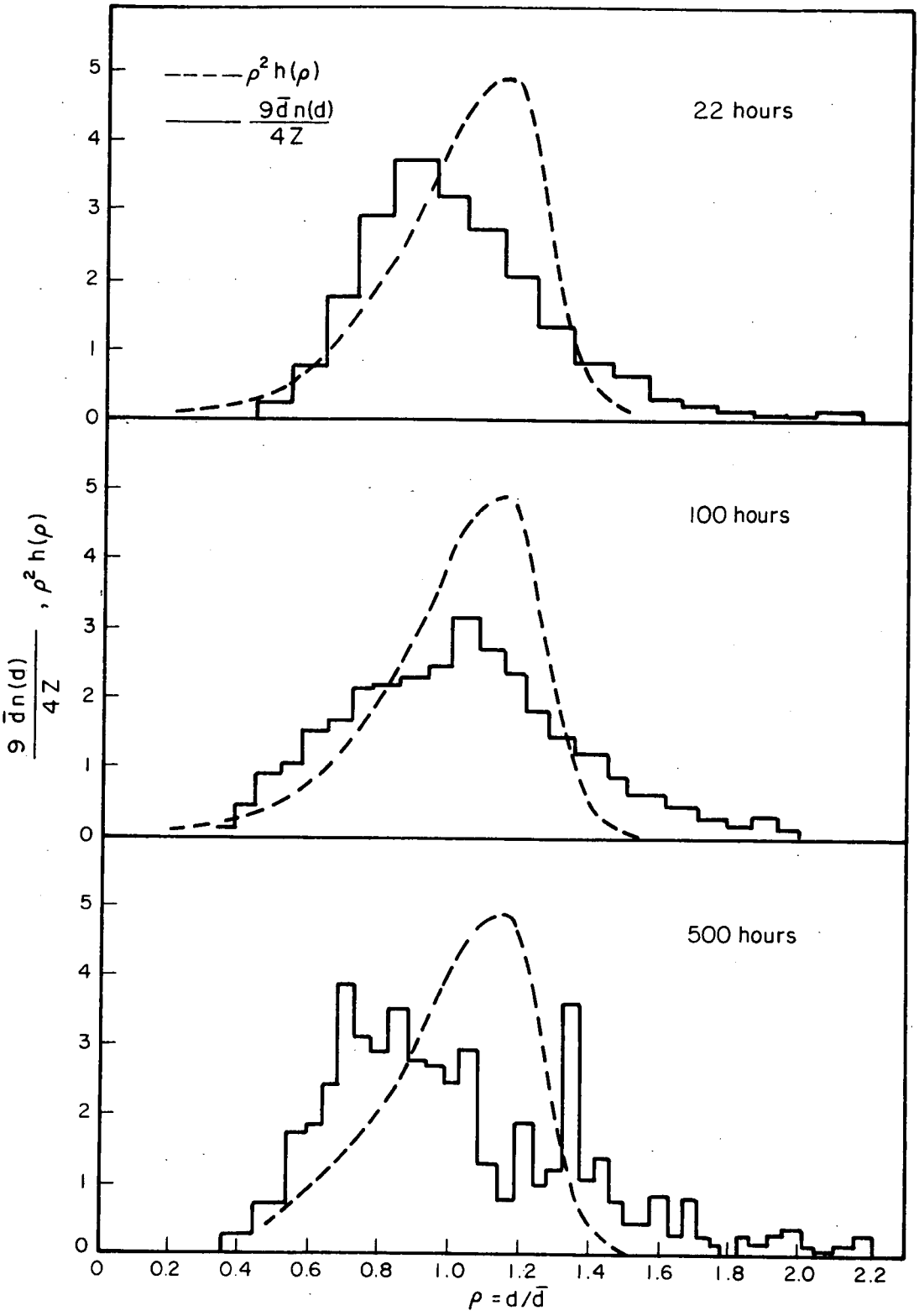

FIGURE 16. EXPERIMENTALLY DETERMINED PARTICLE-SIZE DISTRIBUTIONS FOR DIFFERENT AGING TIMES AT 920 K (1200 F) PLOTTED AS $9\bar{d}n(d)/4Z$ AGAINST $d/\bar{d}$ (SOLID LINE) AND COMPARED WITH THE THEORETICAL STEADY-STATE DISTRIBUTION (BROKEN LINE)

The agreement between the measured size distributions and the theoretical function is sufficiently good in each case to conclude that during aging the Ti_3Al particles are truly coarsening. For coarsening which is controlled by diffusion in the matrix the particle growth rate is given by:[39]

$$\bar{d}^3 - \bar{d}_o^3 = \frac{128\,\gamma\,D\,C_o\,V_m^2}{9\,\pi\,RT}(t - t_o) \qquad (2)$$

where $\bar{d}_o$ is the mean particle diameter at the onset of coarsening, $(t = t_o)$, γ is the particle-matrix interfacial free-energy, D is the diffusivity of aluminum in titanium, C_o is the equilibrium molar concentration of aluminum in titanium at the aging temperature, V_m is the molar volume of Ti_3Al, and RT has its usual meaning. $\bar{d}^3$ is plotted against t in Figure 17, and a least-squares analysis gives the slope of the best-fit line to be 2.88×10^{-24} cm^3-sec^{-1}. Using this experimental value and appropriate values for the other quantities in Equation (2)*, γ is calculated to be of the order of 10^{-5} ergs-cm^{-2}. Additional data at 920K (1200 F) and other aging temperatures are required for a proper evaluation of γ, but it seems safe to conclude that the α-Ti_3Al interfacial energy is negligibly small. This is consistent with the observation that the precipitate-matrix interface was coherent for all the heat treatments that were investigated. The most important consequence of the extremely slow coarsening kinetics is that isothermal aging is not a very efficient method for producing widely different Ti_3Al size distributions.

The stress-strain curves for the 0.635 mm (0.025 in.) thick specimens, unaged, and aged 100 hr at 770K (930 F) are shown in Figure 18. Aging for 100 hr at 770K (930 F) did not significantly change the yield stress or fracture elongation in air, but it did alter the shape of the stress-strain curve. The aged specimens exhibited a yield drop and Lüders extension, whereas these effects were absent for the unaged specimens. When tested in saltwater, the aged specimens failed by subcritical crack growth after approximately 10 percent strain, whereas the tensile properties of unaged specimens were unaffected by a saltwater environment.

* T = 920 K, r = 8.31×10^7 ergs-gm $mole^{-1}$-K^{-1}, D = 1.5×10^{-10} cm^2-sec^{-1} (41), C_o = .0128 gm mole-cm^{-3} (43), V_m = 40.1 cm^3-gm $mole^{-1}$.

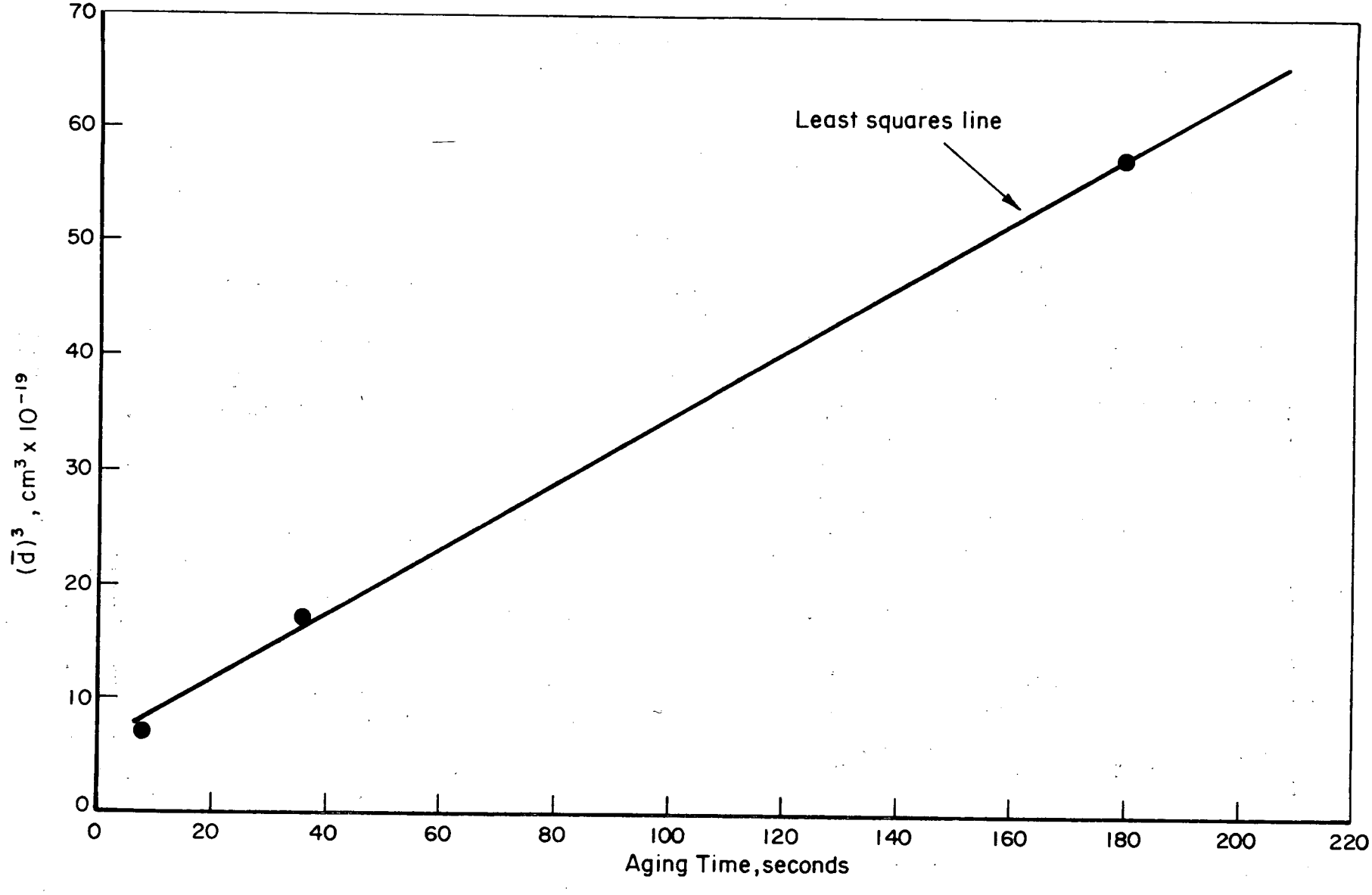

FIGURE 17. PARTICLE COARSENING RATE FOR Ti_3Al AGING AT 920 K (1200 F), PLOTTED AS $\bar{d}^3$ AGAINST t

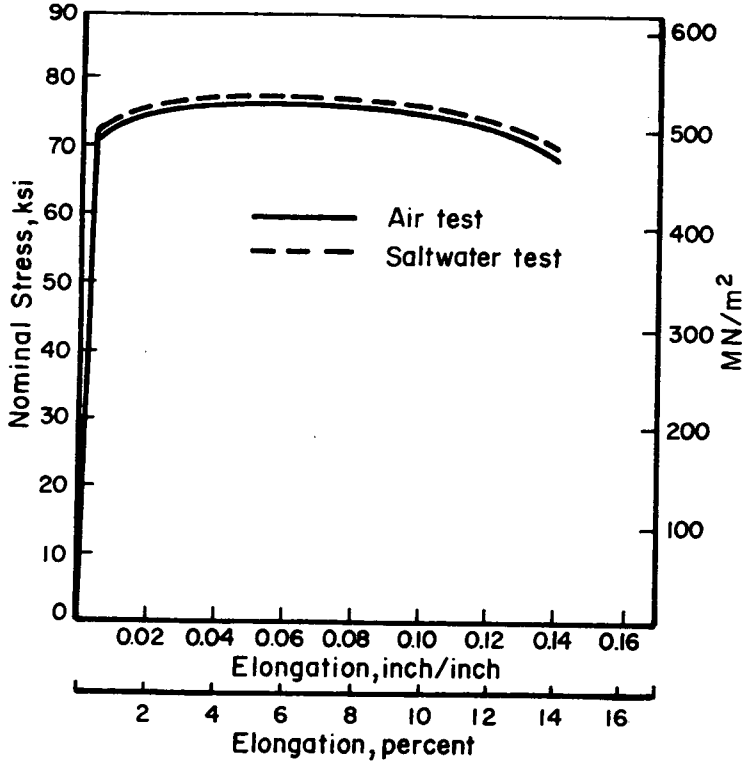

a. 24 Hr at 1170 K (1650 F) W.Q.

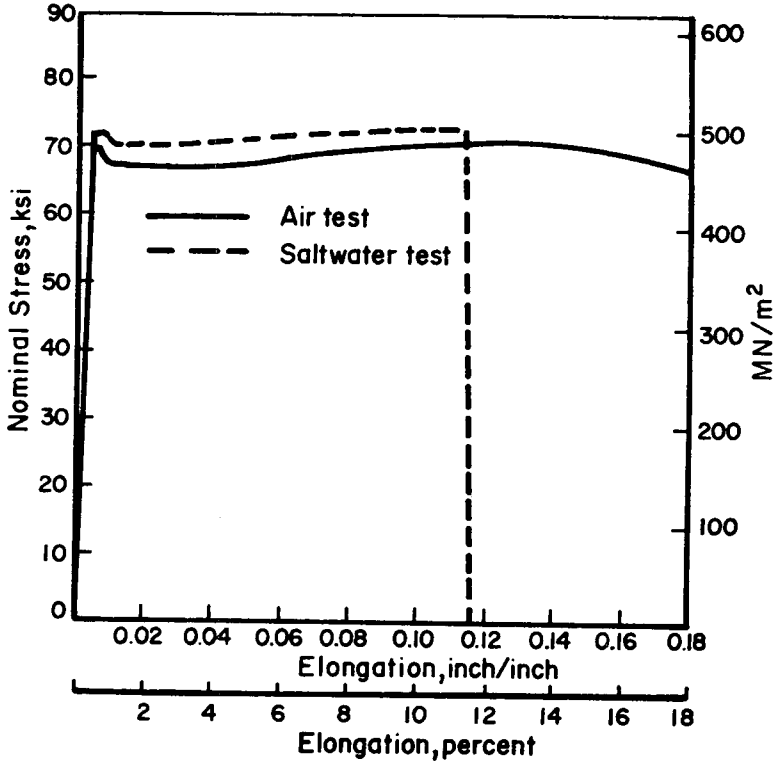

b. 24 Hr at 1170 K (1650 F) W.Q.
+ 100 hr at 770 K (930 F) AC

FIGURE 18. STRESS-STRAIN CURVES FOR 0.635-MM (0.025-IN.) THICK SPECIMENS DEFORMED IN AIR AND IN SALTWATER

The surface slip lines on deformed specimens also showed an effect of heat treatment. In the single-phase material (unaged), slip was nonhomogeneous in that it was generally confined to bands which had an average spacing of 0.2-2 μm ($\sim 10^3$-10^4 b). However, there was much evidence of bands which were wavy on a fine scale (Figure 19a), and often, in the vicinity of an obstacle such as a grain boundary or another slip band, a coarse slip band would disintegrate into a region of fine wavy slip (Figure 19b). By contrast, the slip bands in the aged material were exceedingly straight or composed of perfectly straight segments, and this slip character persisted up to the point of fracture (Figure 20). There was rarely any fine, wavy slip such as that which occurred in the single-phase material. Instead, cracks often formed where slip bands intersected grain boundaries or other slip bands (e.g., Figure 20b at A). Another feature characteristic of the slip bands in the aged material was the existence of trenches along the slip steps. This feature appeared in the two-stage replicas as a black line adjacent to a white shadow (Figures 21b and 21c). The shadows from the trenches were usually very ragged, suggesting the contours of the trenches were quite irregular. The trenches occurred in aged specimens deformed in air as well as in those deformed in saltwater, provided the strain was more than about 5 percent. Trenches were found in approximately half of the grains, and they were specific to a particular slip system in a given grain. For example, in grains deforming by multiple slip, trenches could be found on nearly every slip band belonging to only one or perhaps two of the systems, but were not evident on the remaining slip systems in the grain (Figure 21b).

The dislocation substructures, as revealed by t.e.m., were quite similar in both the aged and unaged specimens. At the low strains which were investigated both alloy conditions produced coplanar arrays of $\frac{a}{3}\langle 11\bar{2}0\rangle$ dislocations lying predominantly on $\{1\bar{1}00\}$ and (0001) (Figures 22 and 23). There was more evidence of cross slip between $\{1\bar{1}00\}$ and (0001) in the single-phase material than in the alloy containing Ti_3Al precipitates (Figure 22b). In the aged specimens the dislocation arrays were somewhat narrower and more rigorously planar. Dark-field microscopy of aged specimens revealed that the density of Ti_3Al particles was much lower in the slip bands than throughout the rest of the grains (Figure 23). The particles which were

a. ε = .02

b. ε = .05

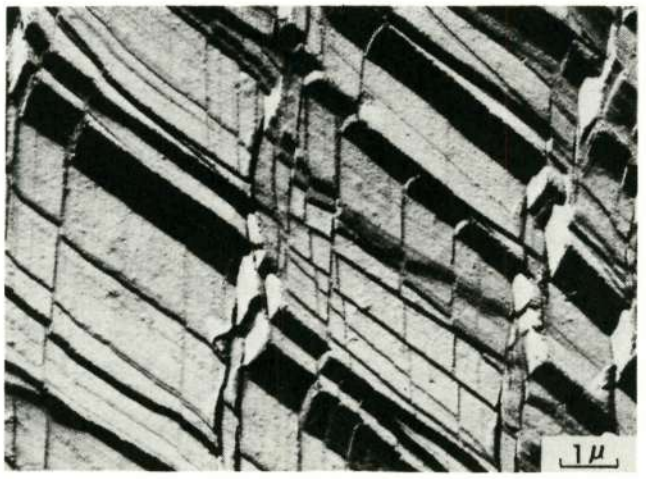

c. Adjacent to Fracture

FIGURE 19. SURFACE SLIPLINES FOR 0.635-MM (0.025-IN.) THICK SPECIMENS, 24 HR AT 1170 K (1650 F), W.Q., DEFORMED IN AIR

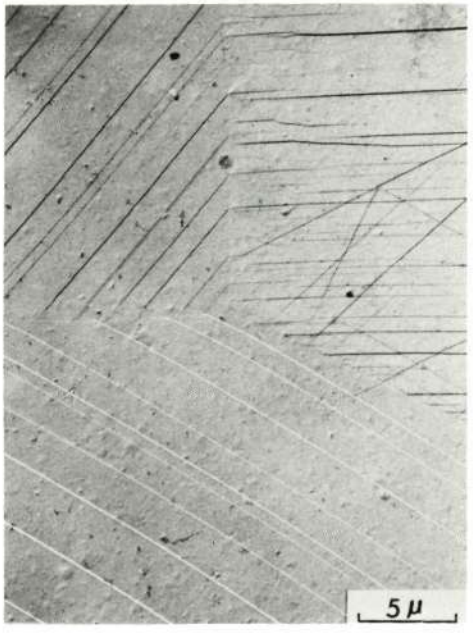

a. ε = .02

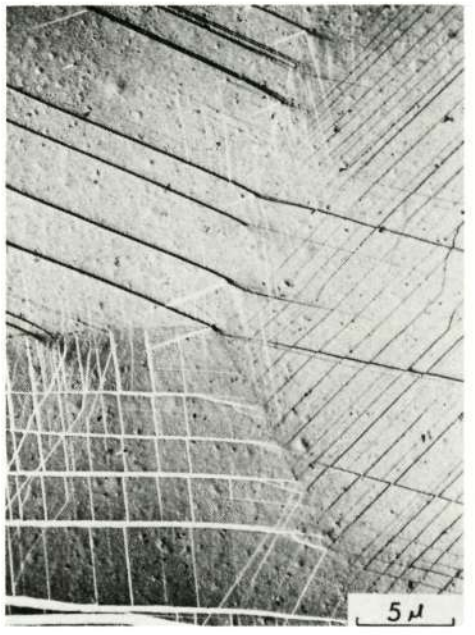

b. ε = .05

c. Adjacent to Fracture

FIGURE 20. SURFACE SLIPLINES FOR 0.635-MM (0.025-IN.) THICK SPECIMENS, 24 HR AT 1170 K (1650 F), W.Q., + 100 HR AT 770 K (930 F) DEFORMED IN AIR

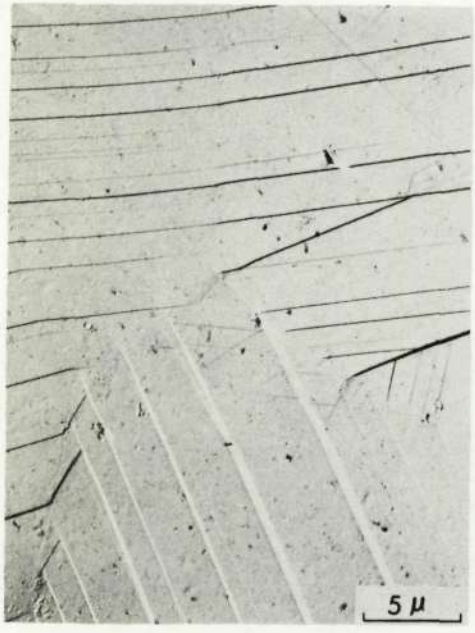

a. ε = .02

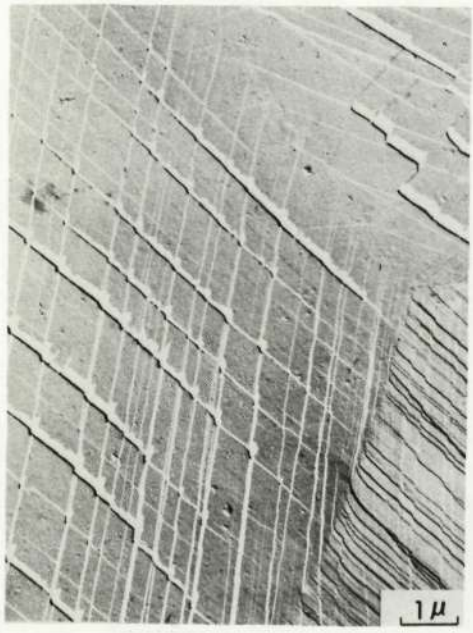

b. ε = .05

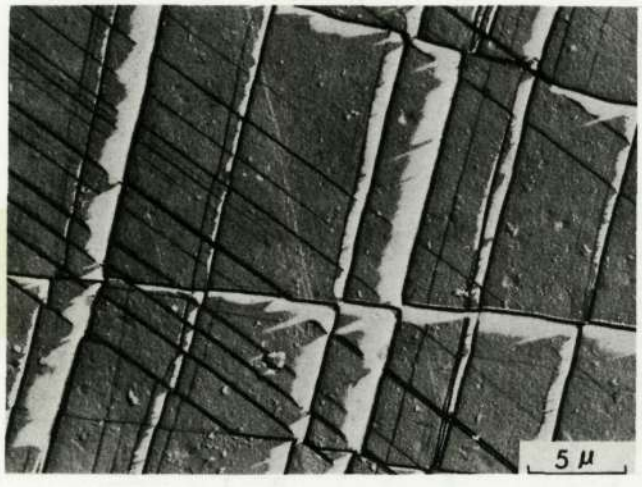

c. Adjacent to a Stress-Corrosion Crack

This page is reproduced at the back of the report by a different reproduction method to provide better detail.

FIGURE 21. SURFACE SLIPLINES FOR 0.635-MM (0.025-IN.) THICK SPECIMENS, 24 HR AT 1170 K (1650 F), W.Q., + 100 HR AT 770 K (930 F) DEFORMED IN SALTWATER

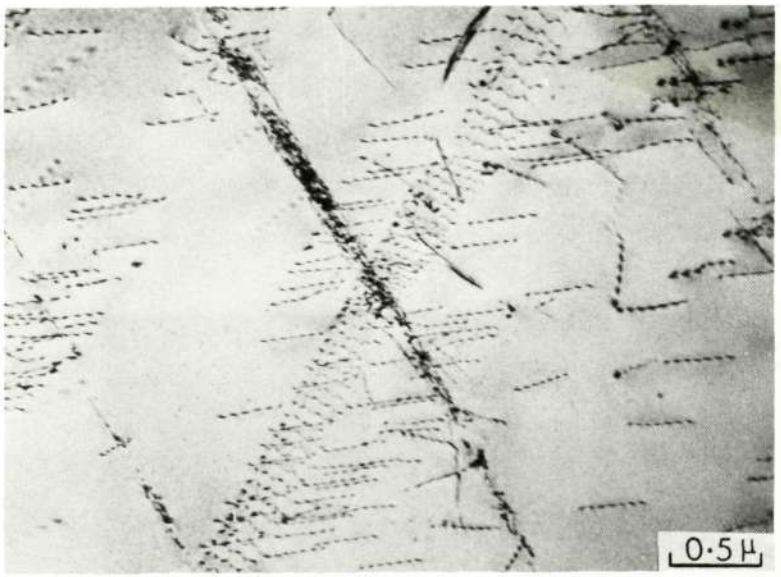

a.

b.

This page is reproduced at the back of the report by a different reproduction method to provide better detail.

FIGURE 22. DISLOCATION SUBSTRUCTURES IN 0.254-MM (0.010-IN.) THICK SPECIMENS, 24 HR AT 1170 K (1650 F), W.Q., + 100 HR AT 770 K (930 F), $\bar{\varepsilon}$ = .02

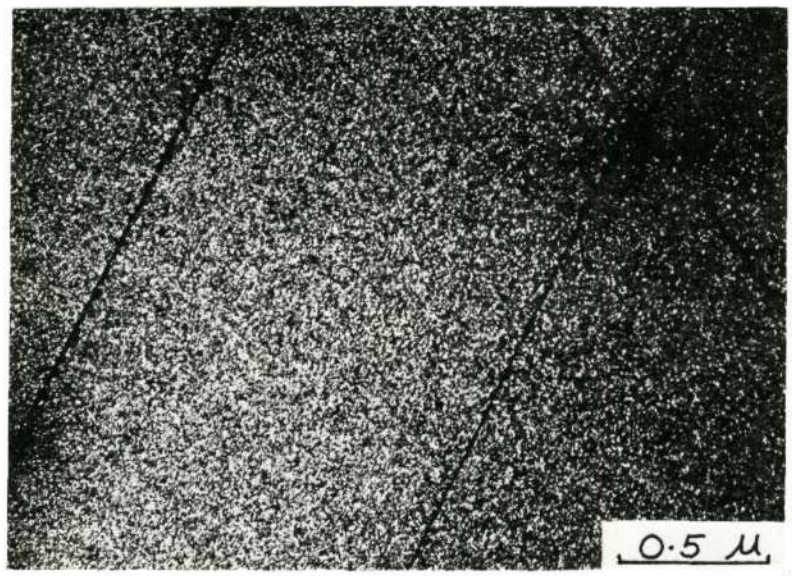

FIGURE 23. SLIP BANDS IN 0.254-MM (0.010-IN.) THICK SPECIMENS, 24 HR AT 1170 K (1650 F), W.Q., + 100 HR AT 570 K (930 F), $\bar{\varepsilon}$ = .01, DARK-FIELD MICROGRAPH

This page is reproduced at the back of the report by a different reproduction method to provide better detail.

visible in a slip band had much weaker images than the others, and in some areas of slip bands there were no particles visible whatsoever.

The results of the tensile tests on the 1.27 mm (0.050-in.) thick specimens are given in Figure 24. Qualitatively the tensile properties of these specimens were the same as for the 0.635 mm (0.025-in.) thick specimens. That is, there was no significant change in the yield stress during aging at 770 K (930 F) but the aged specimens did exhibit a yield point and Lüders extension. However, the thicker specimens consistently had higher yield stresses than the thin specimens.

The stress-strain curves for the 1.9 mm (0.075 in.) thick specimens aged at 920 K (1200 F) are given in Figures 25 (air tests) and 26 (saltwater tests). These data were qualitatively similar to those for specimens aged at 770 K (930 F) but the effects of aging were more pronounced. Note that the yield stresses were all higher than the previous measurements. There was a small increase in the yield stress for aging time up to 1000 hr at 920 K (1200 F). There was a yield point and negligible rate of work hardening in the aged specimens for aging times up to 100 hr. With longer aging times the yield point disappeared, and the stress-strain curve was similar to that for the unaged specimens. The yielding behavior in saltwater was identical to that in air, but those specimens which had been aged for 100 hr. or longer failed by subcritical crack growth. The 100-hr specimen failed in this manner while necking, but the 500-hr and 1000-hr specimens failed after approximately 3 and 6 percent elongation respectively. Thus, there was a very pronounced effect of aging time at 920 K (1200 F) on the stress-corrosion behavior.

T.e.m. of specimens which had been aged at 920 K (1200 F) and 970 K (1290 F), and deformed, also indicated that the density of particles was much lower in the slip bands than in the undeformed areas (Figures 27 and 28*). This effect was easier to study in the specimens aged at these higher temperatures because the Ti_3Al particles were so much larger than those in the 770 K (930 F) specimens. Direct evidence of particle shearing in slipbands was easily observed in these specimens, and there was no evidence of dislocations bowing around Ti_3Al particles.

---

* These results indicate that the $\alpha/\alpha+Ti_3Al$) phase boundary given by Blackburn[43] is somewhat incorrect in the vicinity of 970 K(1290 F) and 8 weight percent aluminum. The phase boundary indicated by the results of Lütjering and Weissmann appears to be more accurate.

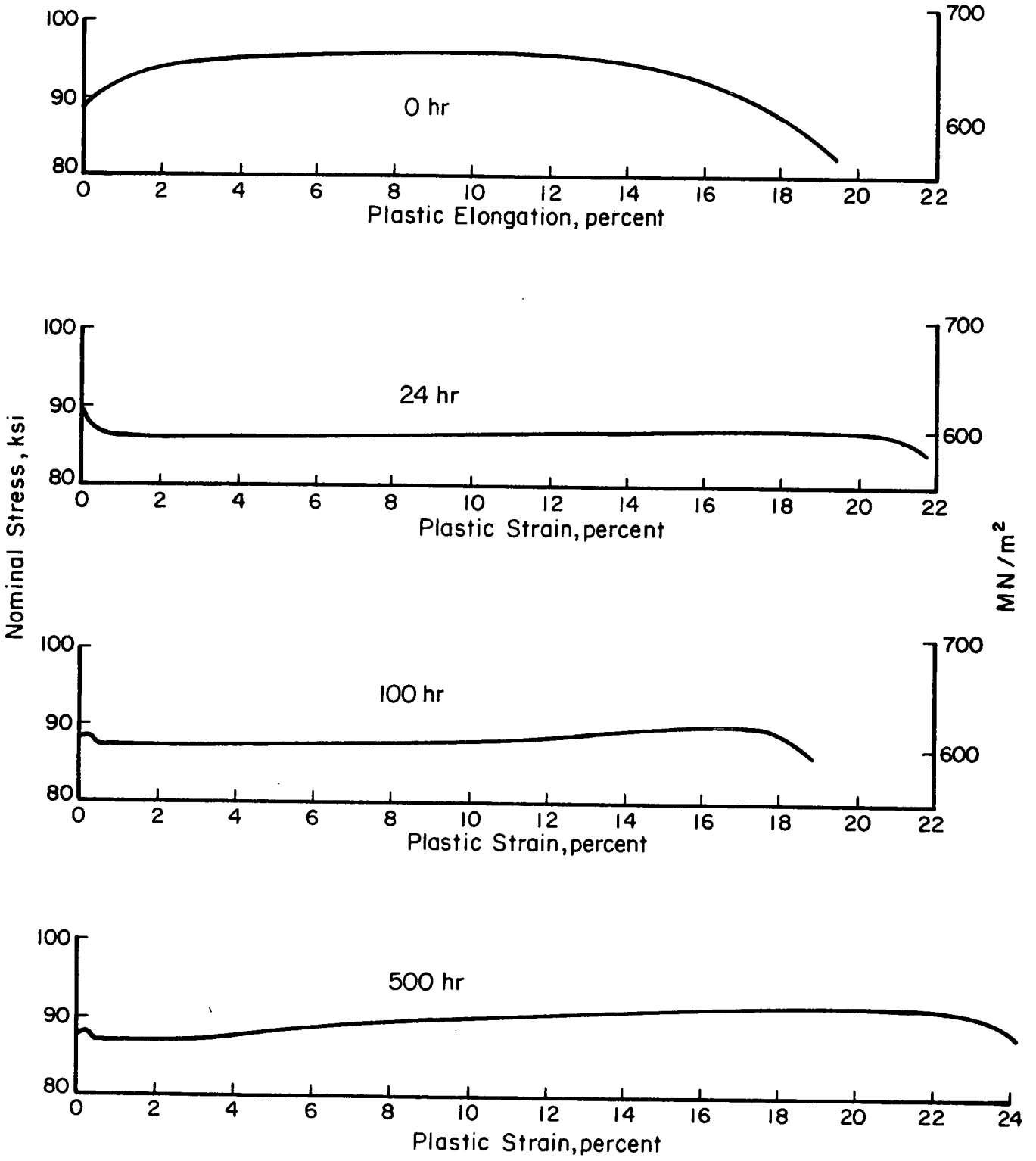

FIGURE 24. STRESS-STRAIN CURVES FOR 1.27-MM (0.050-IN.) THICK SPECIMENS, AGED FOR VARIOUS TIMES AT 770 K (930 F), DEFORMED IN AIR

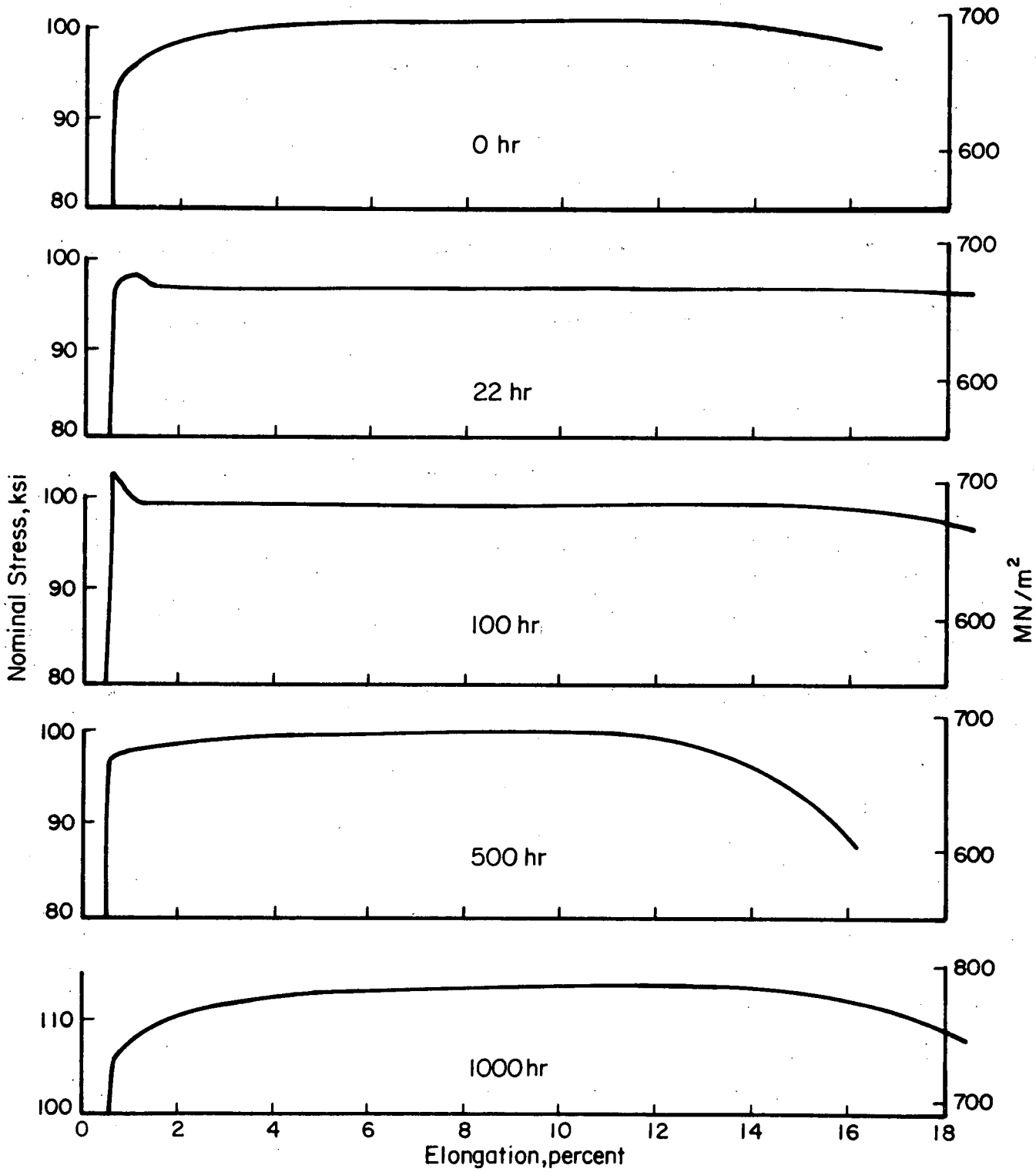

FIGURE 25. STRESS-STRAIN CURVES FOR 1.9-MM (0.075-IN.) THICK SPECIMENS, AGED FOR VARIOUS TIMES AT 920 K (1200 F), DEFORMED IN AIR

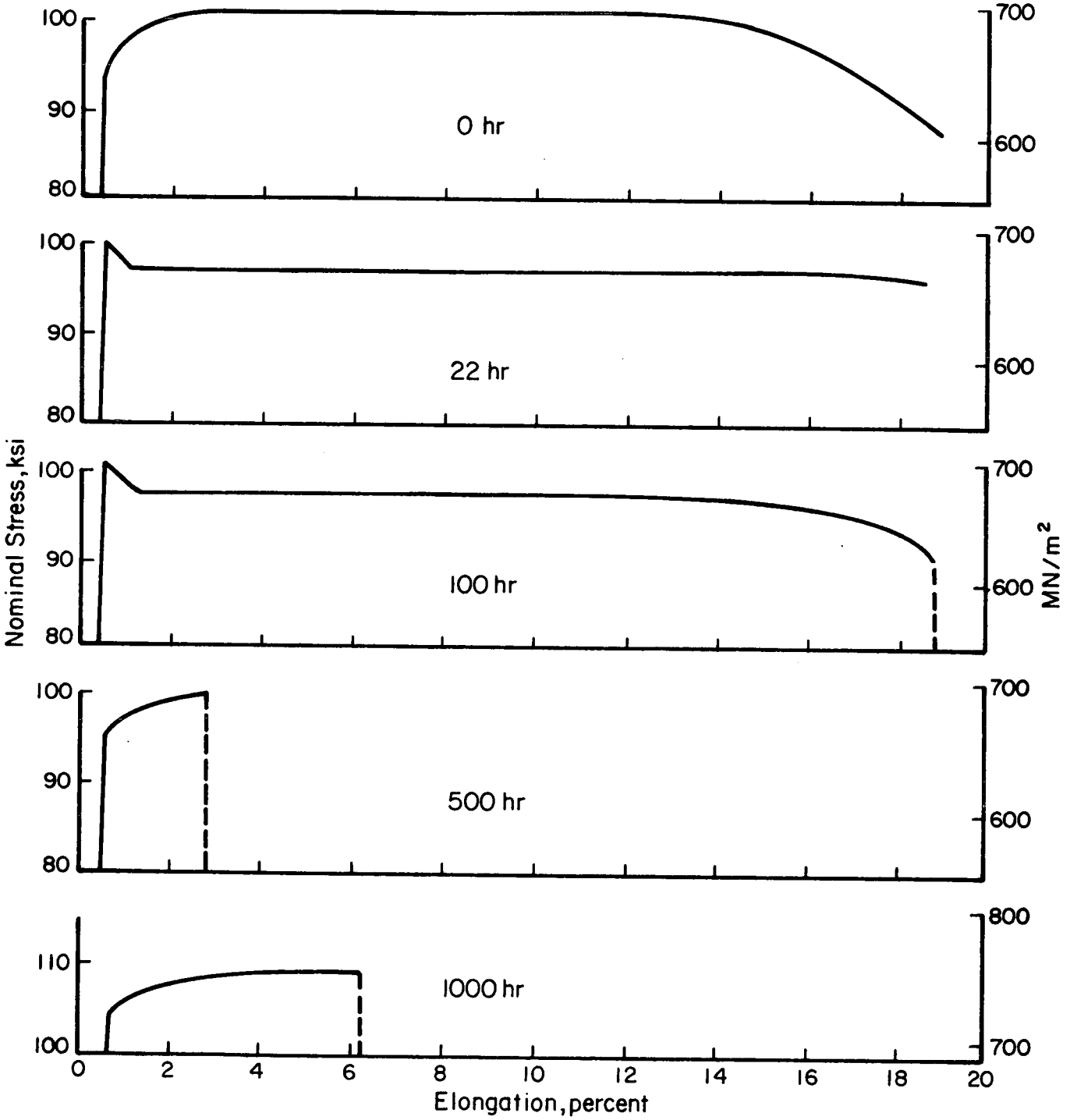

FIGURE 26. STRESS-STRAIN CURVES FOR 1.9-MM (0.075-IN.) THICK SPECIMENS, AGED FOR VARIOUS TIMES AT 920 K (1200 F), DEFORMED IN SALTWATER

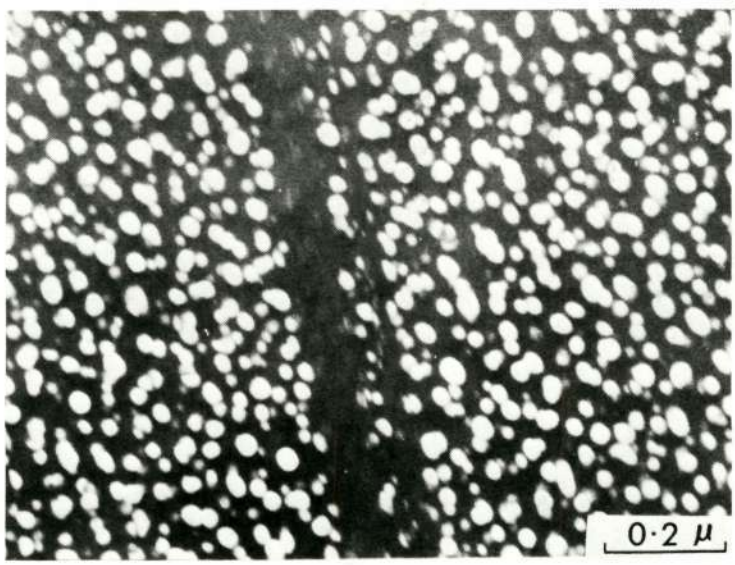

FIGURE 27. SPECIMENS OF 0.254-MM (0.010-IN.) THICKNESS AGED 500 HR AT 920 K (1200 F), $\bar{\varepsilon}$ = .01, SHOWING SHEARED PARTICLES IN A SLIP BAND

This page is reproduced at the back of the report by a different reproduction method to provide better detail.

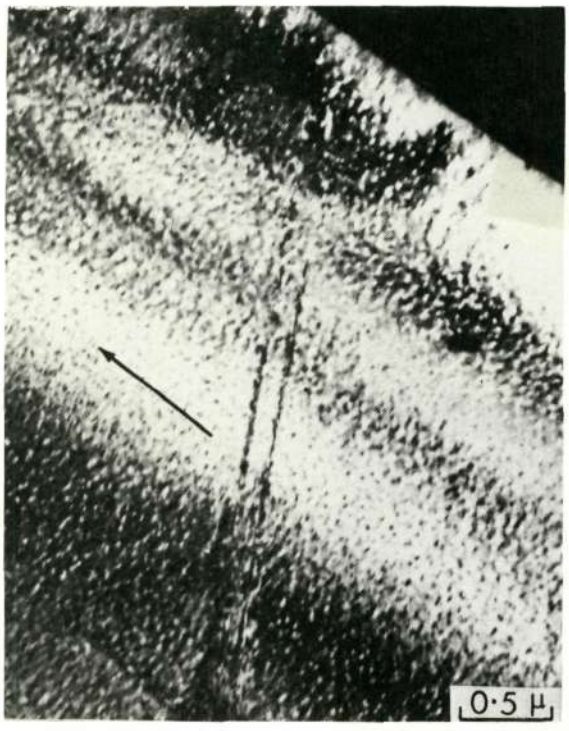

12784

a. Bright Field, $\underline{g} = 11\bar{2}0$

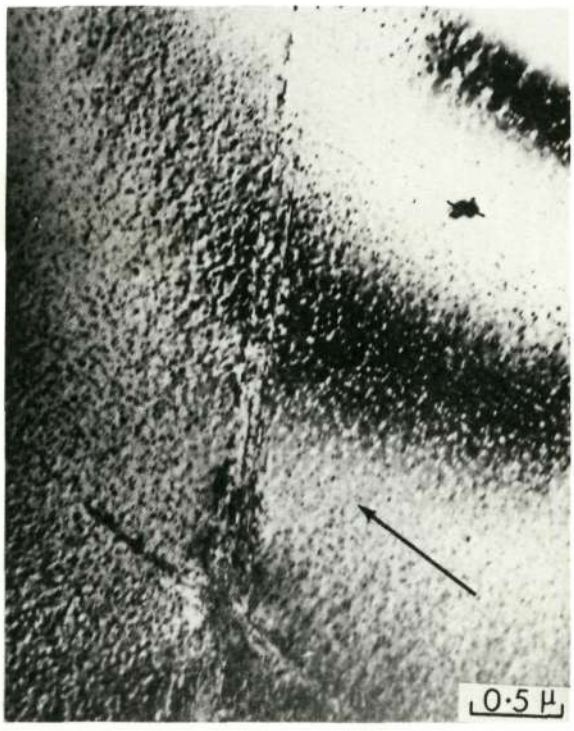

12775

b. Same Area, Dark field, $\underline{g} = 11\bar{2}0\alpha$

12776

c. Same Area, Dark Field, $\underline{g} = \overline{11}20\alpha_2$

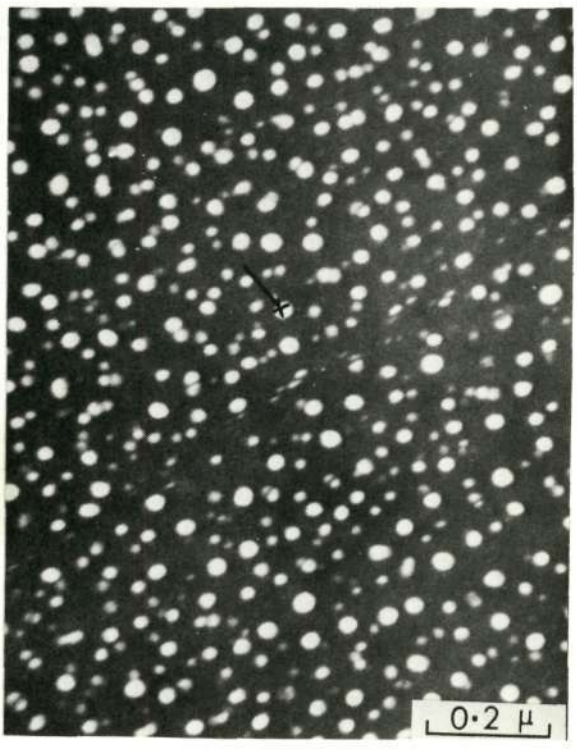

12778

d. Same Area, Dark Field, $\underline{g} = \overline{11}20\alpha_2$

FIGURE 28. SPECIMENS OF 0.254-MM (0.010-IN.) THICKNESS AGED 500 HR AT 970 K (1290 F), $\bar{\varepsilon} = .01$

Arrows indicate diffraction vectors.

Discussion

The tensile data reported in Figures 18, 24, 25, and 26 show that, although there was little scatter in the results of a given set of specimens, there was a wide variation in the measured yield stresses over the whole program. In searching for the cause of this discrepancy it was noted that the values of the yield stress of titanium-aluminum alloys reported in the literature range from 520 MN/m^2 (75 ksi)[35] to 760 MN/m^2 (110 ksi)[32,42] for compositions and heat treatments similar to those employed in the present work. The yield stresses reported here range from 470 MN/m^2 (68 ksi) to 730 MN/m^2 (106 ksi). It is believed that these inconsistencies are due to oxygen contamination which occurs during high temperature processing and heat treatment. In the work reported in references 32 and 42, which produced high yield stresses, the specimens were sealed in evacuated tubes for heat treatment, whereas in the work reported in reference 35, which produced low yield stresses, the specimens were sealed in tubes and heat treated in a dynamic vacuum. In the present work various amounts of material were removed from the specimen surfaces prior to testing thereby eliminating various amounts of contamination. Note that the measured yield stresses varied inversely with the amount of material that was removed by surface grinding. Therefore, it is considered that the tensile data for the 0.635 mm (0.025 in.) thick specimens are the most accurate, and that the surface slip lines observed on these specimens are good representations of the surface slip character.

The t.e.m. observations indicate that the Ti_3Al particles are sheared by the glide dislocations for all of the heat treatments that were investigated. Furthermore, the weak dark-field images of the sheared particles and the sharply reduced density of visible particles in slip bands suggests that the long-range-ordered structure of the particles is destroyed by the slip process. This could occur by the dissolution of fragmented Ti_3Al particles in the slip band, or by an increase in the density of antiphase boundary (APB) in the particles. Alternatively, the apparent low density of particles in the slip bands could be entirely a diffraction-contrast effect. The contrast from the particles is extremely sensitive to the orientation of the specimen relative to the electron beam. Local lattice rotations due to the residual dislocations in the slip band

could make contrast conditions poor for particles in a slip band when they are optimum for matrix precipitates. However, this does not appear to be the cause of the observed effects, because it was not possible to improve the contrast from the particles in a slip band by tilting the specimen. Regardless of the precise description of the precipitates in the slip bands, two important conclusions can be drawn from the observations:

(1) Slip should tend to concentrate in preexisting slip bands because the areal fraction of precipitates per slip plane decreases with the passage of each glide dislocation. Therefore, slip should be nonhomogeneous and planar because it will be difficult for a dislocation to cross slip into an unsheared region.

(2) The chemical potential of the volume of material in a slip band should be higher than the adjacent matrix if the sheared particles redissolve, if the particles in the slip bands have a higher density of APB's, or if they are smaller than the matrix particles (Gibbs-Thompson effect).

Thus, the nonhomogeneous, planar slip character observed for the aged material is consistent with the particle-shearing mechanism. The slip character in the single-phase material is also nonhomogeneous, probably due to short-range order, but in this material cross slip can occur readily on a fine scale (< 25 A). By contrast the slip bands in the aged material are rigorously planar, and there is little evidence of fine, wavy slip. In both alloy conditions the rates of work hardening are low, but only the aged alloy shows a yield drop and Lüders extension. This is also consistent with the particle-shearing mechanism.

The particle-shearing mechanism also accounts for the occurrence of trenches in the aged alloy. The irregular contours of the trenches and their appearance in the early stages of formation as discrete holes along a slip band suggests that they form by localized chemical attack[34], which is promoted by the enhanced chemical potential of the slip bands and the larger surface slip offsets in the aged material. Conversely, in the single-phase material a passivating reaction should dominate when a fresh slip step is produced because the slip steps are smaller and more closely spaced, and there is no gradient in chemical potential between a slip band and the adjacent matrix, other than the small

effect due to the elastic strain energy of the residual dislocations in the slip band. For all of the mechanisms discussed above the chemical potential of a slip band should increase with increasing shear strain. The observations indicate that for specimens aged at 770 K (930 F) conditions are not suitable for trench formation until the average strain is approximately 5 percent. It is likely that this minimum strain for trench formation also depends on the size distribution of the Ti_3Al particles. For instance if the enhanced chemical potential of the slip bands is due to particle dissolution or the Gibbs-Thompson effect, then it is expected that the minimum strain required before trenches are observed will increase rapidly with increasing mean-particle diameter. These qualitative mechanisms are quite plausible for the specimens deformed in an aqueous environment, but it is difficult to explain why trenches occur as frequently in air. For the present it must be assumed that sufficient moisture is available from the atmosphere and from the materials used for replication to support the postulated chemical reactions.

Despite the significant effect of the ordered Ti_3Al precipitates on the slip character, there is little change in the absolute value of the yield stress. There is negligible change in the yield stress during aging at 770 K (930 F) and only a 12 percent increase in the yield stress after aging 1000 hr at 920 K (1200 F). When the particles are cut by the glide dislocations, the dominant strengthening mechanism is the production of APB in the sheared particles. Calculations show that the expected strengthening effect due to this mechanism in titanium-aluminum alloys containing Ti_3Al is indeed very small[32]. Although in this study Ti_3Al does not have a significant effect on the tensile ductility of titanium-8 percent aluminum, it is known to sharply reduce the fracture toughness measured in notched specimens[2]. This can be rationalized by the fact that the nonhomogeneous, planar slip character, which occurs in alloys containing deformable Ti_3Al particles, causes large shear offsets and coplanar pileups of dislocations at obstacles. These conditions promote microvoid nucleation. The nonhomogeneous planar slip character also permits void coalescence by localized shear. Following this reasoning it would be expected that the fracture toughness should be improved when the glide dislocations bypass the particles.

The results of Lütjering and Weissmann[35] appear to support this model. In view of the apparent effect of oxygen contamination on the yield stress of heat treated specimens, some of the available fracture data on titanium-aluminum alloys may be dubious.

The results of the current study indicate a very pronounced effect of aging on the fracture behavior of titanium-8 percent aluminum in saltwater. Since the yield stress does not change appreciably during aging, the stress-corrosion cracking behavior of this alloy must be influenced specifically by the amount and/or size distribution of Ti_3Al. The results for the specimens aged at 770 K (930 F) indicate that the appearance of trenches at the surface slip steps correlates with a susceptible condition. Furthermore, the critical plastic strain required for trench-formation is always somewhat less than that for the onset of subcritical cracking. This suggests that the nonhomogeneous, planar slip character and the enhanced chemical potential of the slip bands caused by the deformable Ti_3Al particles are important factors in the stress-corrosion mechanism. Since the mechanism of subcritical cracking appears to be cleavage on planes near $(0001)_\alpha$[31], it is not likely that the "active" $\{10\bar{1}0\}$ slip bands form a major part of the crack path. Rather, it can be argued that the combination of widely spaced, narrow slip steps, which have a higher chemical potential than the matrix, favor a sustained anodic reaction at the specimen surface. In the absence of these factors the system would be strongly passivating. This reasoning has been discussed in detail by Scully[44]. It does not consider the actual mechanism of crack extension. Instead, it takes the view that the anodic surface reaction is the first necessary event for stress corrosion to proceed, and therefore should be considered first. It also follows that if the conditions for rapid passivation can be maintained, stress-corrosion will not occur, and the problem is solved.

Qualitatively, it would seem that the effects of the Ti_3Al particles on the homogeneity of slip and the chemical potential of the slip bands should be most pronounced for the smallest particle sizes. That is, the strain required to achieve the necessary conditions for the sustained, anodic surface reaction should increase with increasing particle size. However, the results from the specimens aged at 920 K (1200 F) do not bear this out. In fact, quite the opposite was observed, since only those specimens aged longer than 100 hr at 920 K (1200 F)

exhibited sub-critical cracking (Figure 26). Cavallaro and Wilcox[33] reported a similar increase in stress-corrosion susceptibility with aging time at 920 K (1200 F) for titanium-7 percent aluminum, but these results also indicated a decrease in susceptibility for aging times on the order of 500 hr, which was not observed in the present work.

Conclusions

A detailed study was made of the relation between the size distribution of Ti_3Al particles in a Ti-8Al alloy and the tensile properties measured in air and in saltwater. The size distribution of Ti_3Al was varied by isothermal aging for various times at temperatures in the range 770 to 970 K (930 to 1290 F). The aging kinetics were found to be relatively slow. Quantitative measurements of the particle coarsening rate at 920 K (1200 F) showed good agreement with the predicted behavior for coarsening controlled by matrix diffusion, and suggested that the specific free energy of the Ti_3Al-α interface is negligible small. In all cases, the Ti_3Al particles were sheared by the glide dislocations.

It is concluded that there is a definite correlation between the presence of deformable Ti_3Al particles and an alloy's susceptibility to aqueous stress-corrosion cracking. Furthermore, the appearance of the surface slip lines and the dislocation substructure in deformed specimens suggest that the specific effect of the Ti_3Al particles is to cause a nonhomogeneous planar slip character and an enhanced chemical potential of the slip bands. These factors could create the necessary conditions at the specimen-electrolyte interface for a sustained anodic reaction. However, the mechanism is not understood well enough to predict the effects of the size or volume fraction of the Ti_3Al particles on the stress-corrosion behavior. It is suggested that there should be a significant improvement in the resistance to stress-corrosion when the Ti_3Al particles are bypassed by the glide dislocations.

REFERENCES

(1) J. D. Boyd, F. H. Haynie, P. J. Moreland, W. K. Boyd, R. A. Wood, D. N. Williams, and R. I. Jaffee, "The Effect of Composition on the Mechanism of Stress Corrosion Cracking of Titanium Alloys in N_2O_4, and Aqueous and Hot-Salt Environments", Annual Summary Report on Contract NASr-100(09), Jan. 13, 1969.

(2) J. D. Boyd, P. J. Moreland, W. K. Boyd, R. A. Wood, D. N. Williams, and R. I. Jaffee, "The Effects of Composition on the Mechanism of Stress Corrosion Cracking of Titanium Alloys in N_2O_4 and Aqueous and Hot-Salt Environments", Annual Summary Report on Contract NASr-100(09), August 26, 1969.

(3) J. D. Boyd, P. J. Moreland, W. K. Boyd, R. A. Wood, D. N. Williams, and R. I. Jaffee, "The Effect of Composition on the Mechanism of Stress-Corrosion Cracking of Titanium Alloys in N_2O_4, and Aqueous and Hot-Salt Environment", Annual Summary Report on Contract NASr-100-(09), Nov. 20, 1970.

(4) I. R. Lane and J. L. Cavallaro, "Metallurgical and Mechanical Aspects of Sea Water Stress Corrosion of Titanium", Applications Related Phenomena in Titanium Alloys, ASTM STP432, ASTM 1968, p. 147.

(5) H. W. Rosenberg, "Titanium Alloying in Theory and Practice", The Science, Technology, and Application of Titanium, Pergamon Press, 1970, p. 851.

(6) K. S. Jepson, L. Larke, and C. A. Stubbington, "The Effect of the Group Three Elements Al, Ga, and In on the Creep and Stress Rupture of Titanium at 500 C", The Science, Technology, and Application of Titanium, Pergamon Press, 1970, p. 861.

(7) R. P. Elliott, Constitution of Binary Alloys, First Supplement, McGraw-Hill Book Company, New York, 1965, p. 273.

(8) M. Hansen, Constitution of Binary Alloys, McGraw-Hill Book Company, New York, 1958, p. 1222.

(9) R. I. Jaffee, "The Physical Metallurgy of Titanium Alloys," Progress in Metal Physics, 7, Pergamon Press, New York, 1958, p. 144.

(10) W. F. Brown and J. E. Srawley, Plane Strain Crack Toughness Testing of High Strength Metallic Materials, ASTM STP 410 ASTM 1966, p. 23.

(11) S. R. Seagle, R. R. Seeley, and G. S. Hall, "The Influence of Composition and Heat Treatment on the Aqueous Stress Corrosion of Titanium," Application Related Phenomena in Titanium Alloys, ASTM STP 432, ASTM 1968, p. 170.

(12) B. F. Brown, "A New Stress Corrosion Cracking Test for High Strength Alloys", Materials Research and Standards, 6, 1966, p. 129.

(13) I. R. Lane, J. L. Cavallaro, and A.G.S. Morton, "Sea-Water Embrittlement of Titanium", Stress Corrosion Cracking of Titanium, ASTM Special Technical Publication 397, ASTM, 1966, p. 246.

(14) R. A. Wood, J. D. Boyd, and R. I. Jaffee, "The Effect of Composition on the Salt Water Stress-Corrosion Susceptibility of Titanium Alloys Containing Aluminum, Molybdenum, Vanadium, and Oxygen", paper presented at the Second International Conference on Titanium Alloys, May 2-5, 1972.

(15) B. F. Brown, "The Application of Fracture Mechanics to Stress-Corrosion Cracking", Metallurgical Reviews, 13, 1968, p. 171.

(16) D. E. Piper, S. H. Smith, and R. V. Carter, "Corrosion Fatigue and Stress Corrosion Cracking in Aqueous Environments", Metals Engineering Quarterly, 8, Aug., 1968, p. 50.

(17) D. N. Fager and W. F. Spurr, "Some Characteristics of Aqueous Stress Corrosion in Titanium Alloys", ASM Transaction Quarterly, 61, 1968, p. 283.

(18) J. G. Kaufman, "Progress in Fracture Toughness Testing of Metallic Materials", Recent Developments in Plane Strain Fracture Toughness Tests, ASTM Special Technical Publication 463, ASTM, 1970, p. 3.

(19) E. A. Steigerwald and W. D. Benjamin, "Effect of Composition on the Environmentally Induced Delayed Failure of Precracked High Strength Steel", Metallurgical Transactions, 2, 1971, p. 606.

(20) H. H. Johnson and P. C. Paris, "Subcritical Flaw Growth", Engineering Fracture Mechanics, 1, 1968, p. 3.

(21) H. H. Johnson, "Environmental Cracking in High Strength Materials", Fracture, Vol. 3, Fundamentals and Environmental Effects, Academic Press, 1971, p. 679.

(22) G. Sandoz, "Subcritical Crack Propagation in Ti-8Al-1Mo-1V in Organic Liquids, Salt Water, and Inert Environments", Fundamental Aspects of Stress Corrosion Cracking, National Association of Corrosion Engineers, 1969, p. 684.

(23) R. W. Judy, Jr., and R. J. Goode, "Stress Corrosion Cracking of High Strength Steels and Titanium Alloys," NRL Report 7371, March 13, 1972, Naval Research Laboratories.

(24) R. E. Curtis and W. F. Spurr, "Effect of Microstructure on the Fracture Properties of Titanium Alloys in Air and Salt Solutions", ASM Trans. Quarterly, 61, March, 1968, p. 115.

(25) J. C. Williams, "Some Observations of the Stress Corrosion Cracking of Three Titanium Alloys", ASM Transactions Quarterly, 60, December, 1967, p. 646.

(26) R. E. Curtis, R. R. Boyer, and J. C. Williams, "Relationship Between Composition Microstructure and Stress Corrosion Cracking (in Salt Solutions) in Titanium Alloys", Trans. ASM, 62, 1968, p. 457.

(27) Anon., "Tentative Method for Plane Strain Fracture Toughness of Metallic Materials (ASTM Designation E 399-707) Review of Developments in Plane Strain Fracture Toughness Testing", ASTM STP 463, 1970, p. 249.

(28) T. Ingham, G. R. Egan, D. Elliott, and T. C. Harrison, "The Effect of Geometry on the Interpretation of COD Test Data", Inst. Mech. Engineers Preprint C54171 of a paper for the Applied Mechanics Group Conference on Practical Application of Fracture Mechanics to Pressure Vessel Technology.

(29) W. F. Brown, Jr., "Standardization of Crack Toughness Tests", paper presented March 13, 1972, at 1972 Western Metal and Tool Conference, Los Angeles, California.

(30) D. Cox and A. S. Tetelman, "Improving Fracture Toughness of Ti-6Al-4V Through Controlled Diffusion Bonding", AFML Tech Report 71-264, February, 1972, Fracture Analysis Associates Technical Report

(31) M. J. Blackburn and J. C. Williams, "Metallurgical Aspects of the Stress-Corrosion Cracking of Titanium Alloys", in Fundamental Aspects of Stress-Corrosion Cracking, eds. R. W. Staehle, et al., N.A.C.E., Houston, 1969 .

(32) M. J. Blackburn and J. C. Williams, "Strength, Deformation Modes and Fracture in Titanium-Aluminum Alloys", ASM Trans. Quart., 62, 1969, p. 398.

(33) J. L. Cavallaro and R. C. Wilcox, "Embrittlement of Ti-7Al Binary Alloy in Sea Water", Corrosion, 27, 1971, p. 157.

(34) J. D. Boyd and R. G. Hoagland, "The Relation Between Surface Slip Topography and Stress-Corrosion Cracking in Ti-8 Wt. % Al", Presented at the International Symposium on Stress-Corrosion Mechanisms in Titanium Alloys, Atlanta, Georgia, 1971; to be published by N.A.C.E.

(35) G. Lütjering and S. Weissmann, "Mechanical Properties of Age-Hardened Titanium-Aluminum Alloys", Acta Met., 18, 1970, p. 785.

(36) J. D. Boyd and R. G. Hoagland, "Slip in Titanium-Aluminum Alloys Containing Small Ti_3Al Precipitate presented at the Second International Conference on Titanium Alloys, Cambridge, Massachusetts, May 2-5, 1972, to be published by AIME.

(37) K. R. Evans, "The Embrittlement and Fracture of Ti-8 Percent Al Alloys", Trans. Aime, 245, 1969, p. 1297.

(38) M. J. Blackburn and J. C. Williams, "The Preparation of Thin Foils of Titanium Alloys", Trans. AIME 239, 1967, p. 287.

(39) C. Wagner, "Theory of Coarsening of Precipitates by Transfer of Solute in Solution", Z. Elektrochem 65, 1961, p. 581.

(40) A. J. Ardell and R. B. Nicholson, "The Coarsening of in Ni-Al Alloys", J. Phys. Chem. Solids 27, 1966, p. 1793.

(41) D. Goold, "Diffusion of Aluminum, Tin, Vanadium, Molybdenum, and Manganese in Titanium", J. Inst. Met 88, 1960, p. 444.

(42) K. R. Evans, "Deformation Mechanisms in Titanium and Titanium Aluminum Alloys", Trans. AIME 242, 1968, p. 648.

(43) M. J. Blackburn, "The Ordering Transformation in Titanium-Aluminum Alloys Containing up to 25 At. % Aluminum", Trans. Aime, 239, 1967, p. 1200.

(44) J. C. Scully, "Kinetic Features of Stress Corrosion Cracking", Corrosion Science 7, 1967, p. 197.

APPENDIX

Conversion of Units

The following conversion factors were used in converting measurements made in U.S. customary units to SI units. These conversions were made to comply with contract requirements.

Physical Quantity	U. S. Customary Unit	Conversion Factor[a]	SI Unit
Weight	pounds	0.454	kilograms (kg)
Length[b]	inches	2.54	centimeters (cm)
Strength	ksi	6.89	mega-Newtons/meter^2 (MN/m^2)
Stress-Intensity	ksi-in$^{1/2}$	1.1	mega-Newtons/meter$^{3/2}$ (MN/m$^{3/2}$)
Temperature	F	5/9(F+460)	Kelvin (K)

(a) Multiply U.S. units by this number to obtain SI units.

(b) Crack depths are recorded in millimeters (mm), inches x 25.4, and crack opening displacement in micro meters (um), inches x 25400.